

REGULATION OF APOBEC3B CATALYZED MUTATION IN OVARIAN CANCER

A DISSERTATION SUBMITTED TO THE FACULTY OF THE
UNIVERSITY OF MINNESOTA BY

Brandon Charles Leonard

IN PARTIAL FULFILMENT OF THE REQUIREMENTS FOR THE DEGREE OF
DOCTOR OF PHILOSOPHY

Advisor: Reuben S. Harris

August 2015

ACKNOWLEDGEMENTS

I would like to thank the following:

- Present and former Harris lab members - Thank you for your helpful discussions. I am especially grateful to those who directly contributed to these studies.
- Dr. Reuben Harris - Thank you for your guidance over the past 5 years and for giving everyone in lab all of the tools needed to perform any experiment.
- Dr. Bill Brown – Thank you for your help and for answering my persistent questioning. The lab would not run nearly as smoothly without you.
- Drs. Scott Kaufmann and Kimberly Kalli – Thank you for all of your support with the ovarian cancer work. I could not ask for better collaborators.
- Drs. Doug Yee, Anja Bielinsky, and Tim Starr– Thank you for your invaluable advice at our annual thesis committee meetings.
- Minnesota Friends – Thank you for being willing to relax and have a good time. I would especially like to thank Ryan Flynn, Megan Multhaup, Jeff Hall, Valerie Hall, Wade Thomas, and Britnie Thomas. You are all amazing people.
- Dr. Juan Leal and Mrs. Consuelo Alcalde – Thank you for making Minnesota feel like home with your love and support. I also cannot even begin to describe how helpful all of the dog sitting was. Cooper is a lucky pup.
- My family – Thank you for making trips out to Minnesota and for helping me make it back to California. Seeing you was always one of the biggest highlights of the year. To my parents, thank you for encouraging me to pursue science.

DEDICATION

This thesis is dedicated to my amazing wife, Bobbi.

I would not have been able to complete this work without your support.

You are truly inspiring.

ABSTRACT

Cancer is the second highest cause of death in the United States. A greater understanding of the underlying causes of this disease is critical to improve patient outcomes. For years, researchers have known that cancer is primarily a genetic disease, caused by mutations that can activate oncogenes and inactivate tumor suppressors. Several studies have also shown that UV radiation, smoking and certain defects in DNA repair cause some of the mutations that lead to cancer, but the sources of mutations found in many tumor types are yet to be explained. Here, we build upon our initial finding that APOBEC3B is a source of mutation in breast cancer by defining its role in ovarian cancer. Parallel analyses looking globally at mutation in cancer have shown that APOBEC3B also contributes to mutation in several other tumor types. Additional studies have elucidated a major signaling mechanism that regulates APOBEC3B expression in cancer. While many efforts have been made to directly inhibit APOBEC3B enzymatic activity, the advances described here have the potential to inform alternative therapeutic strategies aimed at transcriptionally downregulating APOBEC3B to slow tumor evolution and improve the durability of conventional anti-cancer drugs. Ultimately, a more comprehensive understanding of the basic biology of APOBEC3B catalyzed mutagenesis in cancer will translate to larger impacts in the clinical arena.

TABLE OF CONTENTS

| | |
|--|------------|
| Acknowledgements..... | I |
| Dedication..... | ii |
| Abstract..... | iii |
| Table of Contents..... | iv |
| List of Tables..... | vi |
| List of Figures..... | vii |
| Chapter 1: Pathological consequences of DNA cytosine deamination..... | 1 |
| Summary..... | 2 |
| Sources of mutation in cancer..... | 2 |
| The APOBEC family..... | 3 |
| Previously implicated APOBECs..... | 5 |
| APOBEC3B and cancer..... | 7 |
| Mutagenic outcomes of genomic uracil..... | 8 |
| An APOBEC3B deletion allele..... | 10 |
| Clinical impact of APOBEC3B expression in cancer..... | 11 |
| APOBEC3B regulation by HPV..... | 12 |
| Therapeutic opportunities..... | 13 |
| Overview of thesis chapters..... | 14 |
| Figures..... | 17 |
| Chapter 2: APOBEC3B upregulation and genomic mutation patterns in serous ovarian carcinoma..... | 21 |
| Summary..... | 23 |
| Introduction..... | 23 |
| Results..... | 25 |
| Discussion..... | 32 |

| | |
|--|------------|
| Materials and Methods..... | 35 |
| Additional Contributions..... | 41 |
| Tables and Figures..... | 42 |
| Chapter 3: APOBEC3B upregulation by the PKC-NFκB pathway in multiple human cancers..... | 68 |
| Summary..... | 69 |
| Introduction..... | 69 |
| Results..... | 71 |
| Discussion..... | 79 |
| Materials and Methods..... | 82 |
| Additional Contributions..... | 85 |
| Tables and Figures..... | 86 |
| Chapter 4: APOBEC3G expression correlates with T cell infiltration and improved clinical outcomes in high-grade serous ovarian carcinoma..... | 102 |
| Summary..... | 103 |
| Introduction..... | 103 |
| Results..... | 105 |
| Discussion..... | 108 |
| Materials and Methods..... | 111 |
| Tables and Figures..... | 112 |
| Chapter 5: Conclusions and Discussion..... | 120 |
| Conclusions..... | 121 |
| Discussion..... | 124 |
| Closing remarks..... | 129 |
| Bibliography..... | 131 |

LIST OF TABLES

CHAPTER 2:

| | |
|--|----|
| Table 2.S1 Cell line information..... | 50 |
| Table 2.S2 Quantitative PCR primer and probe sequences. | 51 |
| Table 2.S3 Non-malignant tissues tested..... | 52 |
| Table 2.S4 Early stage serous ovarian tumors used in sequence analyses..... | 54 |
| Table 2.S5 Additional ovarian tumor specimens analyzed..... | 55 |
| Table 2.S6 Microarray analysis of <i>APOBEC3</i> and select control gene probe sets in ovarian TCGA data..... | 58 |

CHAPTER 3:

| | |
|---------------------------------------|----|
| Table 3.S1 ChIP reagents. | 94 |
|---------------------------------------|----|

CHAPTER 4:

| | |
|---|-----|
| Table 4.1 HGSOC clinical characteristics..... | 112 |
| Table 4.S1 Summary of samples used in TCGA analysis..... | 117 |
| Table 4.S2 RT-qPCR primer and probe sets..... | 118 |

LIST OF FIGURES

CHAPTER 1:

| | |
|---|----|
| Figure 1.1 Model for APOBEC3B driven tumor evolution. | 17 |
| Figure 1.2 Introduction to the APOBEC family. | 18 |
| Figure 1.3 An <i>APOBEC3B</i> deletion allele. | 19 |
| Figure 1.4 Therapeutic implications of APOBEC3B mutagenesis..... | 20 |

CHAPTER 2:

| | |
|---|----|
| Figure 2.1 <i>APOBEC3B</i> expression and localization in ovarian cancer cell lines..... | 42 |
| Figure 2.2 Endogenous APOBEC3B activity in ovarian cancer cell lines..... | 43 |
| Figure 2.3 Intrinsic DNA deamination preferences of recombinant APOBEC3B..... | 44 |
| Figure 2.4 <i>APOBEC3B</i> expression in ovarian tumors..... | 45 |
| Figure 2.5 Ovarian cancer genomic mutation patterns..... | 47 |
| Figure 2.6 DNA deamination model for mutation in cancer..... | 49 |
| Figure 2.S1 Polynucleotide cytosine deaminase expression in ovarian cell lines..... | 60 |
| Figure 2.S2 Endogenous DNA deaminase activity in APOBEC3B high and low cell lines..... | 62 |
| Figure 2.S3 Endogenous APOBEC3B activity on alternate dinucleotide substrates.... | 63 |
| Figure 2.S4 Polynucleotide cytosine deaminase expression in ovarian primary samples..... | 64 |
| Figure 2.S5 Polynucleotide cytosine deaminase expression in ovarian TCGA samples by RNAseq. | 66 |

CHAPTER 3:

| | |
|---|----|
| Figure 3.1 APOBEC3B upregulation by PMA..... | 86 |
| Figure 3.2 APOBEC3B upregulation by PMA is dependent on PKC..... | 88 |

| | |
|--|-----|
| Figure 3.3 Non-canonical NFκB signaling is responsible for <i>APOBEC3B</i> upregulation by PMA..... | 90 |
| Figure 3.4 The PKC pathway drives endogenous <i>APOBEC3B</i> expression in cancer cells..... | 92 |
| Figure 3.5 Model for <i>APOBEC3B</i> upregulation by the PKC-NFκB pathway..... | 93 |
| Figure 3.S1 <i>APOBEC3B</i> upregulation by PMA in multiple cell lines..... | 95 |
| Figure 3.S2 <i>APOBEC3</i> mRNA levels in PMA-treated MCF10A..... | 96 |
| Figure 3.S3 Extended timecourse for PMA induction of <i>APOBEC3B</i> | 97 |
| Figure 3.S4 Viability controls for MCF10A cells treated with small molecule inhibitors. | 98 |
| Figure 3.S5 Expanded ChIP data for MCF10A cells treated with PMA alone or in combination with AEB071..... | 100 |
| Figure 3.S6 Viability controls for cancer cell lines treated with AEB071..... | 101 |

CHAPTER 4:

| | |
|---|-----|
| Figure 4.1 Correlations between <i>APOBEC3</i> expression and T cell markers in HGSOC..... | 113 |
| Figure 4.2 Clinical Correlates of <i>APOBEC3</i> and T cell marker expression in HGSOC..... | 115 |
| Figure 4.3 Correlations between <i>APOBEC</i> expression and immune cell markers across 22 cancer types..... | 116 |
| Figure 4.S1 Validation of RT-qPCR assays. | 119 |

CHAPTER 1:

APOBEC3B - pathological consequences of an innate immune DNA mutator

Some sections of this chapter were adapted with permission from: Burns, Leonard, and Harris (2015) Biomedical Journal 38(2):102-110

Authors: Michael B. Burns,^{1,2} Brandon Leonard,^{1,2} and Reuben S. Harris^{1,2}

Affiliations: ¹Biochemistry, Molecular Biology and Biophysics Department, University of Minnesota, Minneapolis, MN 55455, USA. ²Masonic Cancer Center, University of Minnesota, Minneapolis, MN 55455, USA.

SUMMARY *(This section was drafted by M.B. Burns and B. Leonard)*

Cancer is the second largest health burden in the United States. It is a disease that results from alterations in the cellular genome. While new deep sequencing data has detected patterns of mutation caused by known sources, such as UV radiation and tobacco carcinogens, several new patterns are now being uncovered. A major one of which is explained by the enzymatic activity of the DNA cytosine deaminase, APOBEC3B. As a deaminase, APOBEC3B converts cytosines to uracils in single-stranded DNA. A failure to properly repair these uracil lesions can result in a diverse array of mutations. The initial discovery of this mutational phenomenon was described mechanistically using a variety of biochemical, genetic, and cellular assays in breast cancer cell lines. These data were validated using publically available sequencing data from the TCGA and expanded to over 20 different tumor types. Additional studies using large cohorts of breast cancer patients demonstrate that APOBEC3B also manifests clinically and associates with poor outcomes. These reports cumulatively demonstrate that APOBEC3B is a major source of genetic heterogeneity in breast, ovarian, head & neck, bladder, cervical, and lung (adeno- and squamous cell) carcinomas. Future studies should be aimed at determining the diagnostic and therapeutic value of APOBEC3B.

SOURCES OF MUTATION IN CANCER *(This section was drafted by B. Leonard)*

Genome instability was recently described as an enabling hallmark of cancer (1). This hallmark is unique in that it can lead to nearly all malignant phenotypes, including replicative immortality, avoidance of cell death, sustained proliferation and induction of angiogenesis. It is therefore important to understand the sources of genome instability and how each contributes to cancer initiation and progression. Mutation is a major

contributor to genome instability, and has the ability to both activate oncogenes and inactivate tumor suppressors. There are two general categories of mutational sources: exogenous and endogenous. Exogenous sources include ultraviolet (UV) light and carcinogens from tobacco smoke (2-5). The best-studied endogenous sources are DNA replication errors that persist due to defects in DNA repair processes, such as loss of recombination or mismatch repair (MMR) proteins (6-11). While these sources combine to explain some of the observed heterogeneity, the sources of most of the mutations in cancer have yet to be explained mechanistically.

New deep sequencing technologies are allowing for the identification of patterns or “signatures” of mutation in cancer, which reflect the underlying sources of DNA damage (12). For instance, these studies have been able to detect the predicted mutation signatures for aging (characterized by spontaneous deamination of cytosines in CpG motifs) in nearly all cancers, UV light in skin cancer, tobacco usage in lung and head/neck cancer, loss of BRCA1/2 in breast and ovarian cancer, and microsatellite instability in colon cancer (13-19). In addition to confirming these and other known sources, these large datasets have been further deconvoluted to identify completely novel mechanisms of mutation in cancer (13-18,20-25). One of the most significant findings is that APOBEC3B, a member of the APOBEC family of single-stranded DNA polynucleotide cytosine deaminases, is a major contributor to cancer genome mutagenesis [Fig. 1.1; (13-18,21-29)].

THE APOBEC FAMILY (*This section was drafted by B. Leonard*)

The human APOBEC family of cytosine deaminases is composed of 11 members (Fig 1.2A). Apolipoprotein B mRNA Editng enzyme, Catalytic Subunit 1 (*APOBEC1*) is encoded on chromosome 12 and was the first to be described. The innate immune

APOBEC3s (*A*, *B*, *C*, *D*, *F*, *G*, *H*) are encoded in a tandem head-to-tail array on chromosome 22. Activation Induced Cytosine Deaminase (*AID* or *AICDA*), which is responsible for diversifying the antibody repertoire, is encoded on chromosome 6. *APOBEC2* and *APOBEC4* are encoded on chromosomes 6 and 1, respectively, and are the only *APOBECs* not known to be capable of converting cytosine to uracil (C-to-U) in single-stranded DNA (ssDNA) via a deamination reaction (**Fig. 1.2B**).

The *APOBECs* were initially named after the physiologic role of *APOBEC1* in *Apolipoprotein B* mRNA-editing (30). This nomenclature can be misleading as *APOBEC1* is the only family member responsible for this process. In fact, many of these proteins have independent physiological functions (31,32). For example, *AID* is essential for both somatic hypermutation and class-switch recombination through deamination of variable and switch region DNA segments within rearranged immunoglobulin heavy and light chain genes (33).

The *APOBEC3* proteins are also known to have 3 distinct physiologic functions in the human body, all of which are consistent with their role in innate immunity. First, many of the *APOBEC3s* have been described to defend against a diverse array of viral pathogens, including retroviruses, hepatitis viruses, papillomaviruses, and others (34,35). Of note, *APOBEC3D*, *F*, *G*, and *H* have been shown to restrict human immunodeficiency virus-1 (HIV-1) replication by deaminating cDNA intermediates that normally occur during the HIV-1 life cycle (36,37). Second, several *APOBEC3s*, including *APOBEC3A*, *B*, and *F*, have been shown to inhibit retrotransposition of L1 and Alu elements in human cells (38,39). Third, researchers have demonstrated that *APOBEC3A* and other family members have the potential to mediate the clearance of foreign DNA through a deamination dependent mechanism (40-42).

Because the *APOBEC3* family is a result of relatively recent gene duplication events, all members share large amounts of sequence homology (43). For example,

APOBEC3A and the carboxy-terminal domain of *APOBEC3B* share >90% nucleotide identity. This sequence homology has historically complicated expression analyses aimed at deciphering between the various *APOBEC3* proteins. In fact, nearly all commercially available monoclonal antibodies against these proteins lack specificity and are able to detect multiple family members. Additionally, many of the current techniques used to study global changes in mRNA expression are complicated by cross-hybridization issues. For example, the probes used to quantify mRNA levels in microarrays are too short to discretely distinguish between the different *APOBEC3* transcripts and often share homology between multiple family members (23). The longer reads generated by RNA sequencing (RNAseq) and utilization of paired-end sequencing improves upon this issue, but even these are potentially susceptible to inappropriate read mapping. Fortunately, researchers have been able to construct and validate panels of reverse transcription quantitative PCR (RT-qPCR) assays that can be used to specifically quantify each individual *APOBEC* transcript (44,45). Overall, any methods used to detect *APOBEC3* expression must be designed and carefully validated to ensure specificity and efficiency.

PREVIOUSLY IMPLICATED APOBECs (*This section was drafted by B. Leonard*)

The expression of *APOBEC1* in transgenic animals was one of the first experiments to ask whether *APOBEC* mediated cytosine deamination can lead to cancer causing mutations (46). Transgenic expression of rabbit *APOBEC1* in mice resulted in universal liver dysplasia, many of which progressed to hepatocellular carcinoma. While rabbit *APOBEC1* clearly has a dramatic carcinogenic effect when expressed constitutively in transgenic mice, this was not the case when expressed in rabbits and it has not yet proven relevant to human cancers [although a recent study has implicated *APOBEC1* in esophageal adenocarcinomas (47)] . It should also be noted that this

original APOBEC1 study was performed prior to the discovery of AID/APOBEC catalyzed DNA cytosine deamination, and therefore the authors inferred that off-target RNA editing caused the observed malignancies (48,49).

Several APOBEC3 family members have also been hypothesized to play a role in cancer since the initial discovery that they preferentially use DNA as a substrate (48). At that time, the difficulty in differentiating among the many family members made it unclear which, if any, family members might be driving mutation in cancer. More recently, it was reported that APOBEC3G contributes to metastasis in hepatocellular carcinoma, though the research neither proposed nor tested a mechanistic explanation for the observation (50). More recently, with the use of the aforementioned RT-qPCR assays, APOBEC3G is not currently a suspect in cancer onset or progression as there has not yet been a group to discover abnormal levels of APOBEC3G in human cancer tissue when specific assays are applied (23). There is a chance that the normal level of APOBEC3G expressed in a given tissue may be misregulated at the post-transcriptional level, but again, there has been no evidence presented to support this hypothesis.

Because AID is known to deaminate genomic DNA as part of its normal physiological activity, it is easy to imagine that this protein may have detrimental off-target effects. Indeed, body-wide expression of murine AID in mice leads to rapid death due to T-cell lymphomas and lung adenocarcinomas (51). In addition, AID is known to produce well-characterized carcinogenic chromosomal translocations as a side-effect of class switch recombination (52). For example, AID is required for the chromosomal translocation between *c-myc* and the immunoglobulin (*Ig*) locus, which is associated with Burkitt's lymphoma (53). These experiments provide proof of principle and a starting place from which to pursue the potential role of the other family members in cancer.

APOBEC3B AND CANCER (*This section was drafted by M.B. Burns and B. Leonard*)

Burns, Lackey, and colleagues were the first to clearly identify APOBEC3B as the APOBEC family member at work in human cancer (23). They quantified the full repertoire of *APOBEC* family mRNA species in human breast cancer tissues and cell lines. These data showed that *APOBEC3B* was preferentially and specifically upregulated in a majority of the samples tested (23). This allowed subsequent efforts to be focused on elucidating the molecular mechanism by which this enzyme might operate in breast cancer. APOBEC3B is the only family member that constitutively localizes to the cell nucleus (23,36,38,54-57). Additionally, it retains deamination activity, increases the steady-state level of uracil in the cell's genome, and correlates with increased mutation, as determined by selection and enrichment techniques [*TK*-fluctuation assay and 3D-PCR/sequencing; (23)]. These findings indicated that in a large proportion of breast cancer cell lines, APOBEC3B is driving mutations that diversify the genetic landscape.

The key translation of these mechanistic studies to primary patient tumor genomes was the recognition that APOBEC3B deaminates ssDNA at a preferred sequence context. Biochemical assays *in vitro* demonstrated that APOBEC3B prefers substrate cytosines in 5'TCA and 5'TCG contexts (23). Mutation data from three independent primary breast tumor genome datasets clearly indicated that mutations at these sites are significantly enriched (23). Moreover, *APOBEC3B* expression levels correlated positively with both cytosine mutation and overall mutation loads, despite no knowledge of the time that each tumor may have persisted (23).

The work by Burns and colleagues opened the door to larger scale genomic studies aimed at examining the contribution of APOBEC3B to the mutation load across many different tumor types (21,22). These analyses revealed that APOBEC3B is

significantly upregulated in many tumor types relative to its expression in normal tissue derived from the same organ (21,22). Furthermore, the cancer types expressing the highest levels of *APOBEC3B* also contained the most mutations (21,22). The most striking findings came when these groups examined the sequence context of the mutated cytosine bases (*i.e.*, the trinucleotide motifs including the bases immediately 5' and 3' of each mutated cytosine). Here, several tumor types showed a mutation profile similar to that of recombinant *APOBEC3B* (21,22). Together the data produced independently by the Harris and Gordenin labs suggest that *APOBEC3B* contributes most significantly to mutation in six distinct types of cancer: bladder, cervix, lung (adenocarcinoma and squamous cell carcinoma), head and neck, and breast (21,22). Parallel and independent studies looking at general mutation patterns, though non-specific in implicating a particular *APOBEC* family member, have arrived at similar conclusions (13-17,24).

MUTAGENIC OUTCOMES OF GENOMIC URACIL (*This section was drafted by B. Leonard*)

A major challenge to determining which mutations directly result from *APOBEC3B* cytosine deamination events is understanding how genomic uracils are processed in cancer cells. It is established, based on prior research on AID, that U:G mismatches resulting from cytosine deamination can result in all six base substitution mutation types (33). While many U:G lesions are likely repaired in an error free manner by the canonical base excision repair pathway, lesions that escape this process have multiple distinct mutagenic potentials. Briefly, the general steps required for repair include excision of the uracil lesion, nicking of the DNA backbone, and subsequent reincorporation of the correct nucleotides (58). At several of the steps required for repair,

there are alternative outcomes that may lead to a variety of mutation types. Simple DNA replication across uracilated DNA results in C-to-T transitions, mutagenic MMR at U:G mismatches may result in transitions and/or transversions, translesion DNA synthesis across abasic sites can result in transition mutations, and finally, in highly deaminated regions, the repair process may generate nicks on both strands of the DNA double helix that are relatively close to one another potentially resulting in double-stranded breaks.

The above mechanisms are supported not only by the aforementioned work on AID, but also by more recent publications aimed at elucidating the proteins involved in the repair of APOBEC mediated damage in yeast. One study has shown that a deficiency in uracil DNA glycosylase (UNG) or the translesion DNA polymerase REV1 results in a mutation spectrum greatly skewed toward C-to-T transition mutations (at the expense of transversions), particularly in the presence of an active DNA cytosine deaminase (28). Another study used a panel of translesion polymerase mutants to show that REV1 and REV3 contribute most significantly to the formation of transversion mutations in yeast (59). This research provides support for the proposed models, but more studies are needed to identify the mechanisms at play in human tumors (with many more DNA polymerases than yeast) and to determine how other processes, such as mismatch repair, recombination, and cell cycle checkpoints, might also influence mutagenic outcomes.

In breast cancer, Burns, Lackey, and colleagues found that APOBEC3B upregulation correlated with increased levels of transition mutations, suggesting that a proportion of the genomic uracils created by APOBEC3B either persist through DNA synthesis or are generated at a high enough rate that they are detectable in non-replicated DNA. As indicated above, if a uracil is not excised by a DNA glycosylase prior to DNA replication it will template as a thymine and base pair with adenosine. After a

subsequent round of DNA replication, the result is a C-to-T transition mutation. A similar result will occur if the genomic uracil is removed by uracil excision repair and an adenine is inserted opposite the resulting abasic site during local DNA synthesis or replication. While these are perhaps the simplest mutational outcomes of cytosine deamination, many other pathways should be investigated to determine if DNA repair can be harnessed as a potential therapeutic option of cancer treatment.

AN APOBEC3B DELETION ALLELE (*This section was drafted by B. Leonard*)

Several studies have examined the *APOBEC3B* locus in human populations as part of both general surveys and more specific cancer studies (60-65). These analyses have identified an *APOBEC3B* deletion polymorphism circulating in the human population with an allelic frequency ranging from approximately 1% to 93%, dependent upon the biogeographical ancestry of the population examined [Fig. 1.3; (60)]. One group used a small Japanese cohort (<50 patients) to assess breast cancer incidence and the *APOBEC3B* deletion polymorphism and found a statistically insignificant trend toward an inverse correlation between *APOBEC3B* and breast cancer (61). Two other groups used much larger cohorts to assess the relationship between the deletion allele and breast cancer incidence (62,63). These larger studies determined that there was a significant increase in the *APOBEC3B* deletion allele among women with breast cancer. Unlike the Japanese study that collected data on the deletion allele frequency from normal healthy patients recruited into their study, these groups relied on data from the 1000 genomes project to determine the frequency of the deletion allele within their cohorts. Another group found a similar association between the *APOBEC3B* deletion and ovarian cancer risk in a cohort of Chinese women (64). These findings argue that *APOBEC3B* is somehow a protective factor, reducing the incidence of breast cancer in

the populations studied. These observations are intriguing and may reflect compromised innate immune defenses, with increased levels of viral infection and endogenous retrotransposition expected in the absence of this enzyme.

An argument has been presented that an APOBEC mutation pattern persists even in cancer samples that harbor the *APOBEC3B* deletion allele (65). This would imply that the signature is likely the result of another APOBEC since APOBEC3B is absent in the cells homozygous for the *APOBEC3B* deletion. Unfortunately, this study failed to segregate the *APOBEC3B*-deletion allele heterozygotes from the homozygotes and thus confounded interpretations by including as the majority of their “APOBEC3B-deletion” samples, tumors with upregulated, active APOBEC3B. This, coupled with the finding that APOBEC3A when expressed endogenously is confined to myeloid lineage cell types, and the protein itself is located in the cytoplasm and non-genotoxic, indicating that APOBEC3B remains the leading culprit for cancer mutagenesis (42,44,45,66,67). Further work is needed to determine unambiguously whether other APOBEC family members might contribute to cancer mutagenesis and, if so, then deduce their contributions relative to those of APOBEC3B.

CLINICAL IMPACT OF APOBEC3B EXPRESSION IN CANCER (*This section was drafted by M.B. Burns and B. Leonard*)

The *APOBEC3B* deletion allele may be protective with respect to breast cancer incidence, however it was recently shown that once the cancer has formed, certain subsets of patients with tumors expressing high levels of *APOBEC3B* have significantly worse outcomes relative to those that lack expression of the enzyme (26,27). One study showed that this was the case in estrogen receptor (ER)-positive breast cancer patients from the Netherlands, while another used TCGA data to show this correlation in both

Luminal A and Luminal B tumor subsets. One of the Dutch cohorts represented patients that had only been treated by surgical resection indicating that *APOBEC3B* expression levels alone can provide a prognostic indication. This recent study is important because it clearly distinguishes incidence from progression. Additional studies on breast and other *APOBEC3B*-linked tumor types are needed to confirm and extend these initial findings.

***APOBEC3B* UPREGULATION BY HPV** (*This section was drafted by R.S. Harris and B. Leonard*)

A key question is how *APOBEC3B* becomes upregulated in cancer. Original studies eliminated many possibilities including gene amplification, chromosome translocation, promoter mutations, and other *cis* events such as differential methylation (23). Although there are likely to be many answers to this question, one possible clue comes from the strong link between *APOBEC3B* expression and mutagenesis in cervical and head/neck cancers and the fact that many of these cancers are HPV driven (13,15,16,21,22,68). Henderson and colleagues recently demonstrated a clear segregation of exogenous, smoking related mutations and *APOBEC3B*-driven mutations in head/neck cancers (16). Their findings further indicated that *APOBEC3B* upregulation correlated with HPV-positive status. Subsequent functional studies have confirmed these observations and determined that either E6 or E7, two oncoproteins encoded by HPV, are likely responsible for *APOBEC3B* upregulation (69-72). Thus, for these cancer types, there may be an HPV-mediated mechanism of *APOBEC3B* upregulation. The mechanism(s) for *APOBEC3B* upregulation is less obvious for non-viral cancer types.

THERAPEUTIC OPPORTUNITIES (*This section was drafted by M.B. Burns and B. Leonard*)

There is a growing consensus in the field that APOBEC3B is a major and previously unappreciated source of mutation in several different cancer types. This enzyme is likely contributing significantly to genetic, and thus phenotypic, heterogeneity within the tumors in which it is expressed. The full clinical significance of this conclusion has yet to be realized fully, but it may be relevant to diagnosis, prognosis, and ultimately therapy.

Knowledge of APOBEC3B mutagenesis provides a framework for future therapeutic strategies. The most direct method to limit APOBEC3B's impact would be to inhibit the enzyme's deaminase activity using small molecules and thereby to create a hypomutator state in the tumor (**Fig. 1.4**). The goal of this strategy would be to post-operatively (once tumor burden decreases) slow the rate of evolution of the remaining tumor cells, decrease the likelihood of resistance mutations arising, and ultimately render the remaining tumor cells more sensitive to conventional therapeutics. Alternatively, the as yet unknown pathways that drive *APOBEC3B* expression could be targeted to decrease expression levels, highlighting the importance of further research on this topic. Conversely, as has been done for *BRCA1/2*-mutant cancers, DNA repair pathways could be modulated in an attempt to make APOBEC3B dependent damage toxic, creating a hypermutator phenotype, and a synthetic lethal state for tumor cells (**Fig. 1.4**). In either the hypomutation or hypermutation scenarios, the goal is to translate this basic research discovery into successful clinical results that improve and extend the lives of patients.

OVERVIEW OF THESIS CHAPTERS *(This section was drafted by B. Leonard)*

Chapter 2: APOBEC3B upregulation and genomic mutation patterns in serous ovarian carcinoma

Following our publication elucidating APOBEC3B as a major source of mutation in breast cancer (23) , I was interested to determine whether cytosine deamination also contributed to mutation in other cancer types. Since prior reports indicated that breast and ovarian cancer share similar mutation spectra (73) and we had recently forged a collaboration with a group of clinical ovarian cancer researchers at the Mayo Clinic, I led a project to determine if APOBEC3B contributed to mutation in ovarian cancer (74). In Chapter 2, we show that APOBEC3B is the only cytosine deaminase significantly upregulated in ovarian cancer cell lines and primary tumor samples. Functional studies revealed that APOBEC3B is responsible for nearly all of the cytosine deaminase activity in cellular extracts. Furthermore, bioinformatic analysis of whole genome deep sequencing data from 16 low stage ovarian carcinoma samples identified a correlation between mutation loads and APOBEC3B expression. A particularly interesting finding from this work is that APOBEC3B expression correlates with transversion mutations at C/G base pairs rather than transitions as seen in breast cancer, suggesting a role for translesion DNA synthesis in the repair of uracil lesions created by APOBEC3B. During the review process for this article, our lab and others reported APOBEC3B expression and genomic mutation signatures across multiple cancer types (13,21,22). These analyses revealed that 6 human cancers are most significantly affected by APOBEC3B catalyzed mutagenesis. These cancer types include bladder, breast, cervical, head/neck, lung adenocarcinoma, and lung squamous cell carcinoma. While ovarian cancer was not one of the identified cancer types, our work emphasizes the need for comprehensive

studies of specific cancer types and highlights the heterogeneity of ovarian cancer subtypes.

Chapter 3: APOBEC3B upregulation by the PKC/NFκB pathway in multiple human cancers

Our lab is commonly asked how APOBEC3B becomes upregulated in cancer. While I collaborated with a visiting graduate student to elucidate a role for HPV infection in APOBEC3B upregulation (69), I was eager to determine how APOBEC3B becomes upregulated in cancers with no known viral origins. Previous literature suggested that multiple APOBEC3s can become upregulated upon PMA treatment of oral epithelial tissue, but these early studies were unable to distinguish between the high nucleotide level homologies observed between family members (75). In addition, the fact that primary tissue is comprised of multiple cell types was not considered and therefore it was unclear where each APOBEC3 was being upregulated. In Chapter 3, we show that APOBEC3B is specifically upregulated by PMA in multiple cell lines. Furthermore, we found that upregulation by PMA is accomplished through activation of PKCα and subsequent stimulation of non-canonical NFκB signaling. To extend our findings to APOBEC3B upregulation in cancer, a panel of APOBEC3B expressing cancer cell lines were treated with a preclinical PKC inhibitor. Indeed, PKC inhibition reduced APOBEC3B levels by over 50% in nearly half of the cell lines tested. While these studies elucidate a major pathway responsible for APOBEC3B upregulation in cancer, they also indicate that other mechanisms exist.

Chapter 4: APOBEC3G expression correlates with T cell infiltration and improved clinical outcomes in high-grade serous ovarian carcinoma

A major confounding factor when analyzing primary tumor samples is intra- and inter-tumor heterogeneity. While tumor cell specific genetic differences account for intra-tumor heterogeneity, considerable inter-tumor heterogeneity is contributed by immune infiltrates such as T and B cells. Our lab hypothesized that immune cell infiltration accounts for the expression of several APOBEC family members in primary tumor samples, leading to the inappropriate conclusions that some of these primarily innate immune APOBECs contribute to cancer genome mutation. Here, in Chapter 4, we determined that *APOBEC3G* correlates with several markers of T cell infiltration in a cohort of high-grade serous ovarian cancer patients where T cell infiltration is known to contribute to better patient outcomes (76-79). Using clinical data, we discovered that *APOBEC3G* is a better prognostic marker than other T cell markers. We were also able to address whether *APOBEC3B* contributes to patient outcomes in this cohort of ovarian cancer patients. Interestingly, we discovered that *APOBEC3B* does not correlate strongly with either overall or progression free survival. To apply our findings more broadly, we analyzed TCGA data across 22 cancer types and found a strong correlation between several HIV restrictive APOBEC family members and the T cell marker, *CD3D*. As expected, AID also significantly correlates with a B cell specific marker in many tumor types. Overall, our work here clarifies misconceptions about the detection of APOBEC expression in primary tumor samples, elucidates a new biomarker for T cell immune infiltrates, and identifies additional differences between the role of *APOBEC3B* in breast and ovarian cancer.

Chapter 5: Conclusions and Discussion

In chapter 5, I summarize the main conclusions from each chapter and discuss how these studies improve our understanding of *APOBEC3B* catalyzed mutation in ovarian and other cancer types.

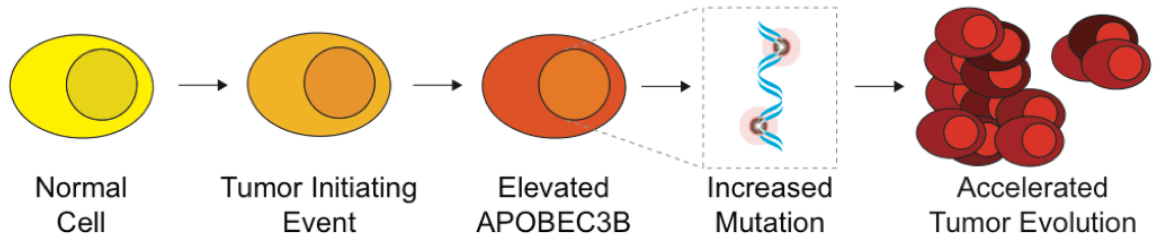


Figure 1.1 Model for APOBEC3B driven tumor evolution.

Upregulation of APOBEC3B in nascent cancer cells or during cancer development increases mutation rates and drives tumor evolution.

This figure was drafted by B. Leonard and published in (80).

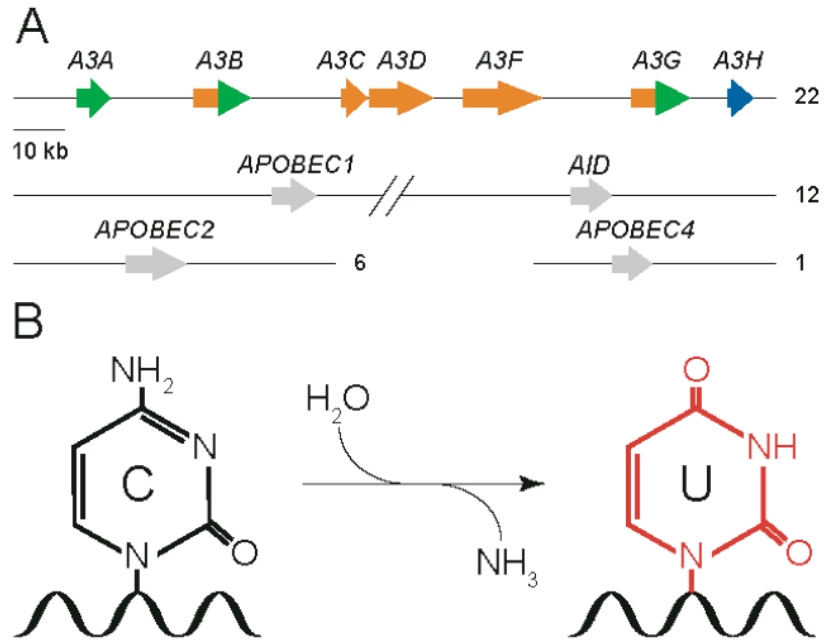


Figure 1.2 Introduction to the APOBEC family.

(A) Depiction of the spatial organization of the APOBEC family members, with the APOBEC3 genes arrayed in tandem on chromosome 22, APOBEC1 and AID located on chromosome 12, and APOBEC2 and APOBEC4 encoded on chromosomes 6 and 1, respectively.

(B) APOBEC3 family enzymes catalyze the hydrolytic reaction of cytosine to uracil in single-stranded DNA.

This figure was drafted by B. Leonard and published in (80).

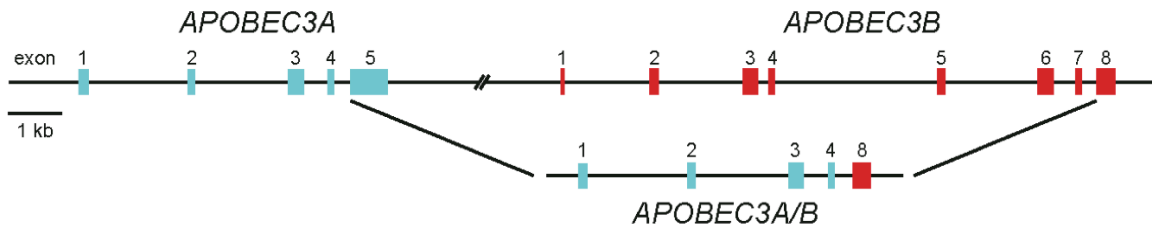


Figure 1.3 An *APOBEC3B* deletion allele.

A germline deletion between homologous regions of *APOBEC3A* and *APOBEC3B* has resulted in a chimeric gene in which exon 4 of *APOBEC3A* is fused to exon 8 of *APOBEC3B*.

This figure was drafted by B. Leonard and published in (80).

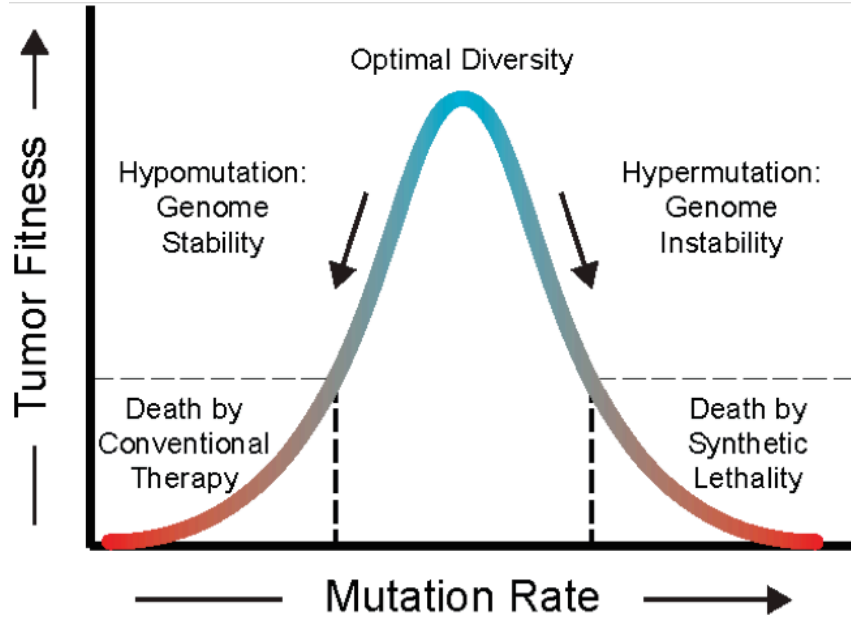


Figure 1.4 Therapeutic implications of APOBEC3B mutagenesis.

Both decreasing or increasing the mutation rate of APOBEC3B-expressing cells is predicted to result in decreased tumor fitness and tumor cell death. Decreasing the mutation rate through APOBEC3B inhibition may result in genome stabilization and a lower probability of drug resistance mutations (*i.e.*, increased durability of conventional chemotherapeutics). Alternatively, increasing the level of APOBEC3B mutagenesis (directly by increasing APOBEC3B levels or indirectly by creating a synthetic lethal state) may result in toxic levels of genomic lesions and tumor death. Adapted from similar concepts proposed for APOBEC3 mutagenesis of HIV-1 (81).

This figure was drafted by B. Leonard and published in (80).

CHAPTER 2:

APOBEC3B upregulation and genomic mutation patterns in serous ovarian carcinoma

This chapter was adapted with permission from: Leonard and Hart et al. (2013) Cancer Research 73(24):7222-7231

Authors: Brandon Leonard,^{1,2,*} Steven N. Hart,^{3,*} Michael B. Burns,^{1,2} Michael A. Carpenter,^{1,2} Nuri A. Temiz,^{1,2} Anurag Rathore,^{1,2} Rachel Isaksson Vogel,² Jason B. Nikas,² Emily K. Law,^{1,2} William L. Brown,^{1,2} Ying Li,³ Yuji Zhang,³ Matthew J. Maurer,³ Ann L. Oberg,³ Julie M. Cunningham,⁴ Viji Shridhar,⁵ Debra A. Bell,⁵ Craig April,⁶ David Bentley,⁶ Marina Bibikova,⁶ R. Keira Cheetham,⁶ Jian-Bing Fan,⁶ Russell Grocock,⁶ Sean Humphray,⁶ Zoya Kingsbury,⁶ John Peden,⁶ Jeremy Chien,⁷ Elizabeth M. Swisher,⁸ Lynn C. Hartmann,⁹ Kimberly R. Kalli,¹⁰ Ellen L. Goode,¹¹ Hugues Sicotte,³ Scott H. Kaufmann,^{12,13} and Reuben S. Harris,^{1,2}

Affiliations: ¹Biochemistry, Molecular Biology and Biophysics Department, University of Minnesota, Minneapolis, MN 55455, USA. ²Masonic Cancer Center, University of Minnesota, Minneapolis, MN 55455, USA. ³Division of Biomedical Statistics and Informatics, Department of Health Sciences Research, Mayo Clinic, Rochester, MN 55905, USA. ⁴Medical Genome Facility and Department of Laboratory Medicine & Pathology, Mayo Clinic, Rochester, MN 55905, USA. ⁵Department of Laboratory Medicine & Pathology, Mayo Clinic, Rochester, MN 55905, USA. ⁶Illumina Cambridge Ltd, Chesterford Research Park, Little Chesterford, Cambridge CB10 1XL, UK. ⁷Department of Cancer Biology, University of Kansas, Kansas City, KS 66160, USA. ⁸Department of Obstetrics & Gynecology, University of Washington School of Medicine,

Seattle, WA 98195, USA. ⁹Division of Medical Oncology, Department of Oncology, Mayo Clinic, Rochester, MN 55905, USA. ¹⁰Women's Cancer Program, Mayo Clinic Cancer Center, Rochester, MN 55905 USA. ¹¹Division of Epidemiology, Department of Health Sciences Research, Mayo Clinic, Rochester, MN 55905, USA. ¹²Division of Oncology Research, Department of Oncology, Mayo Clinic, Rochester, MN 55905 USA. ¹³Department of Molecular Pharmacology & Experimental Therapeutics, Mayo Clinic, Rochester, MN 55905, USA.

* These authors contributed equally to this work

SUMMARY

Ovarian cancer is a clinically and molecularly heterogeneous disease. The driving forces behind this variability are unknown. Here we report wide variation in expression of the DNA cytosine deaminase *APOBEC3B*, with elevated expression in a majority of ovarian cancer cell lines (3 standard deviations above the mean of normal ovarian surface epithelial cells) and primary ovarian cancers. *APOBEC3B* is active in the nucleus of several ovarian cancer cell lines and elicits a biochemical preference for deamination of cytosines in 5'TC dinucleotides. Importantly, examination of whole-genome sequence from 16 ovarian cancers reveals that *APOBEC3B* expression correlates with total mutation load as well as elevated levels of transversion mutations. In particular, high *APOBEC3B* expression correlates with C-to-A and C-to-G transversion mutations within 5'TC dinucleotide motifs in early-stage high-grade serous ovarian cancer genomes, suggesting that *APOBEC3B*-catalyzed genomic uracil lesions are further processed by downstream DNA 'repair' enzymes including error-prone translesion polymerases. These data identify a potential role for *APOBEC3B* in serous ovarian cancer genomic instability.

INTRODUCTION

Ovarian cancer remains the deadliest gynecological malignancy in the United States, with an estimated 22,300 new cases and 15,500 deaths in 2012 (82). Although multiple histological subtypes of ovarian cancer are recognized, including clear cell and endometrioid, the most common and deadly form is serous ovarian cancer. This disease usually escapes detection until it has spread throughout the peritoneal cavity. Previous analyses of high-grade, mostly late-stage serous ovarian cancers have demonstrated mutational inactivation of *TP53* in 95% of cases (83). Mutations in several other genes,

including *BRCA1*, *BRCA2*, and *CDK12*, also collectively occur in roughly a quarter of high-grade serous ovarian cancers; and genomic instability, as manifested by large amplifications and deletions, is common (83,84). In contrast, clear cell and endometrioid ovarian cancers are characterized by mutations in *PIK3CA* and *ARID1A*, with endometrioid ovarian cancers also having frequent *CTNNB1* mutations or *PTEN* loss.

Despite this genetic heterogeneity, ovarian cancers are typically treated with the same chemotherapy after surgical debulking. Most ovarian cancers respond initially to DNA cross-linking chemotherapeutic agents, such as carboplatin (85,86). However, drug resistance commonly develops, with disease recurrence occurring at an average of 18 months after initiating therapy and average survival limited to 3-5 years after diagnosis (86). Mechanisms for resistance remain poorly understood but have been attributed, at least in the case of some *BRCA1/2* mutant tumors, to the acquisition of further mutations (87). The mechanisms responsible for the mutational evolution of these cancers are not completely understood.

We recently discovered a major role for enzyme-catalyzed DNA C-to-U deamination in breast cancer (23). The DNA deaminase APOBEC3B was found upregulated and active in the majority of breast cancer cell lines, and its upregulation in tumors correlated with increased C-to-T transition and overall base substitution mutation loads (23). APOBEC3B is one of seven APOBEC3 deaminases, which have broad and overlapping functions in providing innate immunity to a large number of DNA-based parasites, including retroviruses (with susceptible cDNA intermediates), some DNA viruses, and even naked foreign DNA [(34) and references therein]. These APOBEC3 enzymes are related to the antibody diversification enzyme activation-induced DNA cytidine deaminase (AID) and the *APOB* mRNA editing protein APOBEC1 (31). All nine of these enzymes exhibit DNA deaminase activity in multiple assays. Furthermore, transgenic expression of AID and APOBEC1 can induce tumor formation in mice

(46,51,88). In humans, AID is associated with B cell tumorigenesis, imatinib resistance, and *BCL2* gain-of-function (52,89,90). However, because human AID and APOBEC1 are expressed predominantly in B lymphocytes and gastrointestinal tissues, respectively, it is unlikely that they contribute to tumorigenesis elsewhere. Based on the fact that breast and ovarian cancers have similar mutation spectra (73) and often show high degrees of genomic instability (83,91), here we test the possibility that APOBEC3B is an active source of genomic DNA damage and mutagenesis in ovarian cancer.

RESULTS

APOBEC3B expression and localization in ovarian cancer cell lines

As an initial test for APOBEC3B in ovarian cancer, we used reverse transcription quantitative PCR (RT-qPCR) to survey the mRNA levels of *APOBEC3B* and all of the related deaminase family members in a panel of ovarian cancer cell lines (**Fig. 2.1A**, **Fig. 2.S1**, **Table 2.S1**, and **Table 2.S2**). The expression level of each deaminase family member was normalized to that of the constitutive house keeping gene *TATA binding protein (TBP)*. This analysis revealed that *APOBEC3B* expression varied widely across these cell lines (**Fig. 2.1A**). In contrast, immortalized ovarian epithelial lines (OSE) used as controls showed a much narrower range of *APOBEC3B* expression (**Fig. 2.1A**). 10 of 18 [56%, 95% confidence interval (CI) 30.8-78.5%] ovarian cancer cell lines had *APOBEC3B* mRNA levels more than 3 standard deviations (SD) above the mean of the 5 OSE lines. Cultured fallopian tube epithelial cells (92), another normal control, had *APOBEC3B* levels similar to those found in the OSE lines (**Fig. 2.1A**).

Examination of additional deaminase members revealed that mRNA of the most closely related family member, *APOBEC3A*, was undetectable in 16/18 (88.9%, 95% CI 65.3-98.6%) ovarian cancer cell lines, consistent with its developmental confinement to

myeloid lineage cell types [Fig. 2.S1; (40,44)]. Although some of the other family members were expressed to varying degrees in several of the ovarian cancer cell lines, none were over-expressed in the majority of lines based on the same statistical criteria (3 SD over the mean level in the 5 OSE lines; Fig. 2.S1).

We next investigated whether APOBEC3B protein localizes to the nuclear compartment in ovarian cancer cell lines, as it does in several other cancer and immortalized cell lines (23,36,38,54-57). Because specific antibodies for APOBEC3B are not yet available, we determined the localization of transfected APOBEC3B-eGFP in live ovarian cancer cells and APOBEC3B-HA in fixed and permeabilized cell lines by fluorescence microscopy. Both APOBEC3B-eGFP and APOBEC3B-HA were predominantly nuclear in the OVCAR5, IGROV-1, and A2780 ovarian cancer cell lines (Fig. 2.1B). Taken together these RT-qPCR and localization data suggested that APOBEC3B is positioned to pose a threat to ovarian genomic integrity.

Endogenous APOBEC3B activity in ovarian cancer cell lines

The gold standard for quantifying an endogenous protein is measuring its functional activity. We therefore assayed endogenous DNA C-to-U deaminase activity of the 3 highest and lowest *APOBEC3B* expressing cell lines using a fluorescence-based assay (Fig. 2.2A and 2.S2). Clear endogenous DNA deaminase activity was detected from the *APOBEC3B*-high but not the -low expressing lines suggesting a direct link. To ask which cellular compartment contained the source of this activity, we generated cytoplasmic and nuclear protein extracts from the *APOBEC3B*-high lines and assayed the activity of each fraction. High levels of single-stranded DNA C-to-U activity were detected in the nuclear but not the cytoplasmic protein fractions consistent with localization data (Fig. 2.2B and 2.2C). To test whether this nuclear deaminase activity

was specifically due to endogenous APOBEC3B, we also performed the experiments using protein extracts prepared from pools of cells transduced with control or *APOBEC3B* shRNAs. Two independent knockdown constructs were used, with one causing stronger depletion of endogenous *APOBEC3B* mRNA levels [Fig. 2.2B, blue vs. green bars; (23)]. The level of *APOBEC3B* knockdown correlated directly with loss of nuclear ssDNA C-to-U deaminase activity, with the stronger shRNA causing a larger diminution of activity (Fig. 2.2C). OVCAR5, IGROV-1, and A2780 all yielded similar results.

In parallel, we also assessed the dinucleotide deamination preference of endogenous APOBEC3B in nuclear and cytoplasmic protein extracts from the same cell lines. In all instances, a single-stranded DNA substrate with a 5'TC deamination target was strongly preferred over other dinucleotide-containing substrates (Fig. 2.2C and 2.S3). Taken together, these coupled genetic knockdown and enzyme activity experiments demonstrate that most, if not all, of the measurable DNA deaminase activity in the nuclear compartment of the tested ovarian cancer cell lines is due to the endogenous APOBEC3B enzyme.

Deamination kinetics of recombinant APOBEC3B

Deoxynucleotide identities immediately 5' and 3' of target DNA cytosines can strongly influence the efficiency of DNA deamination by APOBEC3 family members (23,93-95). Therefore, to compare the cell-based studies (above) with mutational data from clinical samples (below), we determined the local sequence specificity and enzyme kinetics of recombinant APOBEC3B *in vitro*. Using the catalytic domain of APOBEC3B (residues 195-382) purified from HEK293 cells, we conducted a series of time course experiments with substrates spanning all 16 permutations of deoxynucleotides

immediately 5' and 3' of the target cytosine (*i.e.*, 5'NCN). Quantification of deamination products accumulating over time enabled catalytic efficiencies to be determined. These analyses revealed that the nucleotide directly 5' of the target cytosine was a stronger determinant of APOBEC3B deamination than the 3' nucleotide. More specifically, we found that 5'TC dinucleotides support the highest reaction rates and 5'AC and 5'GC support the lowest (representative gels in **Fig. 2.3A** and quantification in **Fig. 2.3B**). Overall, these *in vitro* preferences of recombinant APOBEC3B catalytic domain confirmed and extended our prior studies (21,23), and they correlated strongly with and further validated results obtained with the full length endogenous enzyme in nuclear extracts of breast (23) and ovarian cancer cell lines (this study, above). Importantly, these substrate preferences, which represent the intrinsic deamination activity of APOBEC3B, provided a hierarchy of 'signatures' for comparison with the mutation patterns in ovarian cancer genomic mutation data sets described below.

APOBEC3B expression in ovarian tumors

To extend our studies to clinical ovarian cancer specimens, we initially assayed DNA deaminase family member mRNA expression in 8 normal or benign ovarian tissues (**Table 2.S3**) and a series of 23 ovarian cancers, including 16 early stage high-grade serous ovarian cancers that were also subjected to whole genome sequencing (clinical characteristics in **Tables 2.S4** and **2.S5**). High quality RNA was prepared from flash frozen tissues, and each of the deaminase family members were quantified by RT-qPCR as described above. As expected based on our cell line expression analysis, *APOBEC3B* mRNA varied widely in ovarian cancers, but was significantly upregulated in comparison to normal ovary tissue as a control (tumor n = 23 vs. normal tissue n=8; p=0.011 by the Wilcoxon rank sum test; **Fig. 2.S4**). *APOBEC1* was also upregulated in

one tumor ($p=0.006$), but this was considered a rare exception because it was not supported by cell line or additional tumor data. No significant differential expression was apparent for *APOBEC3A* ($p=0.541$), *APOBEC3G* ($p=0.068$), *APOBEC3H* ($p=0.214$), *AID* ($p=0.214$), or *APOBEC4* ($p=0.107$). Interestingly, lower levels were found in the tumor than in normal ovaries for *APOBEC3C* ($p=0.002$), *APOBEC3D* ($p=0.002$), *APOBEC3F* ($p=0.040$), and *APOBEC2* ($p=0.003$) suggesting either that these family members are down-regulated in ovarian cancers or they are poorly expressed in cells that eventually develop into tumors (**Fig. 2.S4**).

Using the same RT-qPCR assay and the data from our initial cohort, we next examined *APOBEC3B* expression in an expanded panel of 77 ovarian tumors (clinical characteristics in **Tables 2.S4** and **2.S5**), and determined whether higher *APOBEC3B* correlates with stage and/or grade (**Fig. 2.4A-D**). *APOBEC3B* mRNA levels in most normal ovarian tissues were only a small fraction of those of the housekeeping gene *TBP* with an average of 0.07 +/- a SD of 0.04 *APOBEC3B/TBP* ($n=20$, excluding OV412 as an outlier; Dixon's Q test confidence limit 99%). Using a strict cutoff of 3 SD above the normal ovary tissue mean, we found that 44/66 ovarian carcinomas without matched normal samples show upregulated *APOBEC3B* mRNA levels (66.7%; 95% CI, 55.3-78.1%; **Fig. 2.4A**). In addition, *APOBEC3B* was upregulated in 9 of 11 instances where both matched normal and tumor tissue was available ($p=0.010$ by Signed rank test; **Fig. 2.4B**). When comparing all 77 tumors, there was no statistical difference in *APOBEC3B* mRNA levels in late vs. early-stage samples ($p=0.222$ by Wilcoxon rank sum test; **Fig. 2.4C**), suggesting that *APOBEC3B* upregulation may occur early in ovarian cancer development. In contrast, there was a significant difference between grade 3 and all lower grade samples ($p=0.044$ by Wilcoxon rank sum test; **Fig. 2.4D**), suggesting that *APOBEC3B* may contribute to tumor dedifferentiation.

As for many cell-of-origin versus tumor comparisons, cells of the ovarian epithelial layer may only represent a fraction of the total bulk ovarian tissue. This factor is further affected by microenvironment changes that occur during tumor development. These and other factors complicate direct comparisons between normal tissues and tumor samples. Therefore, to fortify the above comparisons, we performed an additional analysis using the mean *APOBEC3B* expression values from immortalized OSE lines (**Fig. 2.1A**) and expression values from the tumors described here (**Fig. 2.4A**). Similar to the analysis described above, *APOBEC3B* expression levels were at least three SD above the mean of the immortalized OSE cells in 12 of 77 ovarian tumors. Therefore, regardless of the normal samples used for comparison, a subset of ovarian tumors show upregulated *APOBEC3B* expression levels.

Next, The Cancer Genome Atlas (TCGA) Network microarray and RNA sequencing (RNAseq) data were used to test the robustness of our RT-qPCR approach and to extend expression results to larger, independent data sets (**Fig. 2.4E-F**). TCGA microarray data were available for 581 ovarian cancers and 8 unrelated normal ovarian tissues, and an analysis of these data indicated *APOBEC3A* and *APOBEC3B* upregulation in malignant tissues ($p < 0.0003$ by Mann-Whitney U test; **Fig. 2.4E** and **Table 2.S6**). However, the microarray result for *APOBEC3A* is likely a false-positive because 5/11 *APOBEC3A* probes have >22/25 nucleotides of identity with *APOBEC3B*, and 8/11 *APOBEC3B* probes have >22/25 nucleotides of identity with *APOBEC3A* (23). Moreover, modest *APOBEC3G* down-regulation is also a false positive because the probe set in question has no complementarity to *APOBEC3G* and the second *APOBEC3G* probe set showed no significant difference. RNAseq data largely overcome these technical limitations because the longer paired-end reads enhance the chance of spanning a region of heterology and enabling the correct gene-specific assignment of

sequence reads [e.g., (21,23)]. Analysis of the RNAseq data available on 188 TCGA samples demonstrated that expression of *APOBEC3A* is lower than *APOBEC3B* in high-grade, late-stage serous ovarian cancer specimens, confirming that the *APOBEC3A* measurement on the microarray is likely a false positive (**Fig. 2.S5**). Moreover, quantification of *APOBEC3B* expression by RNAseq across the entire 190 TCGA ovarian cancer samples examined by this technique also yielded data that largely mirrored our RT-qPCR results (**Fig. 2.4F**). A subset of the samples analyzed by RT-qPCR was also part of TCGA studies (n=42; denoted by asterisks in **Fig. 2.4A** and indicated in **Table 2.S5**). Analysis of the 32 TCGA samples analyzed by both RT-qPCR and RNAseq revealed a strong correlation between results obtained with both techniques ($p < 0.0001$, $r = 0.88$ by Spearman's correlation; **Fig. 2.4G**). This concordance lends confidence to the overall data sets and fortifies the conclusion that *APOBEC3B* expression varies widely but appears to be elevated in many of the ovarian cancers studied relative to normal ovarian tissues or immortalized OSE samples used as controls in this study.

Mutation patterns in early-stage ovarian tumors

To gain further insight into the biological consequences of varied *APOBEC3B* expression in ovarian cancer, we performed whole genome sequencing in 16 early-stage, mostly high-grade serous ovarian cancers (**Table 2.S4**) and examined the relationship between *APOBEC3B* expression and the mutations found in these cancers. Importantly, all patients were treatment naïve and had no evidence of other cancers prior to diagnosis. The total load of somatic mutations varied widely among the 16 early-stage serous ovarian cancers, with a range from 1055 to 8249 mutations per specimen (**Table 2.S4**). A significant positive correlation ($p = 0.013$, $r = 0.60$ by Spearman's correlation)

was observed between mutation load and *APOBEC3B* levels (**Fig. 2.5A**). Approximately 60% of base substitutions occurred at C/G base pairs, which is notable given the A/T richness of the human genome.

Surprisingly, we found that the majority of mutations occurring at C/G base pairs in ovarian cancer are C-to-A or C-to-G transversions (**Fig. 2.5B**). Moreover, these transversions correlated with *APOBEC3B* expression levels (**Fig. 2.5C**). This finding was unexpected because the anticipated simplest outcome of a C-to-U genomic DNA lesion is a C-to-T transition through DNA replication or misrepair, as observed for breast cancer (see Discussion). Nevertheless, this transversion pattern is most likely due to *APOBEC3B* enzymatic activity, as these events most frequently occurred within *APOBEC3B*-preferred 5'TC motifs (**Fig. 2.5D**). The rarity of transversion mutation events at 5'TCG sites may be due to a natural scarcity of CpG dinucleotides in the human genome (in comparison to other dinucleotides) and/or to the lower activity of *APOBEC3B* on 5-methyl-cytosine substrates in comparison to non-methylated cytosines [by analogy to the closely related enzyme *APOBEC3A* (42,96)]. Similar results were evident in the subset of genomic mutations confirmed by RNA sequencing (**Fig. 2.5E-H**). These mutation data are consistent with a model in which *APOBEC3B* catalyzed C-to-U genomic DNA deamination events are converted by uracil DNA glycosylase into abasic sites, which template the misinsertion of T or C through error-prone DNA synthesis and ultimately yield C-to-A or C-to-G transversions (after at least one round of DNA replication or repair; model in **Fig. 2.6** discussed further below).

DISCUSSION

In this study, we have shown that *APOBEC3B* expression levels vary widely in ovarian cancer cell lines and clinical samples and are, in a substantial proportion of

samples, higher than those in OSE lines, FTE cultures, or normal ovarian tissues. Knockdown experiments established that APOBEC3B is the only detectable source of DNA cytosine deaminase activity in nuclear extracts from multiple ovarian cancer cell lines. Microscopy images showed that epitope tagged APOBEC3B is predominantly nuclear, in full agreement with subcellular fractionation and activity studies of endogenous APOBEC3B. Biochemical experiments revealed the intrinsic cytosine deamination preferences for the catalytic domain of APOBEC3B and, interestingly, the preferred motif, 5'TC, corresponds to the most abundant sites of C-to-A or C-to-G transversion mutations observed in whole-genome sequencing of early-stage serous ovarian cancer genomic DNA. Importantly, *APOBEC3B* expression levels correlated with mutational load in these tumors, suggesting a potential role for this enzyme in generating mutagenic lesions in ovarian cancer.

A unique finding here is the significant correlation between *APOBEC3B* expression levels, *in vitro* APOBEC3B deamination preferences, and the cytosine transversion signatures in early-stage ovarian cancers. In breast cancer, we recently reported a correlation between endogenous *APOBEC3B* expression and transition mutations at C/G base pairs, which can be easily explained by replication past uracil lesions [Fig. 2.6B, (23)]. Concordant results were observed when APOBEC3B was over-expressed exogenously in HEK293 cells (23,29). In contrast, the C-to-A and C-to-G transversions that predominate here are more complicated outcomes of an initiating genomic C-to-U lesion. The presence of these mutational events in ovarian cancer strongly suggests a model in which genomic uracils are converted by uracil DNA glycosylase (UNG) into abasic sites, which in turn become substrates for error-prone translesion DNA synthesis (TLS; Fig. 2.6D). Several TLS DNA polymerases are strong candidates for such a role in generating transversion mutations downstream of cytosine

deamination, including REV1, which elicits a strong preference for pyrimidine insertion opposite an abasic lesion (97). Indeed, such a model is supported by recent studies in yeast, which showed that both UNG and REV1 proteins are required for heterologous expression of human AID/APOBEC3 proteins to cause transversion mutations (28). Somatic hypermutation of immunoglobulin gene variable regions initiated by AID-dependent C-to-U deamination events also provides precedent that enzyme-catalyzed uracil lesions can result in all six types of base substitutions (33,52). In particular, in mouse models, the AID-induced C-to-A and C-to-G events are largely dependent upon the uracil excision enzyme UNG2 and most likely involve TLS polymerases (33,52).

The transversions observed here in early-stage ovarian cancers in an APOBEC3B preferred dinucleotide context raises many additional questions for future studies, including identifying the causal TLS polymerase (since humans have many more than yeast), explaining the differential processing of APOBEC3B dependent lesions in different tumor types (*e.g.*, breast vs. ovary), and addressing whether other mutagenic outcomes may also be APOBEC3B-dependent. For instance, incomplete repair of even a single uracil lesion can lead to a nicked DNA strand and, together with DNA replication (or even local synthesis), result in double-strand breaks that, in turn, are known to precipitate larger scale chromosomal aberrations such as insertions, deletions, duplications, and translocations (**Fig. 2.6E**). Thus, the elevated APOBEC3B expression documented here might also contribute to some of the larger-scale genomic alterations that are characteristic of many advanced serous ovarian tumors (83). Another critical point to address in future studies is assessing the effect of APOBEC3B expression on clinical outcomes, such as overall and progression-free survival, response to therapy, and rate of recurrence. To do this, large cohorts of clinical specimens with well-documented patient histories will need to be examined.

Recently, three separate analyses of large data collections examined the relationship between mutation pattern, mutation load, and *APOBEC* expression across multiple tumor types, including ovarian cancer (13,21,22). While these analyses showed evidence for *APOBEC*-driven mutagenesis in multiple tumor types, none focused on ovarian cancer. This may be due to the fact that ovarian cancer has more modest *APOBEC3B* expression levels and mutation loads in comparison to some of these other cancers. The present study is the first to focus on ovarian cancer and differs from these recent reports in many ways: i) we used specific RT-qPCR assays to profile *APOBEC3B* in ovarian cancer cell lines and tissues; ii) we performed experiments to show that *APOBEC3B* is active in the nuclear compartment of ovarian cancer cell lines; iii) we studied the relationship between *APOBEC3B* expression and mutation burden among individual ovarian cancers rather than across tumor types; and iv) we examined mutation burden using newly available early stage ovarian cancer whole genome sequences. The results shown here suggest that these prior studies may have been limited by both the specificity of the techniques used to measure gene expression and the limitations of exomic as opposed to whole genome sequencing. Our work also emphasizes the importance of in-depth studies of specific tumor types that may be overlooked by global analyses.

MATERIALS AND METHODS

Cell lines

A2780, IGROV-1, OVCAR3, OVCAR5, OVCAR8, OV17, OV167, OV177, OV202, PEO1, PEO4, and SKOV3IP were obtained from the Mayo Clinic ovarian cell line repository. SKOV3, ES2, and TOV-21G were provided by Dr. Martina Bazarro (University of Minnesota, Twin Cities). RNA from IMCC3, 1816-686, 1816-575, IOSE-

VAN, MA148, CAOV3, OVCA429, HEY, and OVCA433 was provided by Dr. Amy Skubitz (University of Minnesota, Twin Cities) and RNA from OSEts-hTERT was obtained from the Mayo Clinic. Normal fallopian tube epithelial lines were derived by culture of epithelial cells recovered from fimbria (resected at the University of Washington for non-neoplastic indications in accordance with IRB-approved protocol 08#27077). The growth conditions for each of the cell lines are as follows. PEO1 and PEO4 cells were grown in DMEM containing 10% FBS, a 1:250 dilution of nonessential amino acids and 10 µg/mL insulin. OVCAR3 and A2780 were grown in RPMI containing 10% FBS and 10 µg/mL insulin. SKOV3IP and IGROV-1 were grown in McCoy's 5A containing 10% FBS. OVCAR5 and OVCAR8 were grown in RPMI containing 10% FBS. SKOV3, ES2, and TOV-21G were grown in DMEM containing 10% FBS. OV202, OV177, OV17 and OV167 were grown in EMEM containing 20% FBS, as described (98). All fallopian tube epithelial lines were grown in MEM (Cambrex) containing 1% fetal bovine serum, as described (92). All cell lines were grown at 37°C in the presence of 5% carbon dioxide.

APOBEC expression profiling of cell lines

Since specific antibodies for APOBEC3B are not yet available, RT-qPCR was used for mRNA quantification as described (23,40,44). RNA was isolated from 1 - 5 x 10⁶ cells for each cell line using the RNeasy Mini Kit (Qiagen, cat # 74106). cDNA was prepared using random hexamers (IDT), dNTPs (Roche, cat # 11277049001), and Transcriptor Reverse Transcriptase (Roche, cat # 03531287001). qPCR was performed using 2x Probes Master Mix (Roche, cat # 04887301001). All primer and probe combinations are listed in **Table 2.S2**.

Microscopy

For the OVCAR5 cell line, 1×10^6 cells were plated in two wells of a 6-well plate. 24 hours after plating the cells were either transfected with an expression construct encoding APOBEC3B-GFP or APOBEC3B-HA using TransIT LTI (Mirus, cat # MIR 2306). For A2780 and IGROV-1, 2.5×10^6 cells were nucleofected with 2 μ g of each expression construct using the Ingenio Nucleofector Solution (Mirus, cat # MIR 50114) and a Nucleofector II set to the X-001 program. Cells were then immediately plated into 6 well plates. 6×10^4 cells were transferred to a 4 well chamber slide for imaging 24 hours after transfection. Imaging was performed using a DeltaVision microscope at 60X magnification.

***APOBEC3B* knockdown experiments**

Knockdowns were done using pLKO.1-based lentiviral vectors and techniques reported previously (23). Transduced cells were selected with 1 μ g/ml puromycin for 1 week before being harvested for fractionation. APOBEC3B knockdown was confirmed by RT-qPCR, as above.

Cell line fractionation

Fractionation was performed as described (23). 1×10^7 cells were incubated in a 500 μ L of hypotonic solution containing 10 mM Hepes, 10 mM KCl, 1.5 mM MgCl₂, 1 mM DTT, protease inhibitors for 30 min at 4°C. The plasma membrane was ruptured by passing the cell suspension through a 28-gauge needle 4 times and nuclei were pelleted by centrifugation for 1 min at 600 x g. The supernatant was saved as the cytoplasmic fraction. The pelleted nuclei were lysed in 500 μ L GST lysis buffer containing 25 mM HEPES, 10% glycerol, 150 mM NaCl, 0.5% Triton X-100, and 1 mM EDTA, and

sonicated to create the nuclear fraction. Fractionation efficiency was determined by immunoblot. 10 μ L of a 1:10 dilution of each fraction was loaded into a 12% polyacrylamide gel and anti-tubulin (Covance, cat # MMS-407R) and anti-histone H3 (Abcam, cat # ab1791) antibodies were used to detect the cytoplasmic and nuclear fractions, respectively.

Fluorescence-based DNA deaminase assays

Fluorescence-based DNA deaminase assays were performed as described (23). This assay uses fluorescently tagged oligonucleotides with the following sequence, 5'-AAATNCNAATAGATAATGTGA -3', where N represent a T, C, G, or A. Each oligonucleotide is tagged with a fluorescein fluorophore at the 5' end and a TAMRA quencher at the 3' end. 10 pmol of oligonucleotide were incubated with 0-20 μ L of protein extract, 0.02 units of uracil DNA glycosylase (UDG; New England Biolabs), 15 μ L of 50 mM Tris-Cl (pH 7.4) and 10 mM EDTA in Nunc 384-well black plates for 2 hours at 37°C. The reactions were then treated with 100 mM NaOH at 37°C for 30 min to break the DNA back bone at abasic sites. 3 μ L of 4 N HCl and 37 μ L of 2 M Tris-Cl (pH 7.9) was then added to neutralize reactions. Finally, fluorescence was quantified using a spectrophotometer with excitation at 490 nm and emission at 520 nm.

APOBEC3B catalytic domain biochemistry

The catalytic domain of APOBEC3B (residues 195-382) was purified from HEK293 cells using a C-terminal myc-His₆ epitope tag and standard Ni-NTA purification procedures (23). Deamination reactions were performed at 37°C using 400-600 nM substrate, 10 nM purified APOBEC3B, and 0.025 U/rxn UDG for the given incubation times. Reactions were treated with 100 mM NaOH at 95°C for 10 min to achieve

complete backbone breakage. The reactions were then run on 15 or 20% TBE-urea gels to separate substrate from product. Gels were scanned using a FujiFilm Image Reader FLA-500 and densitometry was performed using ImageGauge (FujiFilm).

Analysis of APOBEC expression in clinical samples (Tables 2.S3, 2.S4, and 2.S5)

Review of H & E stained slides by a gynecological pathologist prior to both banking and analysis was performed on all samples. This ensured that the normal samples were tumor free and that the tumor samples contained >70% carcinoma cells. Snap frozen cancers were cryopreserved in OCT medium at -80°C. Cryostat sections were cut into TRIZol (Invitrogen, cat # 15596-026). TRIZol-based RNA extractions were performed in the following manner. After tubes containing cryosectioned tissue and TRIZol were brought to 20°C and mixed with 0.2 mL of chloroform/mL TRIZol used, samples were sedimented at 12,000 x g for 15 min at 4°C. RNA was recovered from the aqueous phase by adding 0.5 mL of isopropanol/mL TRIZol, incubating samples at 20°C for 10 min, and sedimenting the precipitate at 12000 x g for 10 min at 4°C. After the pellet was washed with 75% ethanol, recovered by sedimentation and air dried, RNA was resuspended in 30 µL RNase-free water. cDNA synthesis and RT-qPCR were performed using the same methods as described above (Mayo Clinic IRB#12-000095).

Microarray data analyses

After downloading the raw intensity microarray expression data for 581 ovarian tumors and 8 unmatched normal ovarian tissues from TCGA, the CEL files were analyzed using the MAS5 algorithm (510K FDA approved; standard settings) and the library for the HT-HG-U133A microarray chip provided by the Expression Console Software (Affymetrix). Statistical significance was assessed using two independent

methods based on Mann-Whitney derived p-values and fold-change in gene expression. First, the Mann-Whitney U test was used to derive p-values for non-parametric variables. Since the HT-HG-U133A chip has 7 probe sets targeting the *APOBEC3* genes (A, B, C, F/G, F, G, G) and 22 probe sets that target the 10 control genes used in this study [*TBP* (3), *GAPDH* (3), *TRAP1* (2), *FPGS* (1), *DECR1* (1), *UBC* (2), *TXN* (2), *B2M* (2), *FARP1* (2), and *EEF1A1* (4)], a Bonferroni correction was also applied with significance level set to $\alpha = 0.00172$. Exact probability was used for all Mann-Whitney U tests because none of the non-parametric variables had any sets of ties (a subject from one group having the same expression value as a subject from the other group). Second, fold change (FC) was used to compare expression values in tumor versus normal samples. FC was defined as the mean expression value of the tumor tissue samples over the mean expression value of the normal tissue samples and deemed significant if greater than 2-fold. Therefore, in order for a gene variable to be deemed statistically significant, it had to have $p < 0.00172$ and $FC \geq 2.0$ or ≤ 0.5 . **Table 2.S6** shows the statistical results of all *APOBEC3* genes and all control genes.

Genomic sequencing and re-sequencing

Whole genome and RNA sequencing was applied to previously banked low-stage, high-grade ovarian carcinomas (Mayo Clinic IRB#08-008535). After review of H & E stained slides by a gynecological pathologist, tumor and germline DNA was extracted using Genra Puregene Tissue Kit (Qiagen, cat # 158622) and sequenced on the Illumina GAIIIX with 40X average coverage. Reads were aligned with BWA (99) and realigned around insertions/deletions using the GATK (100). Somatic variants were called using SomaticSniper 1.0 (101), requiring that variants have a somatic score of at least 40 and that variants have at least 2 unique reads containing the mutant allele. To

filter out false positives from low germline coverage, we required that variants not overlap position of SNPs in dbSNP (102) or the 1000 Genomes Project (103) with minor allele frequency of at least 1% (as long as these variants are not annotated as mutations in dbSNP). RNA sequencing data were aligned to hg19 using TopHat (104). We tested our somatic mutation calling by looking for evidence in the RNA. On average, 71% (\pm 13%) of the somatic mutations were supported with at least one read containing the sequence variant. In addition, we performed resequencing of *TP53* by Sanger sequencing (105) and targeted capture sequencing in a subset of tumors and normal samples (84) to confirm *TP53* mutation status and validate a somatic *BRCA2* mutation in one tumor that had been identified in whole genome sequences. All patients had provided prior written consent for the banking and subsequent research on their specimens, including genomic studies (Mayo Clinic IRB#08-005749).

Statistical analyses

Statistically significant differences between normal and tumor tissue, high- and low-grade, and early and late stage were determined using the Wilcoxon Rank Sum test. The Wilcoxon Signed Rank test was used to analyze matched normal and tumor tissues. Association between *APOBEC3B* expression levels and mutation counts were examined graphically, with significance determined using Spearman's correlation coefficients and p-values. Best-fit lines for mutation correlations were estimated using linear regression (Graphpad Prism 5.0).

ADDITIONAL CONTRIBUTIONS

We thank M. Bazarro for cell lines, A. Skubitz for cell line RNA, Paula Schneider for isolating tumor RNA, and several lab members for helpful discussions.

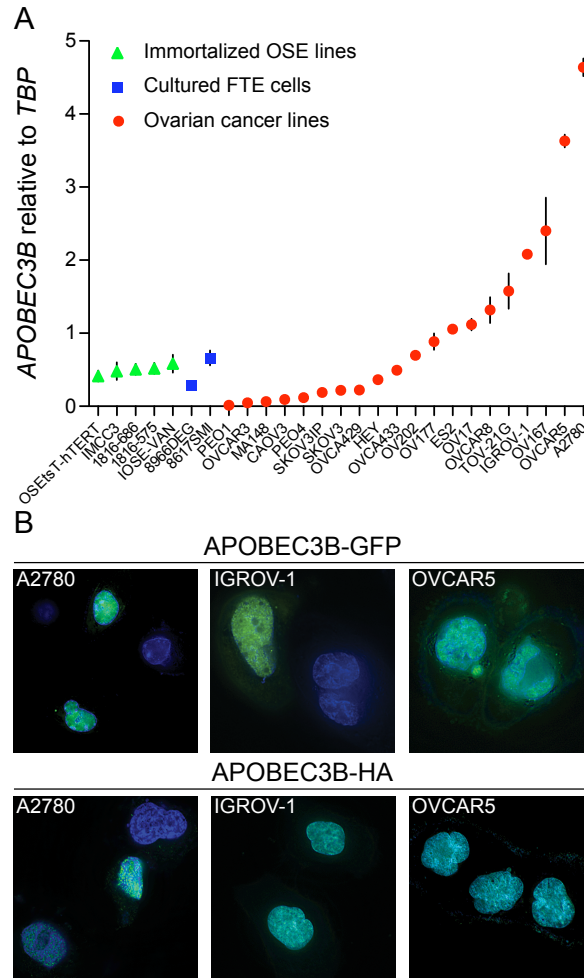


Figure 2.1 *APOBEC3B* expression and localization in ovarian cancer cell lines.

(A) *APOBEC3B* mRNA levels in the indicated ovarian cancer cell lines (red circles, n=18 with sister pairs PEO1/4 and SKOV3/IP counted only once), fallopian tube epithelial (FTE) cells (blue squares, n=2), and immortalized ovarian surface epithelium (OSE) cell lines (green triangles, n=5). Each data point is the mean *APOBEC3B* level of 3 independent RT-qPCR reactions presented relative to mRNA levels of the constitutive housekeeping gene *TBP* (error bars = 1 SD).

(B) GFP and HA-tagged *APOBEC3B* (green) co-localize with Hoescht-stained nuclear DNA (blue) in the indicated ovarian cancer cell lines. All images taken at 60X magnification.

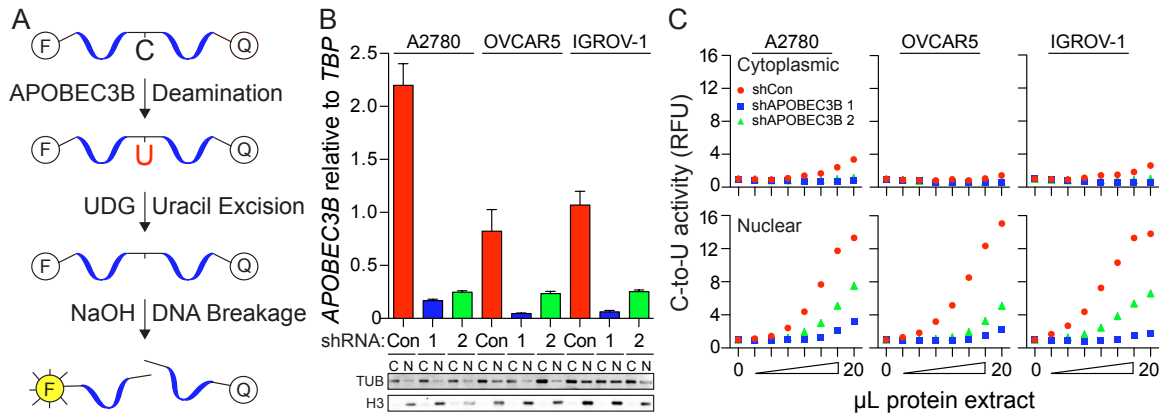


Figure 2.2 Endogenous APOBEC3B activity in ovarian cancer cell lines.

(A) A schematic of the fluorescence-based DNA cytosine deamination assay. The single-stranded DNA substrate has a target cytosine, 5' fluorescent group (F), and 3' fluorescence-quenching group (Q). Deamination and uracil excision create an abasic site, hydroxide breaks the DNA backbone, and the fluorescent group escapes quenching.

(B) *APOBEC3B* RT-qPCR data from the indicated ovarian cancer cell lines expressing control shRNA (Con) or one of two shRNAs specific to *APOBEC3B* (1 or 2) (n=3; mean and SD shown for each condition). Fractionation is confirmed by immunoblots of the cytoplasmic (C) and nuclear (N) protein fractions from each condition (TUB=anti-tubulin; H3=anti-histone H3).

(C) DNA C-to-U deaminase activity elicited by cytoplasmic (upper panels) and nuclear (lower panels) protein extracts from the indicated cell lines. These experiments used a single-stranded DNA substrate with a single 5'-TC deamination target. Symbol colors match the knockdown bar colors in panel B.

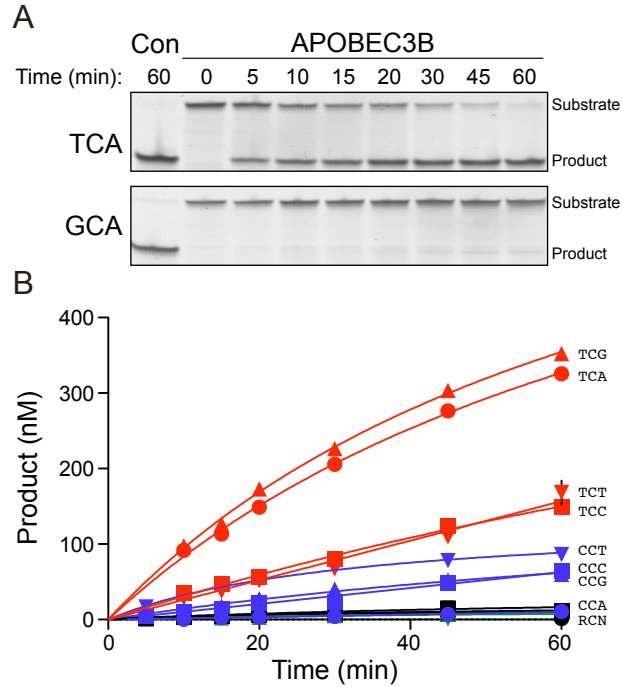


Figure 2.3 Intrinsic DNA deamination preferences of recombinant APOBEC3B.

(A) Representative gel images of APOBEC3B catalytic domain DNA deamination products accumulating over the indicated reaction times for the 5'-TCA (most preferred) and 5'-GCA (least preferred) trinucleotide contexts. Complete deamination by APOBEC3A is shown as a positive control (Con).

(B) APOBEC3B catalytic domain deamination kinetics using 5'-TCN, CCN, GCN, and ACN single-stranded DNA substrates (n=16 reaction conditions done each in triplicate; mean values are shown with SD smaller than symbols in all but one instance). Reactions with 5'-RCN substrates had indistinguishably low activity (R = A or G).

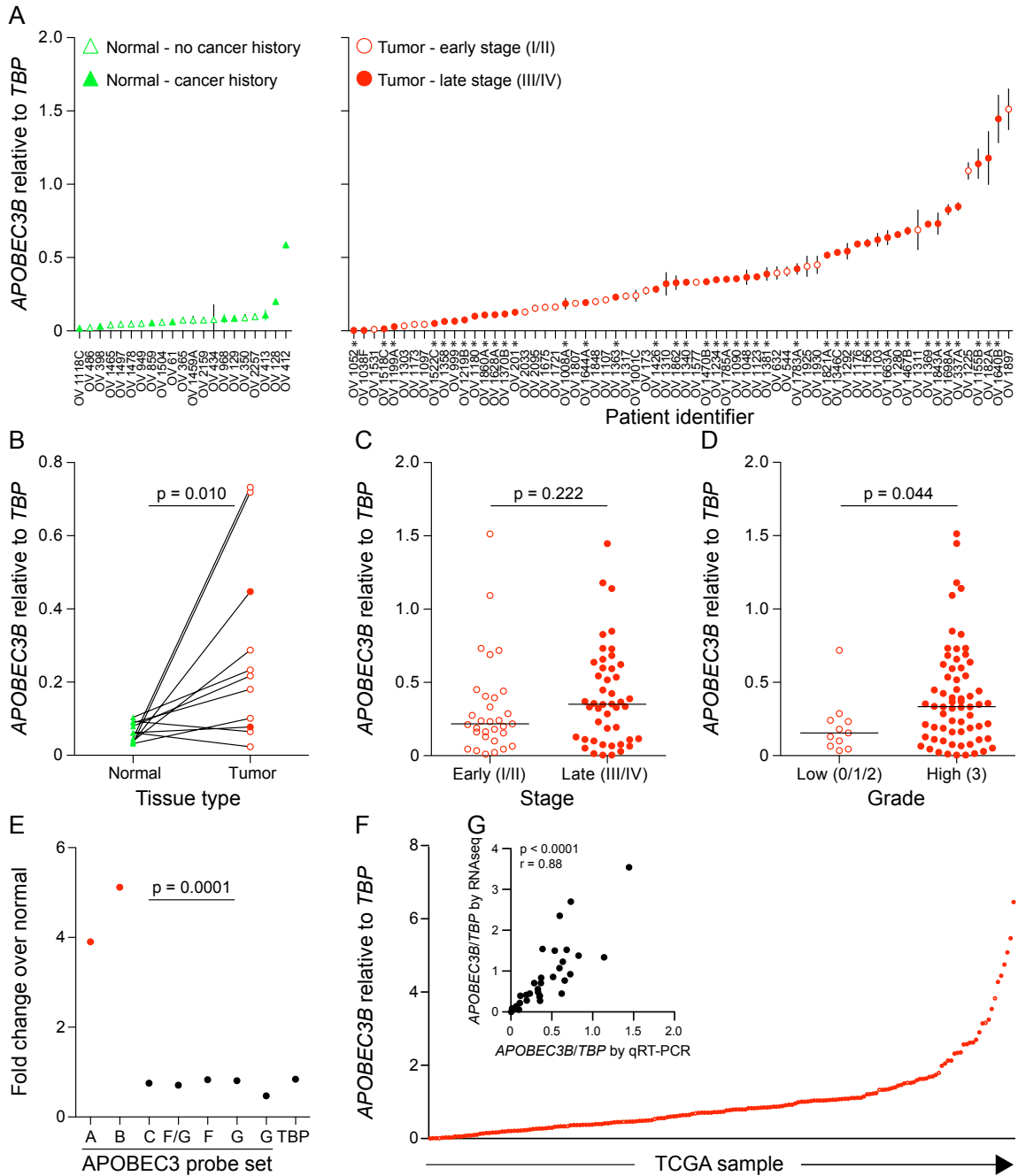


Figure 2.4 *APOBEC3B* expression in ovarian tumors.

(A) *APOBEC3B* levels in the indicated normal (green triangles; n=21) and unmatched cancerous (red circles; n=66) ovarian tissues. Cancer history is indicated by open (no history) or filled green symbols (some history; see **Tables 2.S2** and **2.S4** for additional patient information). Tumor stage is indicated by open (early-stage) or closed (late-

stage) red symbols. Data points in each category are arranged from lowest to highest *APOBEC3B* expression level. Each point reports the mean *APOBEC3B* level of 3 independent RT-qPCR reactions presented relative to mRNA levels of the constitutive housekeeping gene *TBP* (error bars = 1 SD). Asterisks indicate samples that are also in TCGA data sets with the alternative identifiers listed in **Table 2.S5**.

(B) Dot plot showing *APOBEC3B* expression in matched normal and tumor specimens (n=11 unrelated to specimens in panel A). Lines connect matched specimens. P-values were calculated using the Signed rank test.

(C, D) Dot plots showing the relationship between *APOBEC3B* levels (as in panel A) and tumor stage (early vs. late) or tumor grade (low vs. high). P-values were calculated using the Wilcoxon rank sum test.

(E) Relative microarray *APOBEC3* expression levels based on data from the indicated probe sets. A false positive *APOBEC3A* signal is expected due to high nucleotide identity with *APOBEC3B* and cross-hybridizing probe sets [see supplement to (23)].

(F) *APOBEC3B* quantification by RNA sequencing of 190 TCGA ovarian tumors. *APOBEC3B* mRNA levels are presented relative to those of the housekeeping gene *TBP*, and plotted from lowest to highest. No normal tissues were available for comparison.

(G) A 2-dimensional plot comparing RT-qPCR and RNA sequencing data for tumor samples common to each analysis (n=32). P-values calculated using Spearman's correlation.

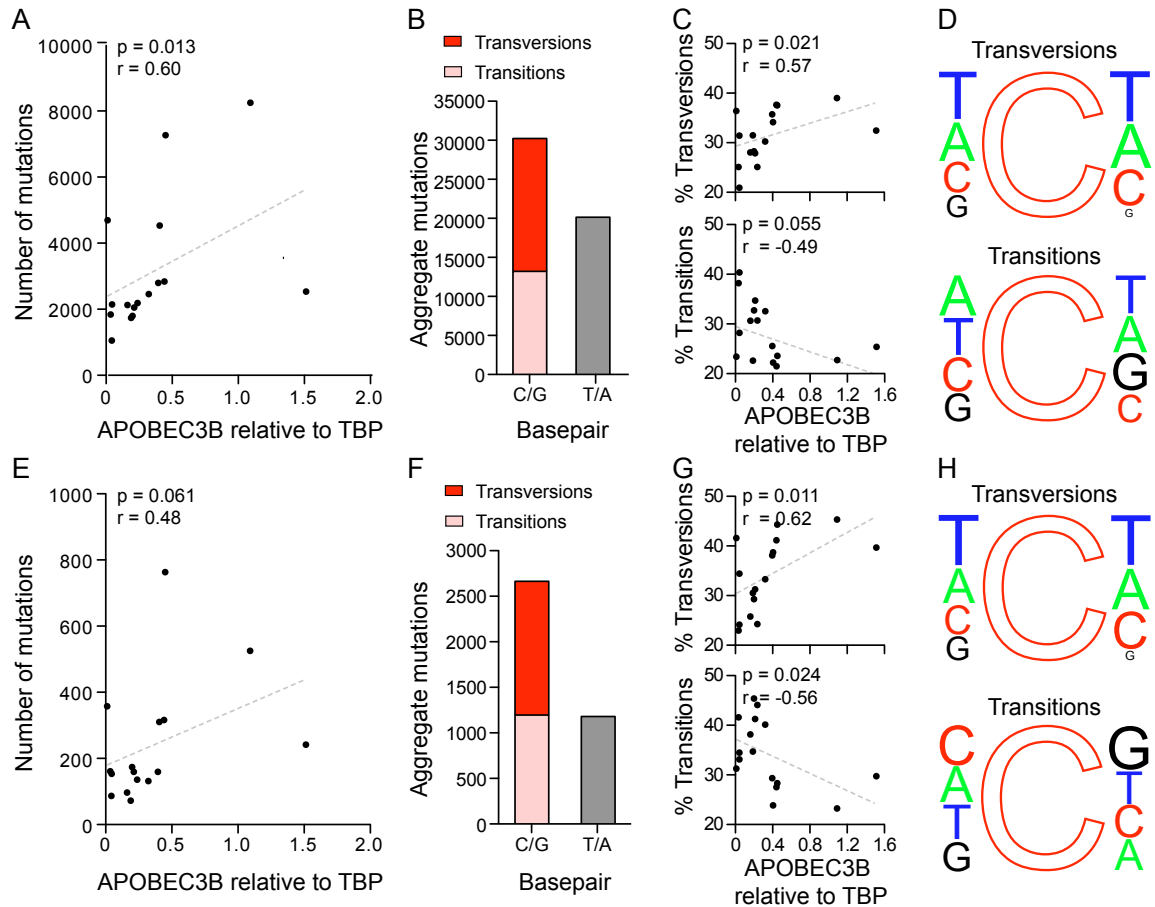


Figure 2.5 Ovarian cancer genomic mutation patterns.

(A) Correlation between *APOBEC3B* expression and total mutation loads in whole genome sequences of 16 early-stage serous ovarian carcinomas (**Table 2.S4**) assessed using the Spearman's correlation.

(B) Grouped analysis of whole genome mutation types in all 16 cancers.

(C) Correlation between *APOBEC3B* expression levels and mutation type at C/G base pairs in whole genome sequences assessed using Spearman's correlation.

(D) Trinucleotide context of the mutated C for transversions (top) and transitions (bottom) in whole genome sequences (16,986 transversions and 13,232 transitions).

(E-H) As above for A-D, except these analyses were done using RNAseq-confirmed

mutations from the same 16 early-stage serous ovarian carcinomas (1,468 transversions and 1,198 transitions).

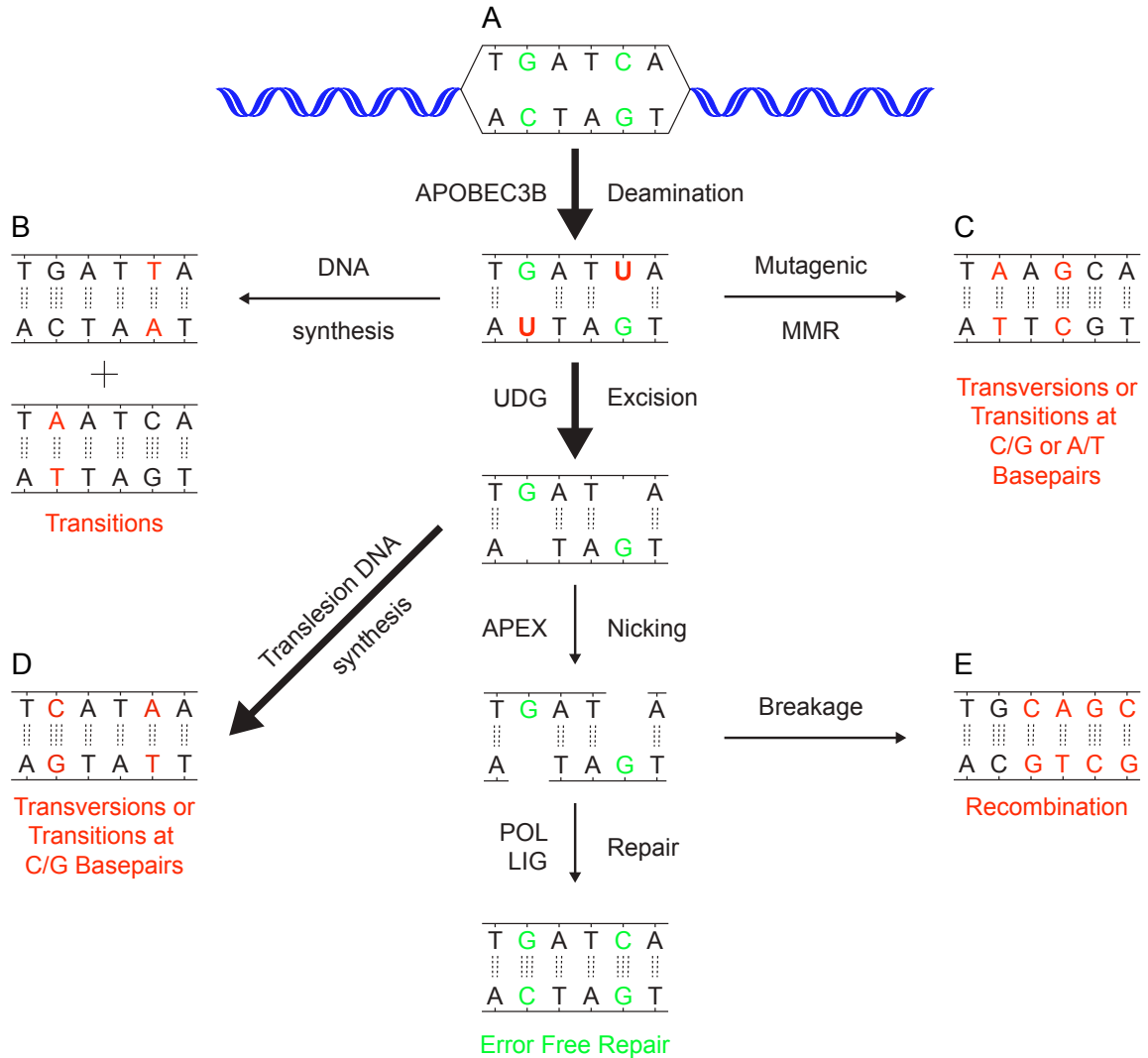


Figure 2.6 DNA deamination model for mutation in cancer.

APOBEC3B catalyzed C-to-U deamination events in single-stranded DNA can be repaired error-free (A) or processed in an error-prone manner by DNA synthesis (B, D), mutagenic repair (C) or recombination (E). This model is adapted from our prior report (23) and based on the DNA deamination mechanism for antibody gene diversification (33,52).

Table 2.S1 Cell line information

| Cell line | Derivation | Site | Subtype | Stage | Grade | <i>APOBEC3B/TBP</i> | Reference |
|--------------|------------|-----------------------|-------------|-------|-------|---------------------|-----------|
| OSEtsT-hTERT | OSE | Benign ovary | n.a. | n.a | n.a | 0.42 | (106) |
| IMCC3 | OSE | Benign ovary | n.a. | n.a | n.a | 0.48 | - |
| 1816-686 | OSE | Benign ovary | n.a. | n.a | n.a | 0.51 | (107) |
| 1816-575 | OSE | Benign ovary | n.a. | n.a | n.a | 0.52 | (107) |
| IOSE-VAN | OSE | Benign ovary | n.a. | n.a | n.a | 0.59 | - |
| 8966DEG | FTE | Benign fallopian tube | n.a. | n.a | n.a | 0.28 | (108) |
| 8617SMI | FTE | Benign fallopian tube | n.a. | n.a | n.a | 0.66 | (109) |
| PEO1* | Cancer | Ascites | Serous | - | 3 | 0.01 | (108) |
| OVCAR-3 | Cancer | Ascites | Serous | - | 3 | 0.05 | (109) |
| MA148 | Cancer | - | Serous | III | - | 0.06 | (110) |
| PEO4* | Cancer | Ascites | Serous | - | 3 | 0.09 | (108) |
| Caov-3 | Cancer | - | - | - | - | 0.12 | - |
| SKOV-3ip** | Cancer | - | - | - | - | 0.19 | - |
| SKOV-3** | Cancer | Ascites | - | - | - | 0.22 | - |
| OVCA429 | Cancer | Ascites | - | Late | High | 0.22 | (111) |
| HEY | Cancer | Peritoneal deposit | Serous | - | 2 | 0.37 | (112) |
| OVCA433 | Cancer | Ascites | Serous | Late | High | 0.49 | (111) |
| OV202 | Cancer | Primary tumor | Serous | III | 4 | 0.70 | (98) |
| OV177 | Cancer | Primary tumor | Serous | III | 4 | 0.89 | (98) |
| ES2 | Cancer | - | Clear cell | - | 3 | 1.06 | - |
| OV17 | Cancer | Primary tumor | Endometriod | III | 3 | 1.12 | (98) |
| OVCAR8 | Cancer | - | - | - | - | 1.32 | - |
| TOV-21G | Cancer | Primary tumor | Clear cell | III | 3 | 1.58 | (113) |
| IGROV-1 | Cancer | Primary tumor | Endometriod | III | 4 | 2.08 | (114) |
| OV167 | Cancer | Primary tumor | Serous | III | 3 | 2.40 | (98) |
| OVCAR-5 | Cancer | Ascites | - | - | - | 3.63 | - |
| A2780 | Cancer | - | - | - | - | 4.64 | (115) |

* and ** specify related cell lines

n.a., not applicable

-, unknown

Table 2.S2 Quantitative PCR primer and probe sequences.

| Gene symbol | mRNA NCBI accession | 5' Primer sequence | 3' Primer sequence | Probe name | Probe sequence^a |
|--------------------|----------------------------|---------------------------|---------------------------|-------------------|-----------------------------------|
| <i>APOBEC3A</i> | NM_145699 | gagaagggacaagcacatgg | tggatccatcaagtgtctgg | UPL26 | ctgggctg |
| <i>APOBEC3B</i> | NM_004900 | gaccctttggtccttcgac | gcacagccccaggagaag | UPL1 | cctggagc |
| <i>APOBEC3C</i> | NM_014508 | agcgcttcagaaaagagtgg | aagtttcggtccgatcgttg | UPL155 | ttgccttc |
| <i>APOBEC3D</i> | NM_152426 | acccaaacgtcagtcgaatc | cacatttctgctggttctc | UPL51 | ggcaggag |
| <i>APOBEC3F</i> | NM_145298 | ccgtttggacgcaaagat | ccaggatgatctggaaacactt | UPL27 | gctgcctg |
| <i>APOBEC3G</i> | NM_021822 | ccgaggacccgaaggttac | tccaacagtgctgaaattcg | UPL79 | ccaggagg |
| <i>APOBEC3H</i> | NM_181773 | agctgtggccagaagcac | cggaatgtttcggctggt | UPL21 | tggtctg |
| <i>AID</i> | NM_020661 | gactttggttatcttcgcaataaga | aggcccagtcagatgta | UPL69 | ggaggaag |
| <i>APOBEC1</i> | NM_001644 | gggaccttgtaaacagtggagt | ccagggtgggtagttgacaaaa | UPL67 | tgctggag |
| <i>APOBEC2</i> | NM_006789 | aagtagggcaactgggcttt | ggctgtacatgtcattgctgtc | UPL74 | ctgctgcc |
| <i>APOBEC4</i> | NM_203454 | ttctaacacctggaatgtgatcc | tttactgtcttctagctgcaaacc | UPL80 | cctggaga |
| <i>TBP</i> | NM_003194 | ccatgactcccatgacc | tttacaaccaagattcactgtgg | UPL51 | ggcaggag |

^a Probe sequence according to Roche UPL, which may be as shown or the reverse complement

Table 2.S3 Non-malignant tissues tested

| OV number | Tissue assayed^a | Surgical outcome | Age | Lifetime cancer^b | APOBEC3B/TBP |
|--------------------|-----------------------------------|----------------------------|------------|------------------------------------|---------------------|
| OV61 | Normal ovary | No malignancy | 54 | yes | 0.06 |
| OV128 | Normal ovary | No malignancy | 38 | yes | 0.20 |
| OV129 | Normal ovary | No malignancy | 38 | yes | 0.09 |
| OV350 | Normal ovary | No malignancy | 60 | no | 0.09 |
| OV365 | Normal ovary | No malignancy | 30 | no | 0.07 |
| OV398 | Normal ovary ^d | No residual uterine cancer | 30 | yes | 0.03 |
| OV410B | Normal ovary ^d | Stage I ovarian cancer | 39 | yes | 0.08 |
| OV412 | Normal ovary | No malignancy | 50 | yes | 0.59 |
| OV413 | Simple ovarian cyst | No malignancy | 89 | yes | 0.11 |
| OV431B | Normal ovary ^d | Stage II ovarian cancer | 62 | yes | 0.06 |
| OV434 | Normal ovary ^d | No malignancy | 46 | no | 0.08 |
| OV462B | Normal ovary ^d | Stage I ovarian cancer | 59 | yes | 0.04 |
| OV473A | Normal ovary ^d | Stage I ovarian cancer | 80 | yes | 0.05 |
| OV480B | Normal ovary ^d | Borderline ovarian cancer | 43 | yes | 0.10 |
| OV486 | Normal ovary | No malignancy | 43 | no | 0.02 |
| OV859 ^c | Normal ovary | No malignancy | 62 | yes | 0.05 |
| OV949 ^c | Normal ovary | No malignancy | 46 | no | 0.05 |
| OV968 | Normal ovary ^d | Uterine cancer | 46 | yes | 0.08 |
| OV1047D | Normal ovary ^d | Stage I ovarian cancer | 28 | yes | 0.09 |
| OV1114C | Normal ovary ^d | Stage I ovarian cancer | 81 | yes | 0.09 |
| OV1118C | Normal ovary ^d | Stage I ovarian cancer | 47 | yes | 0.02 |
| OV1172C | Normal ovary ^d | Stage I ovarian cancer | 50 | yes | 0.03 |
| OV1392E | Normal ovary ^d | Borderline ovarian cancer | 50 | yes | 0.03 |
| OV1459B | Normal ovary | No malignancy | 53 | no | 0.07 |
| OV1465B | Normal ovary | No malignancy | 53 | no | 0.04 |
| OV1478A | Normal ovary | No malignancy | 47 | no | 0.05 |
| OV1497 | Normal ovary | Benign steroid cell tumor | 67 | no | 0.04 |
| OV1504 | Normal ovary | No malignancy | 67 | no | 0.06 |
| OV2139B | Normal ovary ^d | Stage III ovarian cancer | 66 | yes | 0.04 |
| OV2159 | Normal ovary ^d | Borderline ovarian cancer | 32 | yes | 0.07 |
| OV2257 | Normal ovary ^d | Mixed malignant mullerian | 79 | yes | 0.10 |
| OV2290B | Normal ovary ^d | Stage IV peritoneal cancer | 65 | yes | 0.06 |

^a Tissues studied as normal ovaries were shown to be free of cancer by gross pathological examination and microscopic examination of H & E sections at the time of surgical resection

^b “Lifetime cancer” indicates whether the participant had cancer either before sample collection, at the same time as the analyzed tissue was collected, or after the sample was collected

^c *BRCA2* mutation carriers

^d Benign tissue tested from women with cancer at the time of sample collection

Table 2.S4 Early stage serous ovarian tumors used in sequence analyses

| OV number | Stage | Grade ^a | Age | TP53 status | Total mutations | Transversions at C/G basepairs | Transitions at C/G basepairs | <i>APOBEC3B/TBP</i> |
|---------------------|-------|--------------------|-----|--------------------|-----------------|--------------------------------|------------------------------|---------------------|
| OV544 | IC | 3 | 52 | C238F | 4533 | 1548 | 1007 | 0.41 |
| OV632 | IA | 3 | 52 | H214R | 2800 | 1001 | 716 | 0.39 |
| OV1097 | IIC | 3 | 50 | Frameshift | 2149 | 676 | 606 | 0.05 |
| OV1107 | IIB | 3 | 81 | R248Q | 2055 | 573 | 713 | 0.21 |
| OV1173 | IIC | 1 | 82 | Wildtype | 1055 | 221 | 426 | 0.04 |
| OV1225 ^b | IIC | 3 | 84 | M246V | 8249 | 3218 | 1877 | 1.09 |
| OV1303 | IIC | 2 | 79 | R273C | 1842 | 463 | 704 | 0.03 |
| OV1317 | IB | 3 | 82 | R175H | 2464 | 746 | 802 | 0.24 |
| OV1531 | IC | 3 | 71 | C242F | 2193 | 551 | 673 | 0.01 |
| OV1577 | IC | 3 | 50 | Wildtype | 4697 | 1709 | 1100 | 0.33 |
| OV1675 | IIC | 3 | 77 | R248W | 2130 | 598 | 653 | 0.16 |
| OV1807 | IA | 3 | 66 | Frameshift | 1742 | 549 | 394 | 0.19 |
| OV1848 | IIB | 3 | 78 | Frameshift | 1803 | 510 | 590 | 0.20 |
| OV1897 | IC | 3 | 60 | R196X ^c | 2537 | 823 | 644 | 1.51 |
| OV1925 | IIB | 3 | 50 | Frameshift | 2839 | 1069 | 610 | 0.44 |
| OV1930 | IIC | 3 | 54 | Frameshift | 7272 | 2731 | 1717 | 0.45 |

^a Grade according to the FIGO/WHO grading system

^b BRCA2 mutation

^c X = premature stop codon

Table 2.S5 Additional ovarian tumor specimens analyzed

| OV number | Stage^a | Grade^a | Age | Histology | TCGA ID^b | APOBEC3B/TBP |
|----------------------|--------------------------|--------------------------|------------|------------------|----------------------------|---------------------|
| OV173 | IA | 3 | 74 | Endometrioid | None | 0.28 |
| OV182A | IIIC | 3 | 74 | Serous | TCGA-25-1871 | 1.18 |
| OV201 | IIIC | 3 | 81 | Serous | TCGA-25-1877 | 0.13 |
| OV337A | IIIC | 3 | 60 | Serous | TCGA-25-1878 | 0.85 |
| OV410A ^c | IA | 3 | 39 | Endometrioid | None | 0.22 |
| OV431A ^c | IIB | 3 | 62 | Serous | None | 0.02 |
| OV462A ^c | IA | 1 | 59 | Mucinous | None | 0.29 |
| OV473B ^c | IC | 3 | 80 | Clear cell | None | 0.73 |
| OV480A ^c | IA | 0 | 43 | Mucinous | None | 0.23 |
| OV999 | IV | 3 | 42 | Serous | TCGA-25-1314 | 0.07 |
| OV1001C | IA | 1 | 41 | Mucinous | None | 0.24 |
| OV1008A | IV | 3 | 65 | Serous | TCGA-25-1313 ^d | 0.19 |
| OV1038F | IIIC | 3 | 62 | Serous | None | 0.00 |
| OV1047C ^c | IA | 2 | 28 | Endometrioid | None | 0.18 |
| OV1048 | IIIC | 3 | 55 | Serous | TCGA-25-1316 ^d | 0.37 |
| OV1052 | IIIC | 3 | 50 | Serous | TCGA-25-1315 ^d | 0.00 |
| OV1090 | IIIC | 3 | 66 | Serous | TCGA-25-1317 ^d | 0.36 |
| OV1103 | IIIC | 3 | 54 | Serous | TCGA-25-1318 ^d | 0.62 |
| OV1114B ^c | IA | 1 | 81 | Endometrioid | None | 0.06 |
| OV1123 | IIIC | 3 | 73 | Serous | TCGA-25-1319 ^d | 0.37 |
| OV1155B | IIIC | 3 | 65 | Serous | TCGA-25-1321 ^d | 1.14 |
| OV1156 | IIIC | 3 | 65 | Serous | TCGA-25-1320 ^d | 0.60 |
| OV1172B ^c | IC | 1 | 50 | Endometrioid | None | 0.72 |
| OV1176 | IV | 3 | 62 | Serous | TCGA-25-1322 ^d | 0.59 |
| OV1180 | IIIC | 3 | 38 | Serous | TCGA-25-1328 ^d | 0.10 |
| OV1199A | IIIC | 3 | 72 | Serous | TCGA-25-1323 | 0.03 |
| OV1219B | IV | 3 | 69 | Serous | TCGA-25-1312 | 0.08 |
| OV1234 | IIIC | 3 | 74 | Serous | TCGA-25-1324 ^d | 0.35 |
| OV1280 | IIIC | 3 | 61 | Serous | TCGA-25-1326 ^d | 0.66 |
| OV1292 | IV | 3 | 77 | Serous | TCGA-25-1325 | 0.54 |
| OV1310 | IIIB | 3 | 83 | Serous | None | 0.32 |
| OV1311 | IC | 3 | 82 | Clear cell | None | 0.69 |

| | | | | | | |
|----------------------|------|---|----|-----------------|---------------------------|------|
| OV1340 | IIIC | 3 | 76 | Serous | TCGA-25-1329 ^d | 0.33 |
| OV1346C | IIIC | 3 | 71 | Serous | TCGA-25-1635 ^d | 0.54 |
| OV1358 | IIIC | 3 | 75 | Serous | TCGA-25-1634 ^d | 0.07 |
| OV1363 | IIIC | 3 | 64 | Serous | TCGA-25-1633 ^d | 0.23 |
| OV1369 | IV | 3 | 68 | Serous | TCGA-25-1632 ^d | 0.73 |
| OV1370B | IIIC | 3 | 73 | Serous | TCGA-25-1631 ^d | 0.12 |
| OV1381 | IIIC | 3 | 73 | Serous | TCGA-25-1630 ^d | 0.39 |
| OV1392A ^c | IA | 0 | 50 | Serous/mucinous | None | 0.10 |
| OV1426 | IIIC | 3 | 73 | Serous | TCGA-25-1627 ^d | 0.28 |
| OV1467B | IIIC | 3 | 57 | Serous | TCGA-25-2391 ^d | 0.68 |
| OV1470B | IV | 3 | 80 | Serous | TCGA-25-2390 | 0.34 |
| OV1518C | IV | 3 | 75 | Serous | TCGA-25-2392 ^d | 0.01 |
| OV1522C | IIIC | 3 | 81 | Serous | TCGA-25-2393 ^d | 0.05 |
| OV1628A | IV | 3 | 59 | Serous | TCGA-25-2397 | 0.11 |
| OV1640B | IIIC | 3 | 71 | Serous | TCGA-25-2398 ^d | 1.45 |
| OV1644A | IIIC | 3 | 80 | Serous | TCGA-25-2399 ^d | 0.19 |
| OV1663A | IIIC | 3 | 64 | Serous | TCGA-25-2401 ^d | 0.64 |
| OV1698A | IIIC | 3 | 38 | Serous | TCGA-25-2404 ^d | 0.83 |
| OV1721 | IC | 3 | 48 | Serous | None | 0.16 |
| OV1783A | IV | 2 | 37 | Serous | TCGA-25-2408 | 0.42 |
| OV1785A | IV | 3 | 71 | Serous | TCGA-25-2409 ^d | 0.35 |
| OV1821A | IIIC | 3 | 65 | Serous | TCGA-25-1626 ^d | 0.52 |
| OV1843A | IIIC | 3 | 66 | Serous | TCGA-25-1625 ^d | 0.73 |
| OV1860A | IIIC | 3 | 60 | Serous | TCGA-25-2042 ^d | 0.11 |
| OV1862 | IV | 3 | 71 | Serous | TCGA-25-1623 ^d | 0.33 |
| OV2033 | IC | 2 | 69 | Endometrioid | None | 0.13 |
| OV2095 | IA | 2 | 63 | Mucinous | None | 0.15 |
| OV2139A ^c | IIIC | 3 | 66 | Serous | None | 0.45 |
| OV2290A ^c | IV | 3 | 65 | Serous | None | 0.08 |

^a Stage and grade were assigned at the time of original surgical resection. When frozen sections were cut for RNA extraction, an adjacent section was stained with H & E and examined to confirm the presence of >70% tumor cells

^b Samples that were also analyzed through the TCGA project are indicated with their identification numbers

^c Patients who provided both tumor tissues (listed here) and matched normal tissue (corresponding OV number in Table S3). Data are reported in Figure 4B.

^d Samples analyzed by both RT-qPCR and RNAseq

Table 2.S6 Microarray analysis of *APOBEC3* and select control gene probe sets in ovarian TCGA data

| Probe set ^a | Specificity | Cancer (mean ± SD) n=581 | Normal (mean ± SD) n=8 | P value ^b | Fold change ^c | Statistical Significance ^d |
|------------------------|-------------|--------------------------------|------------------------------|----------------------|-----------------------------|--|
| 210873_x_at | APOBEC3A | 108 ± 93.5 | 27.4 ± 28.8 | 0.00029 | 4.0 | Yes |
| 206632_s_at | APOBEC3B | 511 ± 484 | 98.7 ± 40.3 | 0.000014 | 5.2 | Yes |
| 209584_x_at | APOBEC3C | 250 ± 182 | 334 ± 134 | 0.030 | 0.75 | No |
| 214995_s_at | APOBEC3F/G | 188 ± 97.5 | 267 ± 86.5 | 0.0078 | 0.71 | No |
| 214994_at | APOBEC3F | 40.5 ± 29.1 | 48.8 ± 29.0 | 0.29 | 0.83 | No |
| 204205_at | APOBEC3G | 983 ± 725 | 1220 ± 438 | 0.088 | 0.81 | No |
| 215579_at | APOBEC3G | 23.8 ± 22.7 | 51.1 ± 31.6 | 0.0015 | 0.47 | Yes ^e |
| 203135_at | TBP | 211 ± 87.6 | 250 ± 34.3 | 0.026 | 0.84 | No |
| 216226_at | TBP | 57.8 ± 49.1 | 49.5 ± 31.1 | 0.81 | 1.2 | No |
| 209430_at | TBP | 643 ± 284 | 612 ± 107 | 0.89 | 1.1 | No |
| 212581_x_at | GAPDH | 22200 ± 7190 | 18500 ± 2900 | 0.11 | 1.2 | No |
| 213453_x_at | GAPDH | 19300 ± 5800 | 14200 ± 1280 | 0.00046 | 1.4 | No |
| 217398_x_at | GAPDH | 21600 ± 6540 | 17800 ± 2930 | 0.051 | 1.2 | No |
| 201391_at | TRAP1 | 1000 ± 475 | 1010 ± 199 | 0.49 | 0.99 | No |
| 205210_at | TRAP1 | 143 ± 57.9 | 117 ± 46.9 | 0.17 | 1.2 | No |
| 202945_at | FPGS | 130 ± 75.8 | 123 ± 105 | 0.46 | 1.1 | No |
| 202447_at | DECR1 | 1650 ± 746 | 1860 ± 435 | 0.15 | 0.89 | No |
| 211296_x_at | UBC | 20600 ± 6004 | 23700 ± 3280 | 0.017 | 0.87 | No |
| 208980_s_at | UBC | 11500 ± 2922 | 12300 ± 1820 | 0.22 | 0.93 | No |
| 208864_s_at | TXN | 4220 ± 1660 | 5300 ± 1200 | 0.022 | 0.80 | No |
| 216609_at | TXN | 492 ± 251 | 399 ± 82.9 | 0.50 | 1.2 | No |
| 216231_s_at | B2M | 18200 ± 6850 | 17000 ± 4220 | 0.59 | 1.1 | No |
| 201891_s_at | B2M | 22300 ± 7000 | 20200 ± 3830 | 0.46 | 1.1 | No |
| 201911_s_at | FARP1 | 668 ± 418 | 633 ± 145 | 0.68 | 1.1 | No |
| 201910_at | FARP1 | 434 ± 241 | 468 ± 144 | 0.33 | 0.93 | No |
| 204892_x_at | EEF1A1 | 25900 ± 9030 | 30900 ± 6130 | 0.015 | 0.84 | No |
| 213477_x_at | EEF1A1 | 27000 ± 8800 | 28300 ± 5110 | 0.22 | 0.95 | No |
| 213583_x_at | EEF1A1 | 24600 ± 7950 | 26500 ± 4800 | 0.135 | 0.93 | No |
| 213614_x_at | EEF1A1 | 28600 ± 8810 | 29900 ± 4900 | 0.22 | 0.95 | No |

^a Sequences of individual probes in each probeset are publically available at affymetrix.com

^b P values calculated using Mann Whitney t test

^c Fold change is calculated as cancer divided by normal

^d The significance level is set at: $\alpha = 0.0017$, and a gene variable is deemed statistically significant if $p < 0.0017$ and fold change ≥ 2.0 or ≤ 0.50

^e Probe set shows significantly reduced expression in cancer tissue

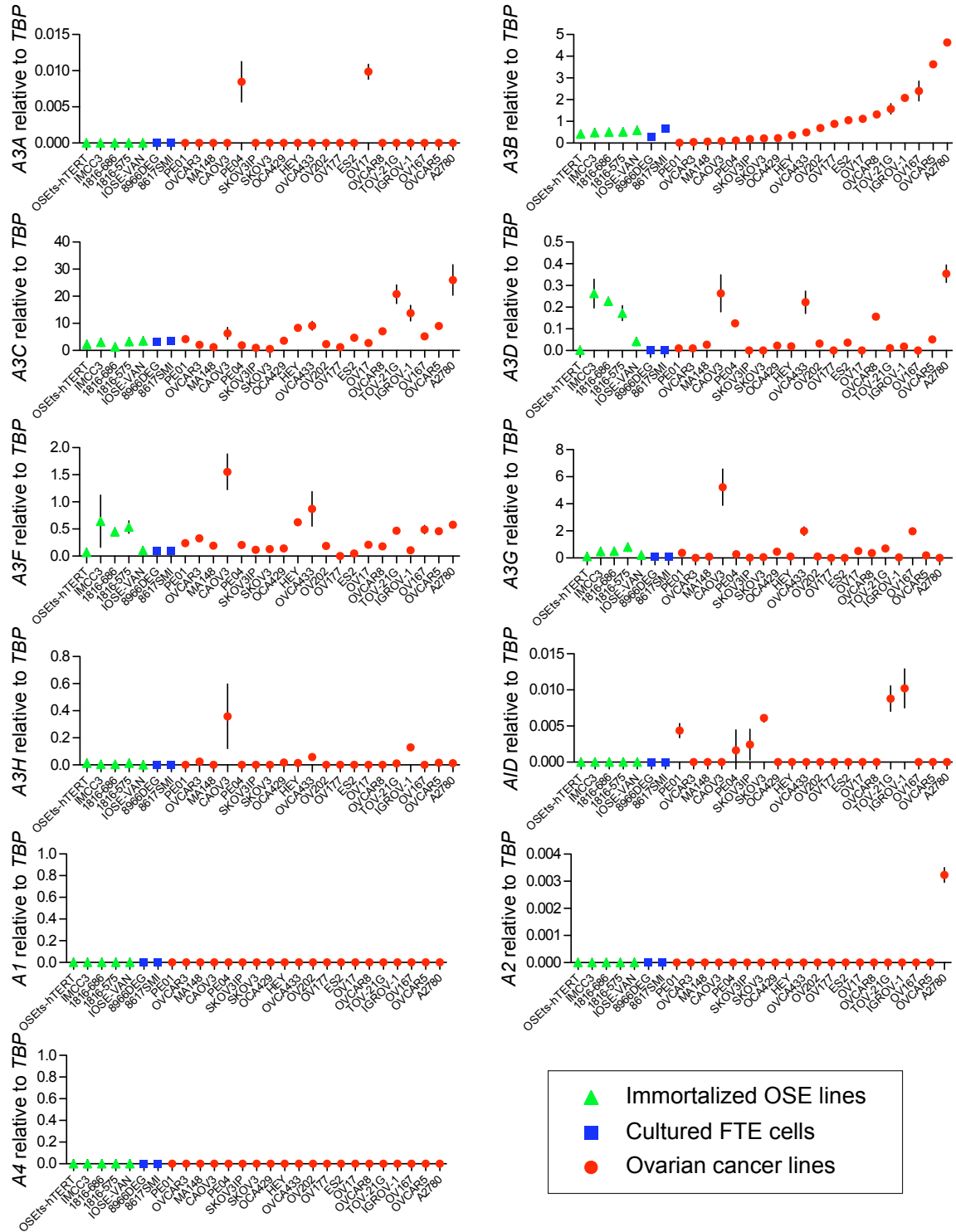


Figure 2.S1 Polynucleotide cytosine deaminase expression in ovarian cell lines.

mRNA levels of *APOBEC3A* (A3A), *APOBEC3B* (A3B), *APOBEC3C* (A3C), *APOBEC3D* (A3D), *APOBEC3F* (A3F), *APOBEC3G* (A3G), *APOBEC3H* (A3H), *Activation induced*

deaminase (AID), APOBEC1 (A1), APOBEC2 (A2), APOBEC4 (A4) in the indicated ovarian cancer cell lines (red circles, n=18 with sister pairs PEO1/4 and SKOV3/IP counted only once), fallopian tube epithelial (FTE) cells (blue squares, n=2), and immortalized ovarian surface epithelium (OSE) cell lines (green triangles, n=5). Each data point is the mean mRNA expression level of 3 independent RT-qPCR reactions presented relative to mRNA levels of the constitutive housekeeping gene *TBP* (error bars = 1 SD).

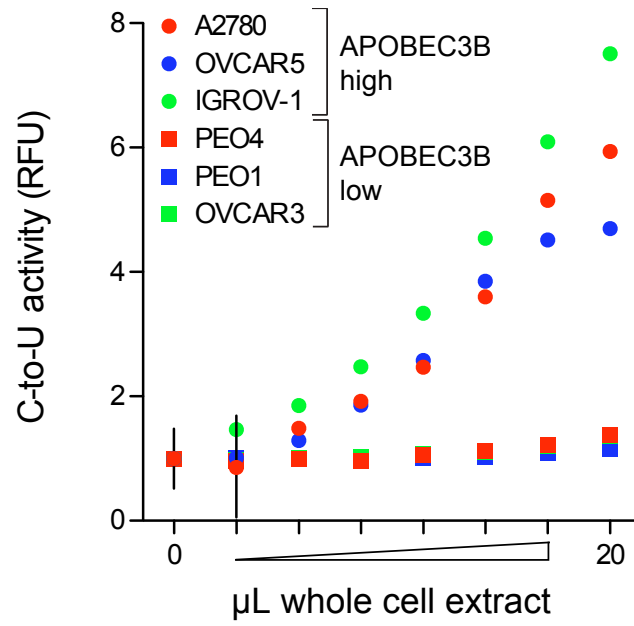


Figure 2.S2 Endogenous DNA deaminase activity in APOBEC3B high and low cell lines. DNA C-to-U deaminase activity in whole cell extracts from the indicated cell lines was measured as described, using a single-stranded DNA substrate with a 5'TC target site.

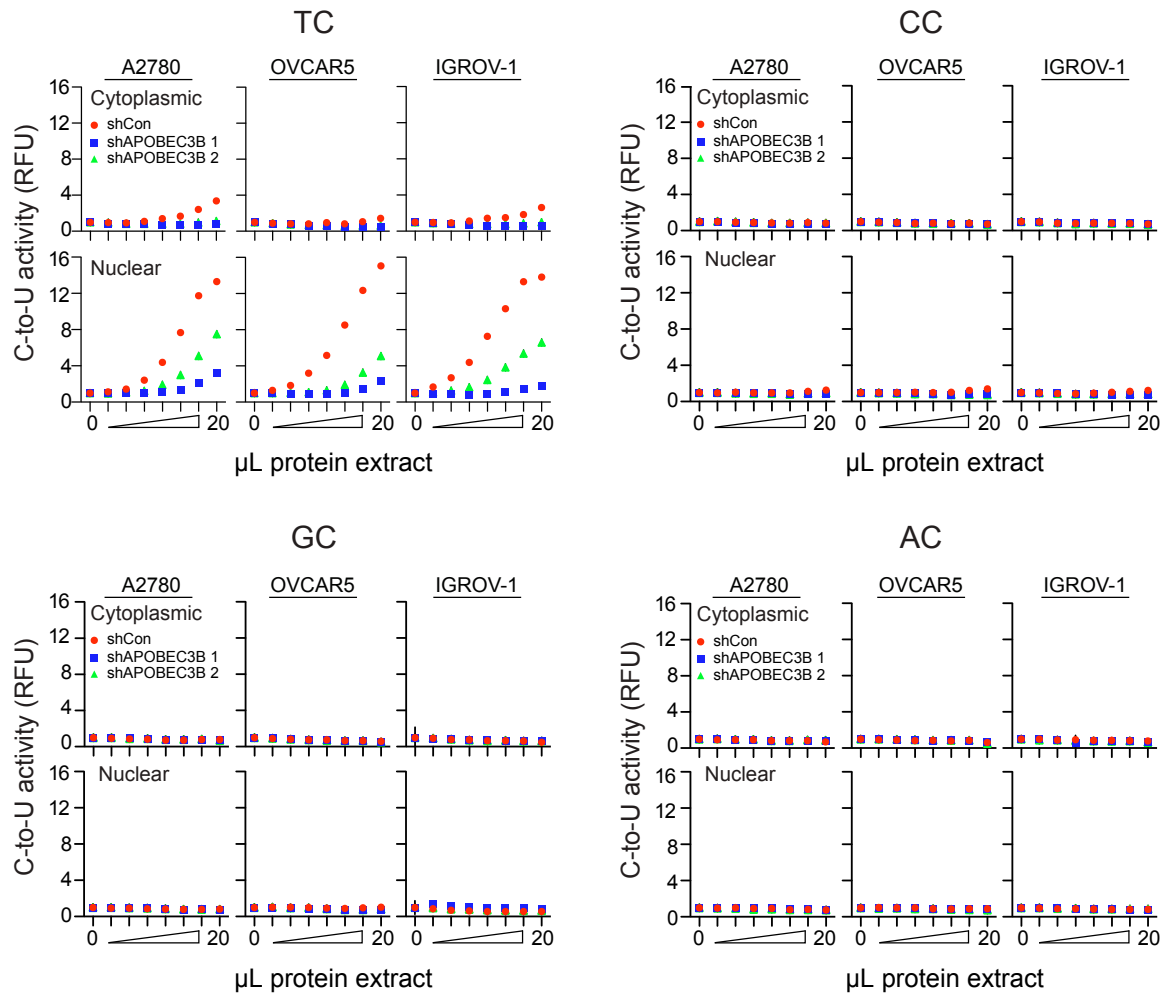


Figure 2.S3 Endogenous APOBEC3B activity on alternate dinucleotide substrates.

DNA C-to-U deaminase activity elicited by cytoplasmic (upper panels for each context) and nuclear (lower panels for each context) protein extracts from the indicated cell lines. These experiments used single-stranded DNA substrates with either 5'TC, 5'CC, 5'GC, or 5'AC dinucleotide target sites. Data in the upper panel with the 5'TC substrate are reproduced from **Fig. 2.2C** for comparison.

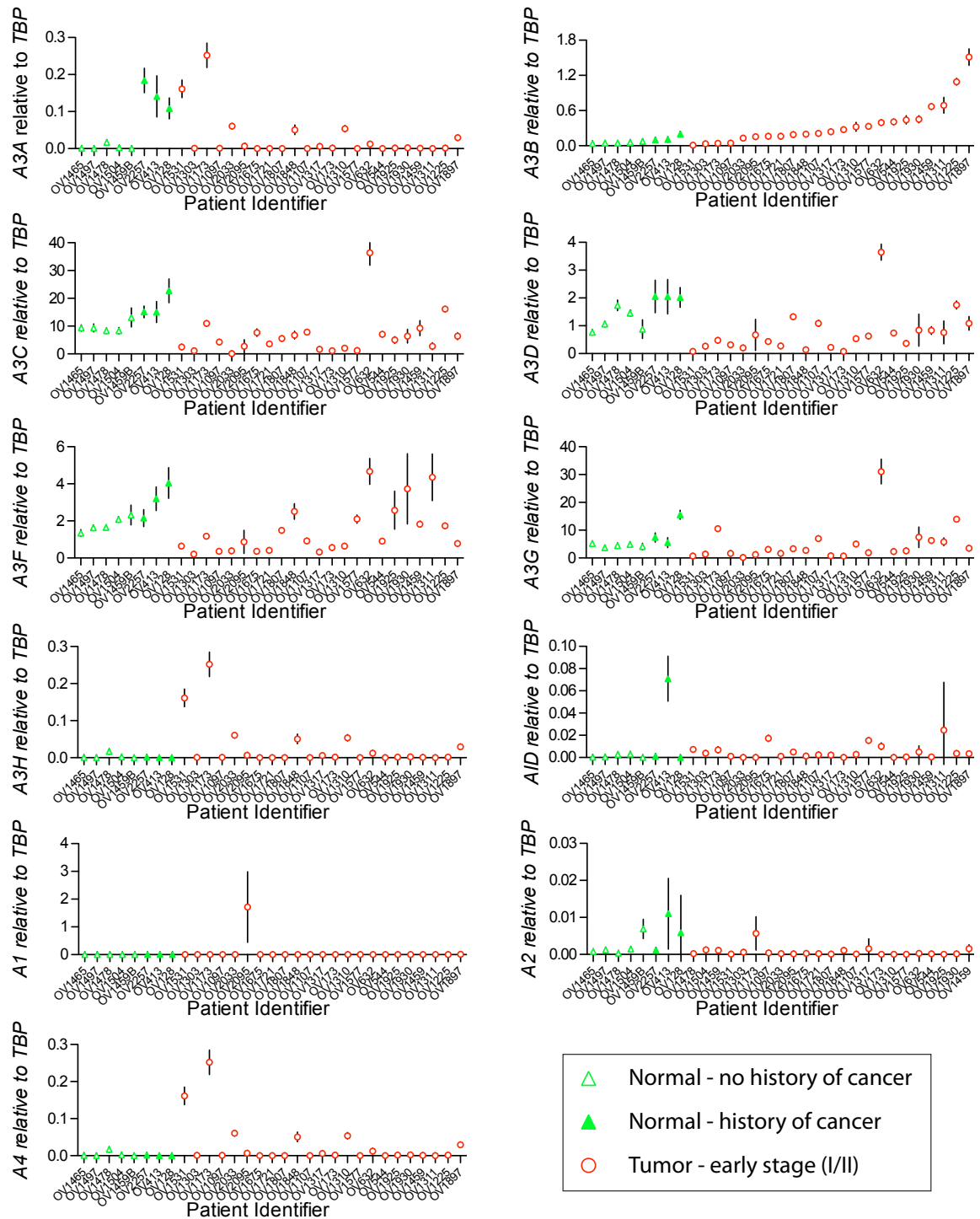


Figure 2.S4 Polynucleotide cytosine deaminase expression in ovarian primary samples. Polynucleotide cytosine deaminase mRNA levels in representative normal (green triangles; n=8) and cancerous (red circles; n=23) ovarian tissues. Cancer history is

indicated by open (no history) or filled green symbols (some history; see **Table 2.S3**, **2.S4**, and **2.S5** for additional patient information). Tumor stage is indicated by open (early-stage) or closed (late-stage) red symbols. Data points in each graph are arranged by lowest to highest *APOBEC3B* expression level (*APOBEC3B* data reproduced from **Fig. 2.4A** for comparison here). Each point reports the mean mRNA expression level of 3 independent RT-qPCR reactions presented relative to mRNA levels of the constitutive housekeeping gene *TBP* (error bars = 1 SD).

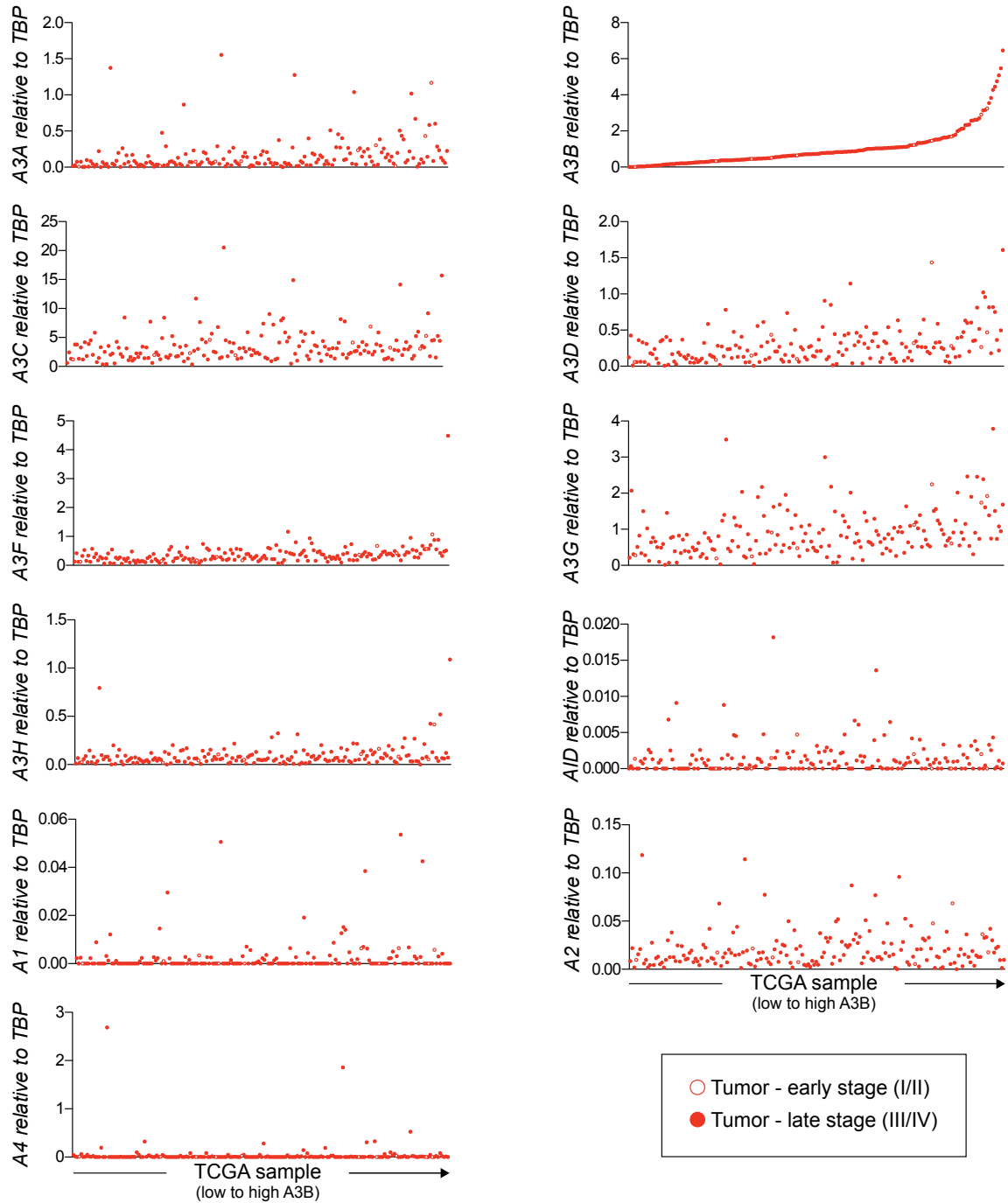


Figure 2.S5 Polynucleotide cytosine deaminase expression in ovarian TCGA samples by RNAseq.

Polynucleotide cytosine deaminase levels in all 188 TCGA ovarian primary cancer samples as measured by RNAseq analysis. Data points in each graph are arranged from

lowest to highest *APOBEC3B* expression level (*APOBEC3B* data reproduced from **Fig. 2.4F** for comparison here).

CHAPTER 3:

APOBEC3B upregulation by the PKC-NFκB pathway in multiple human cancers

Authors: Brandon Leonard,^{1,2} Jennifer L. McCann,^{1,2} Gabriel J. Starrett,^{1,2} Leah Kosyakovsky,^{1,2,3} Elizabeth M. Luengas,^{1,2} Amy M. Molan,^{1,2} Michael B. Burns,^{1,2,4} Rebecca M. McDougle,^{1,2,5} Peter J. Parker,⁶ William L. Brown,^{1,2} and Reuben S. Harris,^{1,2}

Affiliations: ¹Biochemistry, Molecular Biology and Biophysics Department, University of Minnesota, Minneapolis, MN 55455, USA. ²Masonic Cancer Center, University of Minnesota, Minneapolis, MN 55455, USA. ³Faculty of Medicine, University of British Columbia, Vancouver, BC V6T 1Z3. ⁴Department of Genetics, Cell Biology, and Development, University of Minnesota, Minneapolis, MN 55455, USA. ⁵Medical School, University of Minnesota, Minneapolis, MN 55455, USA. ⁶Protein Phosphorylation Laboratory, Cancer Research UK London Research Institute, London WC2A 3LY, UK

SUMMARY

Overexpression of the antiviral DNA cytosine deaminase APOBEC3B has been linked to somatic mutagenesis in many cancers. HPV infection accounts for APOBEC3B upregulation in cervical and head/neck cancers. However, the responsible mechanisms are unclear for non-viral malignancies. Here, we demonstrate APOBEC3B upregulation through the PKC-NFκB pathway. PKC activation by the diacylglycerol mimic PMA causes specific and dose-responsive increases in APOBEC3B mRNA, protein, and activity levels, which are strongly suppressed by PKC or NFκB inhibition. Induction correlates with RELB (but not RELA) recruitment to endogenous *APOBEC3B* implicating non-canonical NFκB signaling. Relevance to tumors is supported by PKC inhibitor-mediated APOBEC3B downregulation in multiple cancer cell lines. These data establish the first mechanistic link between a common signal transduction pathway and APOBEC3B upregulation, suggesting that existing PKC-NFκB inhibitors could be repurposed to suppress cancer mutagenesis, dampen tumor evolution, and decrease the probability of adverse outcomes such as drug resistance and metastases.

INTRODUCTION

Somatic mutations are essential for nearly every hallmark of cancer (1,116). Mutations occur when DNA damage escapes repair. Cancer genome deep sequencing studies are confirming previously known sources of mutation as well as helping to discover new ones (13-15). Established sources of mutation include ultraviolet light in skin cancer, tobacco carcinogens in lung cancer, and water-mediated deamination of methyl-cytosine as a function of age in nearly all cancers. One newly discovered source is the plant derived dietary supplement aristolochic acid, which causes A-to-T transversion mutations in liver and bladder cancers (20). A second and larger source of mutation is the APOBEC family of DNA cytosine deaminases, which cause signature C-

to-T transition and C-to-G transversion mutations in breast, head/neck, bladder, cervical, lung, and ovarian cancers (13-16,21-23,47,74,117). An additional feature of APOBEC mutagenesis is that the majority of these mutational events are dispersed throughout the genome, but an interesting minority are found in dense strand-coordinated clusters termed kataegis (14,118).

Expression profiling and functional studies independently discovered APOBEC as a major source of mutation in cancer (23,74). In particular, we demonstrated APOBEC3B upregulation in breast and ovarian cancer cell lines and primary tumors (23,74). APOBEC3B is predominantly nuclear, and knockdown experiments demonstrated that it accounts for all measurable DNA cytosine deaminase activity in cancer cell line extracts and, likewise, is also responsible for elevated levels of genomic uracil and higher mutation rates. In addition, APOBEC3B levels correlated with higher C-to-T and overall base substitution mutation loads. Importantly, the biochemical preference of recombinant APOBEC3B deduced *in vitro* closely resembles the actual cytosine mutation bias in breast cancer as well as in several of the other tumor types listed above (*i.e.*, strong bias toward 5'-TC dinucleotides).

Human cells have the potential to express up to seven distinct antiviral APOBEC3 enzymes [(31,32) and references therein]. Each enzyme has a biochemical preference for deaminating cytosines in single-stranded DNA, but activity is strongly influenced by flanking bases at the -2, -1, and +1 positions relative to the target cytosine [shown originally by (48) and elaborated by (119,120) and references therein]. APOBEC3B is the only family member clearly upregulated in the cancers listed above (16,21-23,74). HPV infection was recently shown to induce APOBEC3B expression in cell culture experiments, which helps explain APOBEC3B upregulation and mutation biases in virus-positive cervical and head/neck tumors (69,70). However, the mechanism responsible for APOBEC3B upregulation in other tumor types (*i.e.*, non-HPV cancers) is

presently unknown, but not due to obvious processes such as chromosomal translocation, gene amplification, or promoter demethylation (23).

Here, we show that the PKC-NF κ B pathway specifically induces APOBEC3B expression, providing the first mechanistic link between a major signal transduction pathway and cancer mutagenesis. A variety of pharmacological approaches, gene knockdown, RNA sequencing, and chromatin immunoprecipitation experiments were used to demonstrate direct transcriptional upregulation of APOBEC3B by a signal transduction pathway involving the classical PKC isoform PKC α and activation of the non-canonical NF κ B transcription factor RELB. We also demonstrate that PKC inhibition leads to APOBEC3B downregulation in a variety of cancer cell lines suggesting that existing compounds can be repurposed for a new therapeutic strategy centered upon controlling mutagenesis in cancer.

RESULTS

Specific upregulation of APOBEC3B by PMA

The first reported cDNAs representing *APOBEC3A* and/or *APOBEC3B* were cloned from primary human keratinocytes treated with phorbol-myristic acid (PMA) (75). PMA is a diacylglycerol (DAG) analog known to trigger protein kinase C (PKC) signaling as well as activate a number of other cellular processes [(121-124) and references therein]. Due to high levels of homology between *APOBEC3A* and *APOBEC3B* (92%) including long stretches of perfect identity, it is not clear which gene may have been actually represented by these original cDNAs. Moreover, the primary tissues used in this original study consisted of multiple epithelial cell types and most likely also infiltrating immune cells making it unclear where the cDNAs may have originated. These distinctions are important given the fact that *APOBEC3A* (not *APOBEC3B*) is upregulated >100-fold by interferon- α treatment of myeloid cell types (40,67), and that

APOBEC3B (not APOBEC3A) is upregulated by HPV infection of keratinocytes (69,70).

To resolve these issues and get a molecular handle on *APOBEC3B* transcriptional regulation, a panel of cell lines was treated with PMA or equal amounts of DMSO as a negative control, and previously validated reverse transcription quantitative PCR (RT-qPCR) assays were used to measure mRNA levels of all eleven human *APOBEC* family members (44). *APOBEC3B* mRNA was induced at least 2-fold by PMA treatment of all lines (except 293T), with the highest level of fold induction observed for the immortalized normal breast epithelial cell line MCF10A (**Fig. 3.S1**). Under standard cell culture conditions MCF10A expresses low levels of *APOBEC3B* and *APOBEC3F*, even lower levels of *APOBEC3G* and *APOBEC3H*, high levels of *APOBEC3C*, and undetectable levels of all other *APOBEC* family members. Remarkably, PMA treatment caused a specific 100-fold upregulation of *APOBEC3B* mRNA, with no detectable changes in the expression levels of any other *APOBEC* family members (**Fig. 3.1A** and **3.S2**).

APOBEC3B was induced with as little as 1 ng/mL PMA, and its induction was dose responsive and near maximal at 25 ng/mL PMA (**Fig. 3.1B**, histogram). *APOBEC3B* mRNA levels correlated with a rise in steady-state protein levels as measured by immunoblotting with a new rabbit anti-APOBEC3B monoclonal antibody (**Fig. 3.1B**, immunoblot) and with enzymatic activity as measured by a gel-based single-stranded DNA cytosine deamination assay (**Fig. 3.1B**, polyacrylamide gel, and **Materials and Methods**). Moreover, significant *APOBEC3B* mRNA induction was detected 30 minutes after PMA treatment and maximal levels were observed by 3 hours post-treatment (**Fig. 3.1C**, histogram). *APOBEC3B* protein and activity levels lagged shortly behind mRNA levels and persisted through the duration of the 6-hour time course (**Fig. 3.1C**, immunoblot and polyacrylamide gel). An extended time course revealed that *APOBEC3B* mRNA levels begin to decrease by 12 hours with a return to near basal

levels by 24 hours post-PMA treatment (**Fig. 3.S3**). Importantly, *APOBEC3B* upregulation is likely to be a direct result of signal transduction as the kinetics of mRNA upregulation were not affected by simultaneously treating cells with the protein translation inhibitor cyclohexamide (**Fig. 3.1D**, histogram). Cycloheximide treatment was effective as evidenced by disrupted *APOBEC3B* protein accumulation (**Fig. 3.1D**, immunoblot and poly acrylamide gel). Altogether, these data demonstrate that *APOBEC3B* is strongly and specifically upregulated by a PMA-induced signal transduction mechanism in multiple cell lines and most strongly in the immortalized normal breast epithelial cell line MCF10A. Notably, upregulation can be as high as 100-fold and this maximal level of *APOBEC3B* mRNA is on par with that observed in many different cancer cell lines and tumor types including a large fraction of breast and ovarian cancers [*i.e.*, mRNA levels 2- to 5-fold higher than those of the constitutively expressed housekeeping gene *TATA binding protein (TBP)* (21,23,69,74)].

PKC is required for *APOBEC3B* induction by PMA

PMA is a known agonist of PKC signaling, but it is also capable of affecting other cellular processes [(121-124) and references therein]. To determine whether *APOBEC3B* induction by PMA occurs through PKC signal transduction or an alternative mechanism, we leveraged a panel of existing PKC inhibitors that each vary with respect to class selectivity. MCF10A cells were pre-treated for 30 minutes with varying concentrations of the pan-PKC inhibitor Gö6983 (125) and then treated for 6 hours with an optimal amount of PMA (25 ng/mL). In comparison to strong *APOBEC3B* upregulation observed with PMA treatment alone, pretreatment with Gö6983 caused a dose responsive suppression of *APOBEC3B* induction (**Fig. 3.2A**). *APOBEC3B* was suppressed to background levels by 5 μ M Gö6983, as well as by higher concentrations (**Fig. 3.2A** and data not shown). Moreover, no morphological defects or viability issues

were observed at these concentrations of Gö6983 (**Fig. 3.S4**). As additional controls, MCF10A cells were pretreated in parallel with the phosphoinositol 3 kinase (PI3K) inhibitor, LY294002, and the mitogen-activated protein kinase (MEK) inhibitor, UO126, prior to PMA induction (**Fig. 3.2B-C**). In both instances, no suppression of *APOBEC3B* upregulation was observed. Collectively, these data indicated that the PKC pathway regulates *APOBEC3B* expression in the MCF10A breast epithelial cell line, and the PI3K and MEK pathways are unlikely to be involved.

Human cells can express up to 9 different *PKC* genes [(121-124) and references therein]. The resulting 9 distinct PKC proteins (conventionally called isoforms) are divisible into 3 classes based on activation mechanism: classical PKC (cPKC) isoforms require both DAG and increased levels of intracellular calcium, novel PKC (nPKC) isoforms require only DAG, and atypical PKC (aPKC) isoforms are activated by other signals. To test which class of PKC isoforms is responsible for *APOBEC3B* upregulation, we utilized two additional inhibitors known to have similar potency as Gö6983, but greater selectivity for certain PKC classes. First, we pretreated MCF10A cells with bisindolylmaleimide-1 (BIM-1), which is known to inhibit both the cPKC and nPKC classes (126), and then induced with optimal PMA concentrations. A nearly identical dose dependent suppression of *APOBEC3B* induction was observed (**Fig. 3.2D**). This result was expected as DAG mimics do not generally activate aPKCs. Second, we pretreated MCF10A cells with Gö6976, which is an inhibitor of the cPKC class of proteins (127). The dose responsiveness of *APOBEC3B* repression was again similar to Gö6983 (**Fig. 3.2E**). Taken together, these chemical inhibition data strongly implicated a cPKC isoform in *APOBEC3B* induction by PMA.

One of the most potent and clinically advanced PKC inhibitors is AEB071, which selectively inhibits cPKC and nPKC isoforms (128-130). AEB071 has shown positive results in preclinical studies and phase I clinical trials for treatment of uveal melanoma

(131-134). To fortify the pharmacologic approaches elaborated above, we asked whether pretreatment of MCF10A cells with AEB071 would produce a similar reductive effect on PMA induced *APOBEC3B* expression as the above PKC inhibitors. Indeed, a clear dose dependent response was observed and, importantly, AEB071 caused a complete suppression of *APOBEC3B* expression at 500 nM, which is approximately 10-fold more potent than Gö6983, BIM-1, or Gö6983, consistent with previously reported lower IC₅₀ values for this molecule [Fig. 3.2F; (125-130)].

RNA sequencing (RNAseq) revealed that *PKCα* (*PRKCA*) is the only cPKC isoform expressed in MCF10A cells (Fig. 3.2G). *PKCα* mRNA levels were unchanged by PMA treatment, in comparison to DMSO as a negative control, consistent with a mechanism in which PMA signals through *PKCα* to ultimately stimulate *APOBEC3B* transcription (Fig. 3.2G). To further test the involvement of *PKCα* in this regulatory pathway and to provide an orthologous approach to the chemical probes used above, we knocked down *PKCα* expression using 3 independent shRNA-encoding lentiviral constructs. In each case, *PKCα* knockdown resulted in a corresponding reduction in the level of *APOBEC3B* mRNA induced by PMA (Fig 3.2H). Immunoblots confirmed *PKCα* knockdown and proportional reductions in *APOBEC3B* (Fig 3.2I). Altogether, the pharmacologic and genetic approaches used here provide a compelling case for *PKCα* as the predominant PKC isoform driving PMA-mediated upregulation of *APOBEC3B*.

NFκB is required for *APOBEC3B* induction by PMA

We next asked which downstream transcription factor is responsible for driving *APOBEC3B* upregulation in response to PMA. PKC is known to signal through several different transcription factors, including ERK, JNK, NFκB, and others [(121-124) and references therein]. We therefore started at the DNA level and examined the *APOBEC3B* promoter region for binding sites of known PKC-regulated transcription

factors. Interestingly, these *in silico* analyses revealed several NFκB binding sites within 2.5 kb of the *APOBEC3B* transcriptional start site (5'-GGRRNNYYCC). NFκB is known to have multiple roles in immunity and inflammation [(135,136) and references therein], and a direct NFκB-mediated relay to *APOBEC3B* expression could be physiologically beneficial, given *APOBEC3B*'s known roles in innate immunity [(31,32) and references therein].

To test for a mechanistic link between NFκB and *APOBEC3B* transcription, we used two compounds known to block NFκB signaling through independent mechanisms. First, we treated MCF10A cells with varying amounts of BAY 11-7082, which is an NFκB inhibitor that acts by inhibiting upstream ubiquitin assembly (137), and then added optimal PMA concentrations for *APOBEC3B* induction. This small molecule caused strong dose-responsive drops in *APOBEC3B* induction by PMA treatment, analogous to studies above with PKC inhibitors (**Fig. 3.3A**). Second, we pretreated MCF10A cells with a titration of the proteasome inhibitor, MG132, prior to PMA stimulation. It is well known that both the canonical and non-canonical NFκB signaling pathways require proteasome-mediated degradation of IκB and processing of p100, respectively, for efficient signal transduction [(135,136) and references therein]. Indeed, *APOBEC3B* expression decreased in a dose dependent manner in response to MG132 treatment (**Fig. 3.3B**), further suggesting a role for NFκB signaling since the pathway of interest requires protein degradation by the proteasome for productive signal transduction. As above, neither BAY 11-7082 nor MG132 caused cell cycle or morphological changes through the durations of these experiments (**Fig. 3.S4**).

RNAseq data sets revealed that MCF10A expresses both the canonical NFκB components, *RELA* and *NFKB1*, and the non-canonical NFκB components, *RELB* and *NFKB2*, and levels of these mRNAs are unaffected by PMA treatment (**Fig. 3.3C**). Canonical signaling is known to require IKKβ, whereas non-canonical NFκB signaling is

strictly dependent on IKK α -catalyzed phosphorylation of p100 [(135,136) and references therein]. To distinguish between these pathways, we used TPCA-1, which is known to have a 22-fold selectivity for IKK β (canonical) over IKK α (non-canonical) (138). MCF10A cells were pretreated with a titration of TPCA-1 concentrations spanning the IC₅₀ values of both proteins, and then PMA was used to induce *APOBEC3B* upregulation. *APOBEC3B* expression was inhibited closer to the reported IC₅₀ of IKK α , consistent with involvement of the non-canonical NF κ B pathway (**Fig 3.3D**). As an additional control, we also analyzed *TNF α* , which is regulated by the canonical pathway (139,140). As expected, *TNF α* expression was inhibited by much lower concentrations of TPCA-1 confirming the differential selectivity of this compound and further implicating the non-canonical NF κ B pathway in *APOBEC3B* upregulation (**Fig 3.3D**).

RELB and p100/p52 are recruited to the *APOBEC3B* promoter region in response to PMA

We next performed a series of chromatin immunoprecipitation (ChIP) experiments to further test whether the non-canonical NF κ B pathway is responsible for upregulating *APOBEC3B*. Primer sets were designed for each of the predicted NF κ B binding sites near the *APOBEC3B* transcriptional start site (**Fig. 3.3F**). As a control, an additional primer set was made for the promoter region of *NFKBIA*, which contains NF κ B binding sites and is also upregulated by PMA with similar kinetics as *APOBEC3B* (note, *NFKBIA* encodes I κ B; **Figs. 3.3E and F**). ChIP was performed for RELA, RELB, p100/p52, RNA POL II (positive control), and isotype matched IgG (negative control). As expected, RELA, RELB, p100/p52, and RNA POL II were all bound to the *NFKBIA* promoter following PMA treatment (**Fig. 3.3G**). We also found RNA POL II bound to the *APOBEC3B* gene near the transcriptional start site and throughout the gene body in response to PMA (**Fig. 3.3G**). Interestingly, both RELB and p100/p52 were recruited to

the same sites as RNA POL II following PMA treatment, indicating that these factors are also involved in driving *APOBEC3B* expression in response to PMA (**Fig. 3.3G**). An expanded ChIP experiment replicated these data and showed that RNA POL II, RELB, and p100/p52 binding are dependent on PKC signaling as treatment with AEB071 completely ablated all binding to the *APOBEC3B* promoter (**Fig. 3.S5**). These ChIP data strongly implicate the non-canonical NFκB pathway, specifically the RELB and p100/p52 heterodimer (and not RELA and p105/p50), in directly inducing *APOBEC3B* transcription in response to PMA induced activation of PKC.

Endogenous *APOBEC3B* expression requires PKC in multiple cancer cell lines

We next asked whether the constitutively high levels of endogenous *APOBEC3B* observed in many human cancer cell lines occurs through the PKC pathway (23,69,74). For this series of experiments, we selected 4 breast, 4 ovarian, 4 bladder and 4 head/neck cancer cell lines expressing a 10-fold range of endogenous *APOBEC3B* mRNA levels (**Fig. 3.4A**). Each line was treated for 48 hrs with 10 μM AEB071, the most potent PKC inhibitor identified above, and then *APOBEC3B* mRNA and protein levels were quantified by RT-qPCR and immunoblotting. As above, no effects on the cell cycle or cell viability were observed (**Fig. 3.S6**). This is important since higher concentrations of AEB071 are known to cause cell cycle perturbations and apoptosis in certain cell types (131-133). *APOBEC3B* mRNA levels were reduced by more than half in 7/16 cell lines, including the breast cancer cell lines MDA-MB-468, MDA-MB-453, and HCC1806, the ovarian cancer cell line OVCAR5, and the head/neck lines SQ-20B, JSQ3, and TR146 (**Fig. 3.4B**, histogram). Changes of protein levels largely mirrored the mRNA results (**Fig. 3.4B**, immunoblot). Interestingly, several cell lines including all of the bladder cancer cell lines showed little decrease in *APOBEC3B* expression upon treatment with AEB071, suggesting that at least one additional induction mechanism

exists. Altogether, these data demonstrate that the PKC axis is responsible for the constitutive upregulation of endogenous *APOBEC3B* in a variety of cancer cell lines representing multiple distinct cancer types.

DISCUSSION

These studies are the first to establish mechanistic linkages between the PKC-NF κ B signal transduction pathway and upregulation of the DNA mutating enzyme, *APOBEC3B*, in cancer. Our studies suggest a model in which PKC α activation signals through the non-canonical NF κ B pathway and results in the recruitment of RELB to the *APOBEC3B* gene and its transcriptional activation (**Fig. 3.5**). This mechanism is remarkably specific to *APOBEC3B*, as expression of the related *APOBEC* family members is not affected. This specificity is concordant with our prior studies indicating that *APOBEC3B* is the only DNA deaminase family member upregulated in these and other cancer types in comparison to normal tissues (21,23,69,74). Moreover, PKC inhibitor studies with breast, head/neck, and ovarian cancer cell lines indicated that the PKC-NF κ B pathway contributes to the constitutively high levels of endogenous *APOBEC3B* that have been associated previously with cancer mutagenesis. Additional studies will be needed to determine the precise proportions of each tumor type affected by this *APOBEC3B* upregulation mechanism that, based on prior studies from our laboratory and others, is expected to endow cancer cells with mutational fuel for accelerated tumor evolution.

A recent publication implicated both the interferon response and the canonical and non-canonical NF κ B pathways in *APOBEC3A* and *APOBEC3B* upregulation and clearance of HBV episomes from infected cells (141). Activation of the lymphotoxin- β receptor through treatment of infected hepatocytes with bivalent or tetravalent antibodies led to the nuclear translocation of both RELA and RELB and the activation of known

NFκB pathway genes. These antibody treatments also led to the upregulation of *APOBEC3A* and/or *APOBEC3B* and to the gratuitous deamination of HBV cccDNA cytosines, viral DNA degradation, and long-term virus suppression. Taken together with our results presented here, it is tempting to speculate that both the PKC and the lymphotoxin-β receptor signaling mechanisms converge upon the non-canonical RELB-dependent NFκB pathway in order to activate *APOBEC3B* expression. Thus, our work suggests additional strategies such as PMA treatment to induce *APOBEC3B* upregulation and clearance of HBV from infected hepatocytes. However, these strategies may induce collateral damage through genomic DNA mutagenesis and should be approached carefully.

Clear evidence for *APOBEC3B* overexpression and mutation signatures in cervical and head/neck cancers suggested that HPV infection might trigger an innate immune response that includes DNA deaminase upregulation (21,22). Subsequent work demonstrated that infection by high-risk HPV types (not low-risk types) causes the specific upregulation of *APOBEC3B*, suggesting that this is not simply a gratuitous innate immune response to viral infection (69,70). Moreover, the E6 oncoprotein alone from high-risk types (again, not low risk) was sufficient to trigger *APOBEC3B* upregulation (69). It is notable that the overall fold induction by HPV is lower than that described here, due partly to higher background and partly to a smaller magnitude of induction (*i.e.*, 10-20 fold vs. >100-fold here). An independent study suggested that the E7 oncoprotein may also contribute to *APOBEC3B* upregulation (70). The mutator phenotype induced by HPV infection is likely fueling tumor evolution as the pattern of PI3K-activating mutations in HPV-positive tumors is biased toward cytosine mutations in *APOBEC*-like motifs in the helical domain of the kinase, whereas the pattern in HPV-negative tumors is split between the helical and kinase domains of the enzyme (16,117). Obviously, HPV-mediated upregulation of *APOBEC3B* only impacts cervical cancers and

a proportion of head/neck and bladder carcinomas. In contrast, many more tumor types are likely to be susceptible to the mechanism described here. Comprehensive mutation surveys estimate that APOBEC (predominantly APOBEC3B) impacts approximately half of all human cancers (13,21,22). It will be interesting to determine in future studies whether viral and non-viral mechanisms are synergistic, additive, or mutually exclusive.

Another major conclusion from our studies is the likelihood that virus infection and PKC activation are not the only mechanisms responsible for APOBEC3B induction in cancer. PKC inhibition caused little decrease in *APOBEC3B* mRNA levels in the breast cancer cell line HCC1569, the ovarian cancer cell lines A2780, IGROV-1, and OVCAR8, the head/neck cancer cell line SSC58, and all 4 bladder cancer cell lines, strongly implying independence from this signaling pathway. Several of these lines have been deep-sequenced as part of the Cancer Cell Line Encyclopedia, HPV is not present, and therefore a viral mechanism does not appear to play a role (although other head/neck and bladder cancer lines are known to be HPV-positive and the viral mechanism discussed above is a contributing factor). Future studies are therefore likely to reveal additional mechanisms for *APOBEC3B* upregulation, but it is possible that non-canonical NFκB activation will emerge as a common denominator and hub for *APOBEC3B* upregulation.

It will also be interesting to determine the relationship between upregulation of APOBEC3B and immunotherapy responsiveness, as recent reports have suggested that increased tumor mutation loads correlate with stronger anticancer immune responses (3,142). It may therefore be useful to induce APOBEC3B, as described here, to create even more tumor neoantigens in order to boost efficacies of current immunotherapies.

Although *PKC* mutations are rare in cancer, altered expression of several PKC isoforms is observed and associated with poor clinical outcomes [(121,122) and references therein]. In addition, mutations in *GNAQ* and *GNA11* occur in approximately

half of all uveal melanoma samples [(143,144); illustrated as Gq in **Fig. 3.5**]. Inhibition of PKC in these uveal tumors leads to clinical benefits attributed to cell cycle arrest and apoptosis (131-134). It is possible that downregulation of APOBEC3B and a subsequent decrease in tumor evolution through lowered mutation rates may also contribute to these encouraging clinical responses. Based on substantive prior work from our lab and others demonstrating a major role for APOBEC3B in cancer mutagenesis and correlating high levels of APOBEC3B with poor prognoses for ER-positive breast cancers (26,27), together with the studies presented here, we propose that existing inhibitors of the PKC-NFκB axis such as AEB071 may be repurposed to treat primary tumors in combination with existing therapies and help prevent detrimental outcomes such as drug resistance and metastases.

METHODS

Cell lines

MCF10A, 293T, HeLa, HCC1569, MDA-MB-468, MDA-MB-453, HCC1806, T24, RT4, TCCSUP, and J28 were purchased from the American Tissue Culture Collection (ATCC) and cultured as recommended. N/TERT-1 and NIKS were provided by Drs. Peter Howley (Harvard University) and Paul Lambert (University of Wisconsin), respectively, and grown as reported (69). A2780, OVCAR5, IGROV-1, and OVCAR8 were obtained from Dr. Scott Kaufmann (Mayo Clinic) and cultured as reported (74). MCF-7L were provided by Dr. Douglas Yee (University of Minnesota) and grown in IMEM containing 5% fetal bovine serum (FBS), penicillin (100 U/ml), streptomycin (100 ug/ml) and 11.25 nM recombinant human insulin. SQ20B, JSQ3, TR146, and SCC58 were obtained from Dr. Mark Herzberg (University of Minnesota) and cultured at 37°C with 5% CO₂ in DMEM/F12 with 10% FBS, penicillin, streptomycin, and 400 ng/mL hydrocortisone.

Reverse transcription quantitative PCR

For RT-qPCR, cells were trypsinized and pelleted prior to RNA extraction using the Roche High Pure RNA Isolation Kit. Triplicate cDNA reactions were made using Roche Transcriptor Reverse Transcriptase. qPCR was performed on each reaction using previously reported primer-probe combinations for each APOBEC (44). For PKC α , the forward and reverse primers were 5'-TGGTTTTGGTCCCATTTCT and 5'-CATCCGGGTTTCCTGATTC, respectively, and were used with Roche UPL 1. For TNF α , the forward and reverse primers were 5'-CAGCCTCTTCTCCTTCCTGAT and 5'-GCCAGAGGGCTGATTAGAGA, respectively, and were used with Roche UPL 29

Immunoblotting

The development and validation of the rabbit monoclonal antibody (mAb) against APOBEC3B will be described elsewhere (Brown and Harris, *in process*). The mAb used here is called 10-87-13, and it effectively binds endogenous APOBEC3B in a variety of assays including immunoblotting as demonstrated in several experiments. In some cell lines, this mAb cross-reacts with endogenous APOBEC3G, but the faster migrating APOBEC3B can be readily distinguished from the slower migrating APOBEC3G by SDS-PAGE (*e.g.*, **Fig. 3.4B**). The anti-tubulin (Covance, cat # MMS-407R) and PKC α (Cell Signaling, cat # 2056P) antibodies were used in accordance with the manufacturer's specifications.

Deaminase activity assays

Deaminase activity assays were performed as previously reported (69). In short, 4 pmol of a fluorescently labeled oligo with a single target cytosine (5'-ATTATTATTATTCAAATGGATTTATTTATTTATTTATTTATTT-fluorescein) was treated with cell extract containing 0.025 U/rxn UDG (New England BioLabs), UDG buffer, and

1.75 U/rxn RNase A (Qiagen) for 2 hours. Abasic sites were cleaved by treatment with 100 mM NaOH at 95°C for 10 min. Substrate was separated from product using 15% TBE-urea gel electrophoresis. Gels were scanned using a FujiFilm Image Reader FLA-7000.

PMA induction and PKC-NFκB Inhibitors

For induction experiments, 2.5×10^5 cells were plated in a 6-well plate 1 day prior to drug treatment. PMA was then added to the media and incubated at 37°C with 5% CO₂ for 6 hours unless otherwise indicated. For experiments utilizing inhibitors, cells were pretreated with inhibitors 30 minutes prior to PMA induction (25ng/mL). PMA (Fisher Scientific), cyclohexamide (Acros Organics), Gö6983 (Cayman Chemical), LY294002 (EMD Chemicals), UO126 (EMD Chemicals), BIM-1 (Cayman Chemical), Gö6976 (Enzo Life Sciences), AEB071 (Medchem Express), BAY 11-7082 (R&D Systems), MG132 (Fisher Scientific), and TPCA-1 (Cayman Chemical) were stored as recommended.

PKC knockdown experiments

shRNA encoding pLKO.1-based lentiviruses were produced in 293T cells as reported (23). MCF10A cells were transduced with PKCα #1 (Open Biosystems, TRCN0000001691), PKCα #2 (Open Biosystems, TRCN0000001692), or PKCα #3 (Open Biosystems, TRCN0000001690) or a control lentivirus. 96 hours later the transduced pools were treated with 25ng/mL PMA for 3 (RNA) or 6 (protein) hours, and were harvested and analyzed as described above.

RNA sequencing experiments

Two sets of MCF10A cells in duplicate were treated every 8 hours with media supplemented with PMA or DMSO for 48 hours. At 48 hours, RNA was extracted using

an RNeasy Mini Kit (Qiagen). Total RNA was submitted to the University of Minnesota Genomics Center for sequencing on the Illumina HiSeq 2000 platform. Raw reads were analyzed using both DESeq2 (145) and the Tuxedo suite (146) to identify changes in mRNA expression in PMA treated versus untreated cells.

Chromatin immunoprecipitation experiments

MCF10A cells were treated with either DMSO or 25 ng/mL PMA for 2 hours. Cross-linking was performed with 1% formaldehyde for 10 min at room temperature and quenched with 150 mM glycine. Cells were then lysed in Farnham Lysis Buffer at 4°C for 30 minutes. Nuclei were pelleted, resuspended in RIPA Buffer, and sonicated (Diagenode Pico Sonicator) to generate approximately 600 bp DNA fragments. Immunoprecipitations were done using Protein G Dynabeads (Invitrogen) and 2 µg antibody per sample. Samples were washed in 1 mL low salt wash buffer, 1 mL high salt wash buffer, 1 mL LiCl wash buffer, and eluted at 65°C for 30 minutes. Samples were reverse cross-linked using 200 mM NaCl and treated with Proteinase K for 12 hours at 65°C. DNA was purified using a CHIP DNA Clean and Concentrator Kit (Zymo Research) and qPCR was performed with SYBR Green master mix (Roche) on a Roche LightCycler 480. Values represent the percentage of input DNA immunoprecipitated (IP DNA) and are the average of three independent qPCR reactions. All CHIP reagents can be found in the supplementary information (**Table 3.S1**).

ADDITIONAL CONTRIBUTIONS

We thank lab members for critical discussions and P. Howley, P. Lambert, S. Kaufmann, D. Yee and M. Herzberg for providing cancer cell lines, C. McDonald-Hyman and B. Blazar for PKC inhibitors, and C. Deip and C. Lange for PI3K and MEK inhibitors.

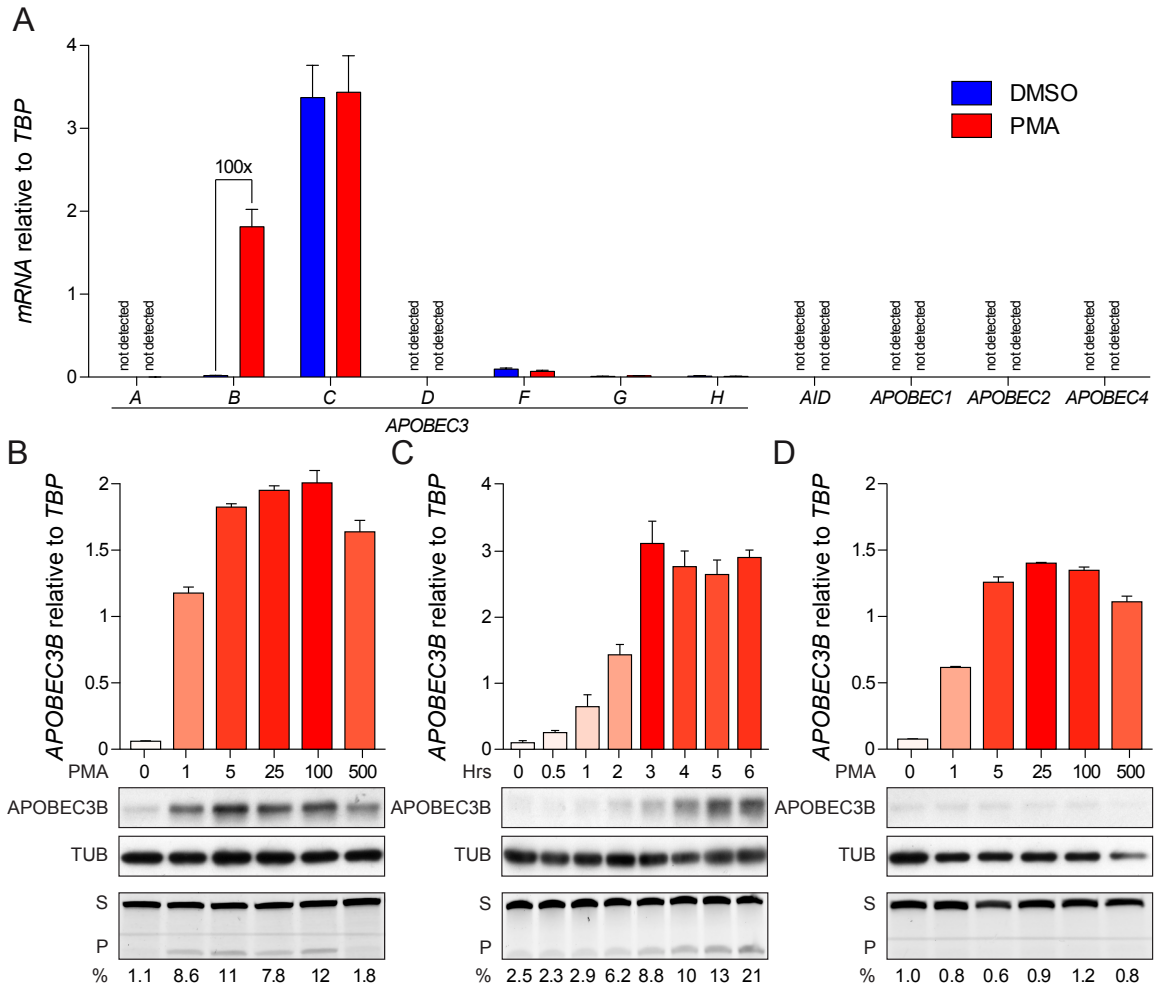


Figure 3.1 APOBEC3B upregulation by PMA.

(A) A histogram showing the specific upregulation of *APOBEC3B* mRNA by PMA. MCF10A cells were treated with PMA (25 ng/ml) or vehicle control for 6 hrs, and mRNA levels were measured by RT-qPCR (mean and SD are shown for triplicate RT-qPCR reactions normalized to *TBP*). The same data points are shown in the context of a larger PMA dose response experiment in Fig. S1.

(B) A histogram demonstrating the dose responsiveness of *APOBEC3B* upregulation by PMA. Normalization and quantification were calculated as in Fig. 1A. The middle images show immunoblots for corresponding APOBEC3B and TUBULIN proteins levels, and the lower image shows DNA cytosine deaminase activity for the corresponding whole cell

extracts (S, substrate; P, product; percent deamination quantified below each lane).

(C) A histogram depicting the rapid kinetics of APOBEC3B upregulation following PMA treatment. MCF10A cells were treated with a single concentration of PMA (25 ng/ml), and mRNA, protein, and activity levels are reported as in Fig. 1B.

(D) New protein synthesis is dispensable for *APOBEC3B* mRNA upregulation by PMA. Representative dose response experiment for MCF10A cells treated with the indicated concentrations of PMA following a 30 min pretreatment with 10 µg/mL cyclohexamide. mRNA, protein, and activity levels are reported as in Fig. 1B

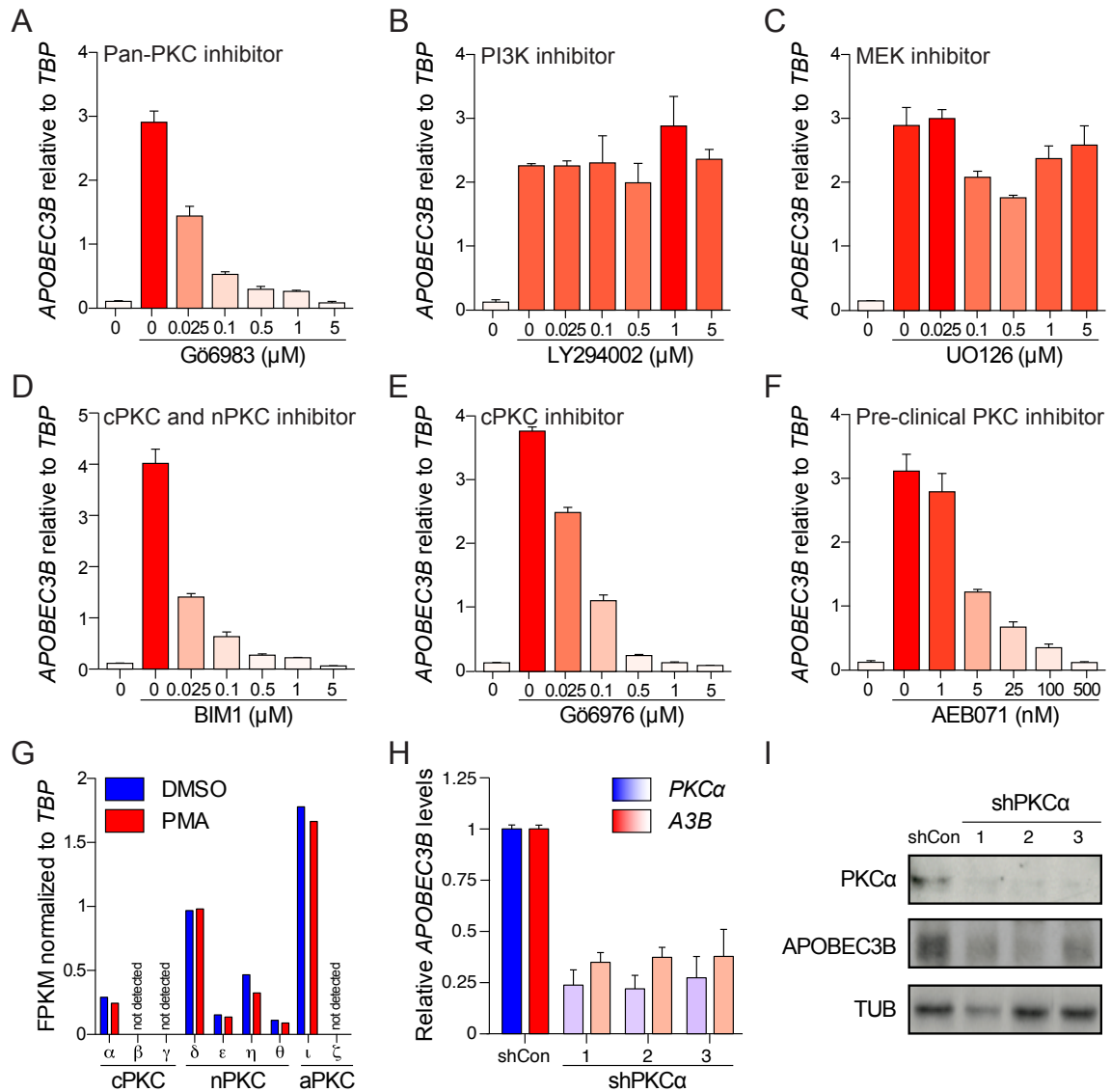


Figure 3.2 APOBEC3B upregulation by PMA is dependent on PKC.

(A-F). Histograms reporting the impact of the indicated small molecules on PMA-induced *APOBEC3B* upregulation. *APOBEC3B* induction was inhibited by Gö6983 (pan-PKC inhibitor), BIM-1 (classical and novel PKC inhibitor), Gö6976 (classical PKC selective inhibitor), and AEB071 (preclinical PKC inhibitor) but not by LY294002 (PI3K inhibitor) or UO126 (MEK inhibitor). MCF10A cells were treated with PMA following a 30 min pretreatment with the indicated concentrations of each inhibitor. mRNA expression is reported as the mean of 3 independent RT-qPCR reactions normalized to *TBP* (error

bars report SD from triplicate assays).

(G) Histogram depicting *PKC* isoforms expressed in MCF10A cells treated with PMA or vehicle control. mRNA expression was determined by RNA-seq and is reported as fragments per kilobase of exon per million fragments mapped (FKPM) and normalized to *TBP*.

(H) Histogram showing that *PKC* α knockdown inhibits *APOBEC3B* induction by PMA. MCF10A cells were treated with PMA following *PKC* α knockdown using 3 independent *PKC* α specific shRNA encoding lentiviruses and a control. mRNA levels for both *PKC* α (blue) and *APOBEC3B* (red) are reported.

(I) Immunoblots confirming *PKC* α knockdowns and proportional reductions in *APOBEC3B* protein levels.

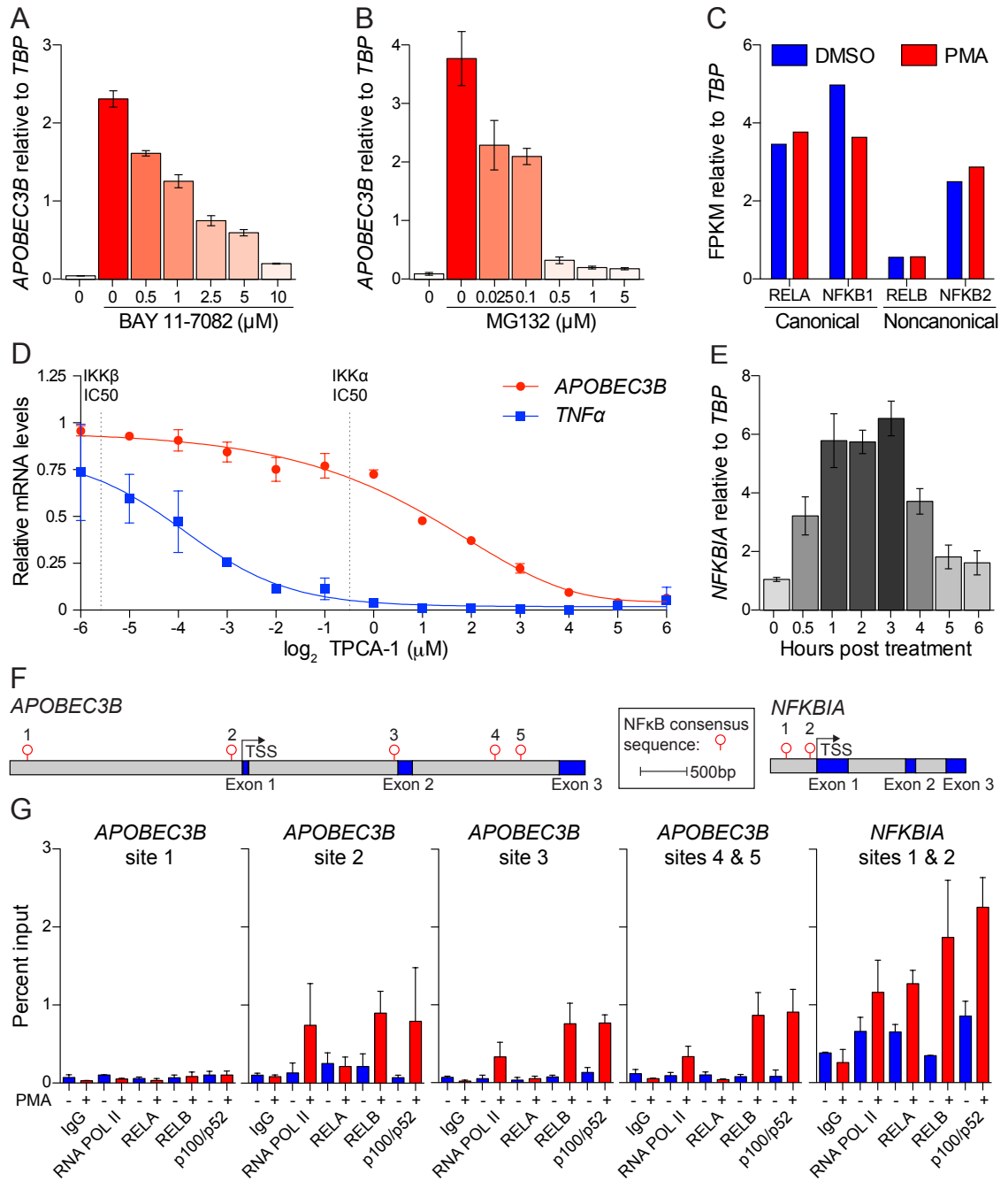


Figure 3.3 Non-canonical NF κ B signaling is responsible for *APOBEC3B* upregulation by PMA.

(A-B) Histograms depicting the dose responsive inhibition of PMA-induced *APOBEC3B* upregulation by BAY 11-7082 (ubiquitination inhibitor) and MG132 (proteasome inhibitor). MCF10A cells were treated with PMA following a 30 min pretreatment with the indicated

concentrations of each inhibitor. *APOBEC3B* mRNA expression is reported as the mean of 3 independent RT-qPCR reactions normalized to *TBP* (error bars report SD from triplicate assays).

(C) Histogram depicting *NFκB* subunit mRNA levels in MCF10A cells treated with PMA or vehicle control. Expression was determined by RNA-seq and is reported as fragments per kilobase of exon per million fragments mapped (FKPM) and normalized to *TBP*.

(D) Plot depicting inhibition of PMA-induced *APOBEC3B* expression by the IκB kinase (IKK) inhibitor, TPCA-1, near the IC₅₀ for IKKα, not IKKβ. MCF10A cells were treated with PMA following treatment with varying concentrations of TPCA-1. *TNFα* (blue) and *APOBEC3B* (red) mRNA levels are reported as the mean of 3 independent RT-qPCR reactions normalized to *TBP* (error bars report SD from triplicate assays). The dotted lines denote previously reported *in vitro* IC₅₀ values for IKKα and IKKβ inhibition by TPCA-1 (138).

(E) Histogram showing the kinetics of *NFKBIA* upregulation by PMA. MCF10A cells were treated with PMA for the indicated times and mRNA values were quantified as in Fig. 3A.

(F) The *APOBEC3B* and *NFKBIA* promoter regions contain several putative NFκB binding sites (TSS, transcriptional start site).

(G) RELB and p105/p52 are specifically and robustly recruited to the *APOBEC3B* promoter region by PMA. ChIP was performed after a treatment with PMA or vehicle control for 2 hrs. *APOBEC3B* sites 4 & 5 and the two *NFKBIA* sites are reported together because they are too close to be distinguished by this procedure. qPCR results are reported as percent of the total chromatin input.

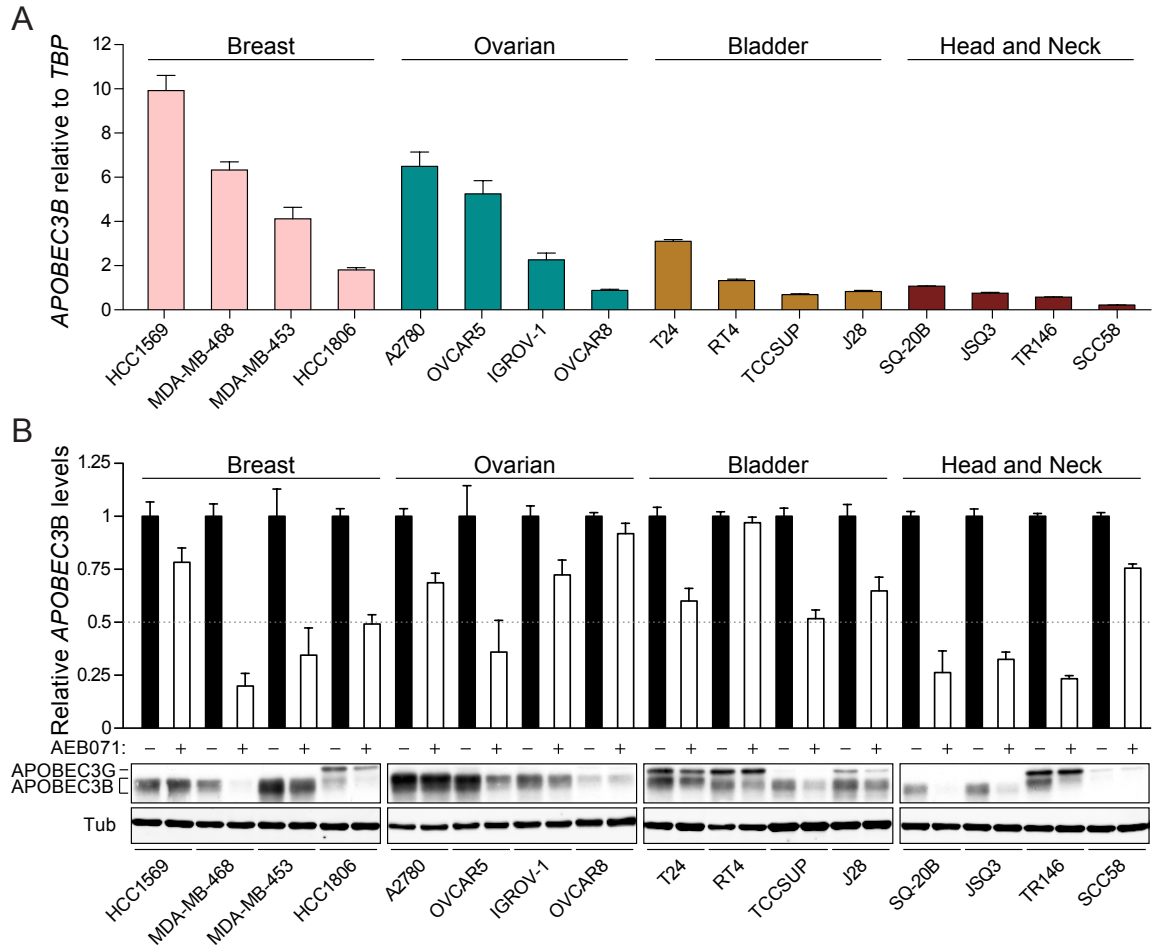


Figure 3.4 The PKC pathway drives endogenous APOBEC3B expression in cancer cells. **(A)** *APOBEC3B* mRNA levels in representative breast, ovarian, bladder, and head/neck cancer cell lines. mRNA expression is reported as the mean of 3 independent RT-qPCR reactions normalized to *TBP* (error bars report SD from triplicate assays). **(B)** AEB071 downregulates APOBEC3B in multiple cancer cell lines. The histogram reports *APOBEC3B* mRNA levels normalized to the vehicle treated control for each line. The dotted line represents a 50% decrease in *APOBEC3B* expression. The corresponding immunoblots show APOBEC3B and TUBULIN levels. Each line was treated with AEB071 (10 μ M) or vehicle control for 48 hours prior to mRNA and protein analysis.

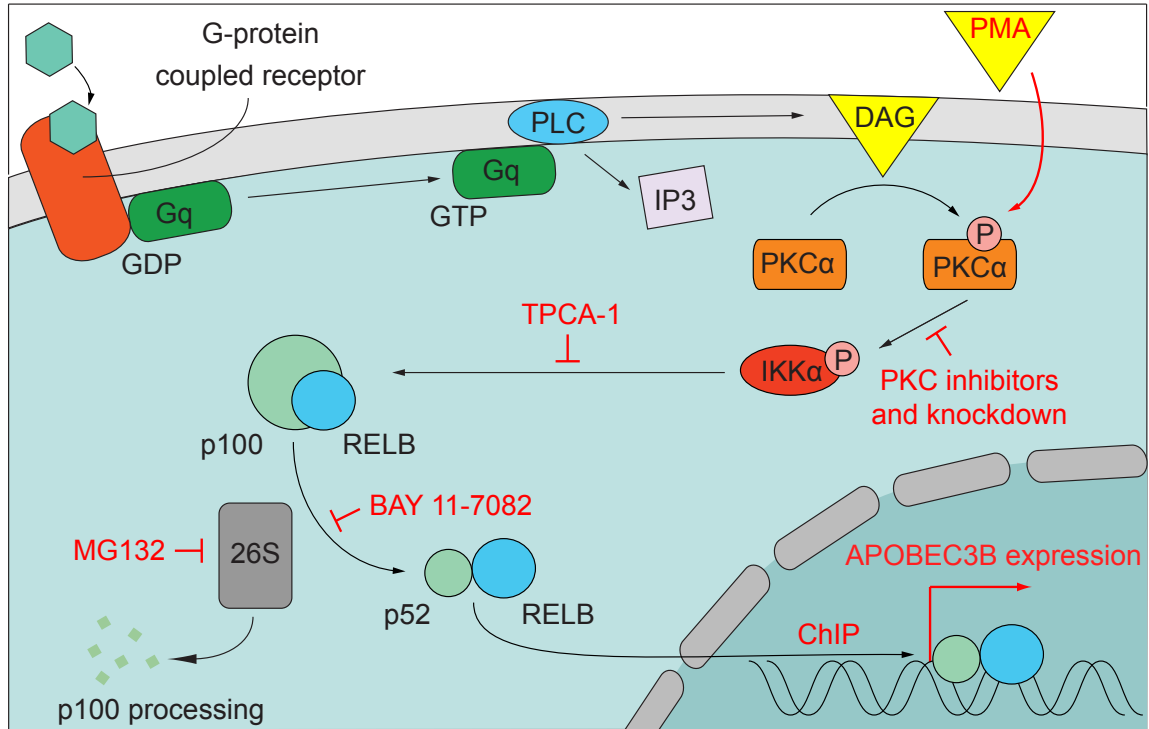


Figure 3.5 Model for APOBEC3B upregulation by the PKC-NFκB pathway.

PKCα activation by DAG or PMA leads to IKKα phosphorylation and proteasome-dependent cleavage of NFκB subunit p100 into the transcriptionally active p52 form. The non-canonical NFκB heterodimer containing p52 and RELB is then recruited to the *APOBEC3B* promoter to drive transcription. Red labels represent the small molecules and approaches used to interrogate this signal transduction pathway.

Table 3.S1 ChIP reagents.

| Category | Name | Description |
|-----------------|-----------------------|---|
| Antibody | Normal Rabbit IgG | Santa Cruz (sc-2027) |
| Antibody | RNA Pol II (Ser 5) | Abcam (ab5131) |
| Antibody | Rel A (p65) | Santa Cruz (sc-372x) |
| Antibody | p105/p50 | Millipore (06-886) |
| Antibody | Rel B | Santa Cruz (sc-226x) |
| Antibody | p105/p52 | Cell Signaling (3017) |
| Buffer | Farnham lysis buffer | 5 mM PIPES pH 8 85 mM KCl 0.5% Nonidet P-40 1x EDTA-free Protease Inhibitor Cocktail (Roche) |
| Buffer | RIPA buffer | 50 mM Tris-HCl pH 8 150 mM NaCl 5 mM EDTA 1% Nonidet P-40 0.5% Deoxycholate 0.1% SDS 1x EDTA-free Protease Inhibitor Cocktail (Roche) |
| Buffer | Low salt wash buffer | 20 mM Tris-HCl pH 8 150 mM NaCl 2 mM EDTA 0.1% SDS 1% Triton X-100 |
| Buffer | High salt wash buffer | 20 mM Tris-HCl pH 8 500 mM NaCl 2 mM EDTA 0.1% SDS 1% Triton X-100 |
| Buffer | LiCl wash buffer | 20 mM Tris-HCl pH 8 0.5 M LiCl 1% Nonidet P-40 1% deoxycholate 1 mM EDTA |
| Buffer | Elution buffer | 100 mM NaHCO ₃ 1% (w/v) SDS |

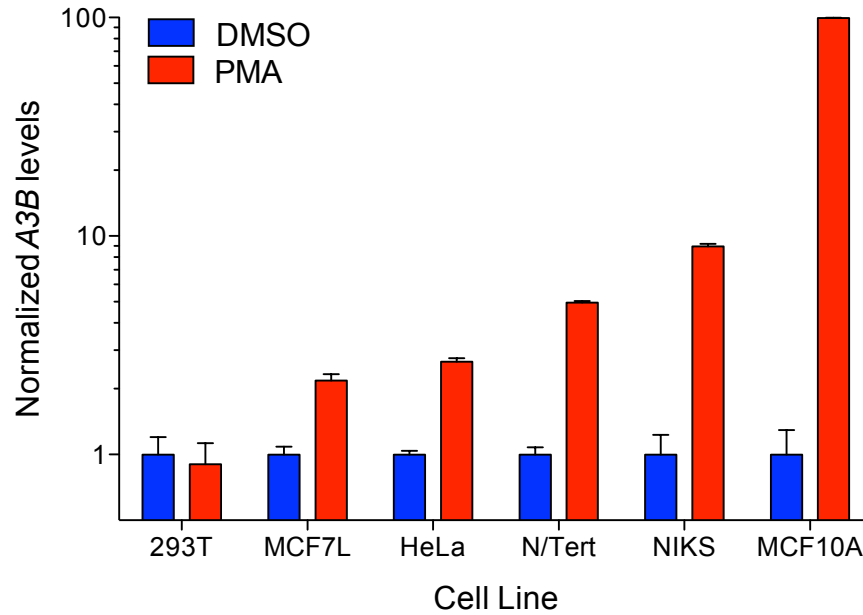


Figure 3.S1 *APOBEC3B* upregulation by PMA in multiple cell lines.

A histogram reporting PMA-induced *APOBEC3B* mRNA levels in the indicated cell lines (red bars) relative to the same lines treated with DMSO as a vehicle control (blue bars). Cells were treated with 25 ng/ml PMA or DMSO for 6 hrs prior to RNA preparation and RT-qPCR. DMSO-treated *APOBEC3B* expression values relative to those of the housekeeping gene *TBP* are 0.04, 0.07, 0.19, 0.47, 0.30, and 0.02 for 293T, MCF7L, HeLa, N/Tert, NIKS, and MCF10A, respectively. Each histogram bar reports the mean of 3 independent RT-qPCR reactions (error bars show SD from triplicate assays).

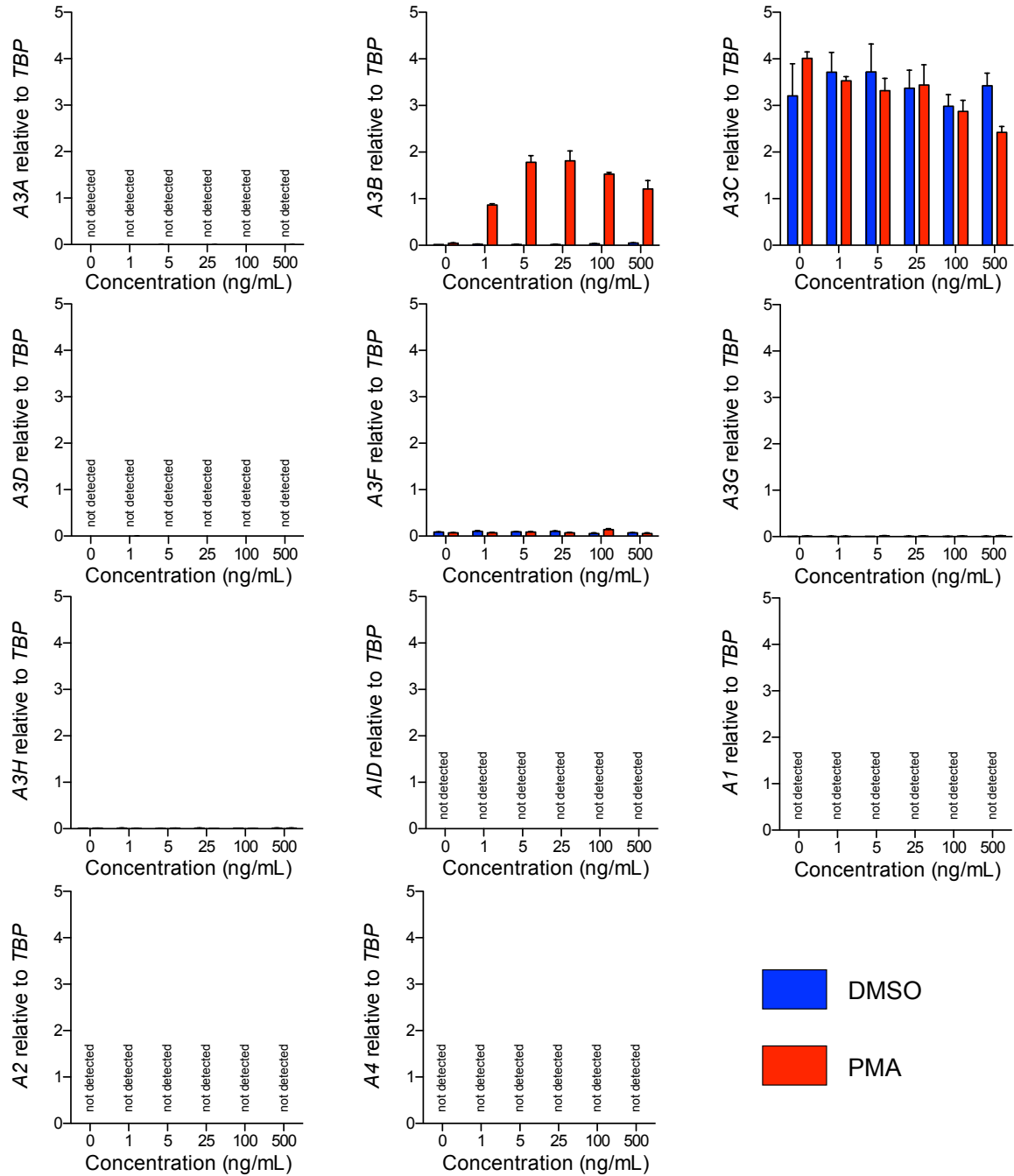


Figure 3.S2 APOBEC3 mRNA levels in PMA-treated MCF10A.

APOBEC family member mRNA levels in MCF10A cells treated with the indicated PMA concentrations or DMSO as vehicle control for 6 hrs. mRNA expression is reported as the mean of 3 independent RT-qPCR reactions normalized to *TBP* (error bars show SD from triplicate assays). The 25 ng/ml data are shown in **Fig. 3.1A**.

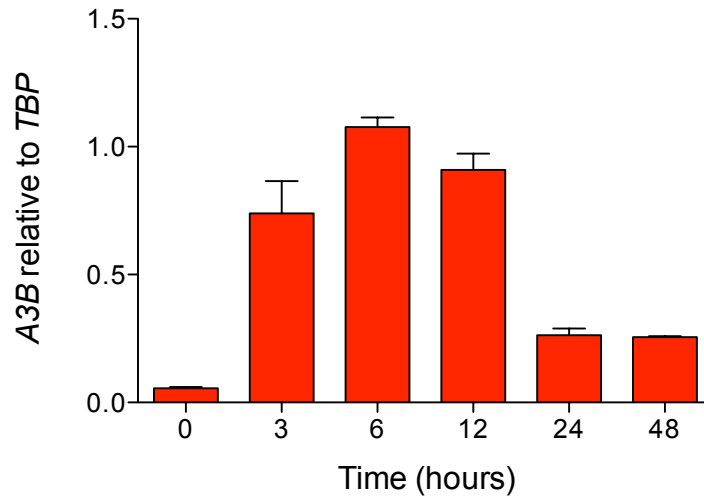


Figure 3.S3 Extended time course for PMA induction of *APOBEC3B*.

APOBEC3B mRNA levels in MCF10A cells treated with 25ng/mL PMA for the indicated times. mRNA expression values are normalized to those of the housekeeping gene *TBP* and reported as the mean of 3 independent RT-qPCR reactions (error bars show SD from triplicate assays).

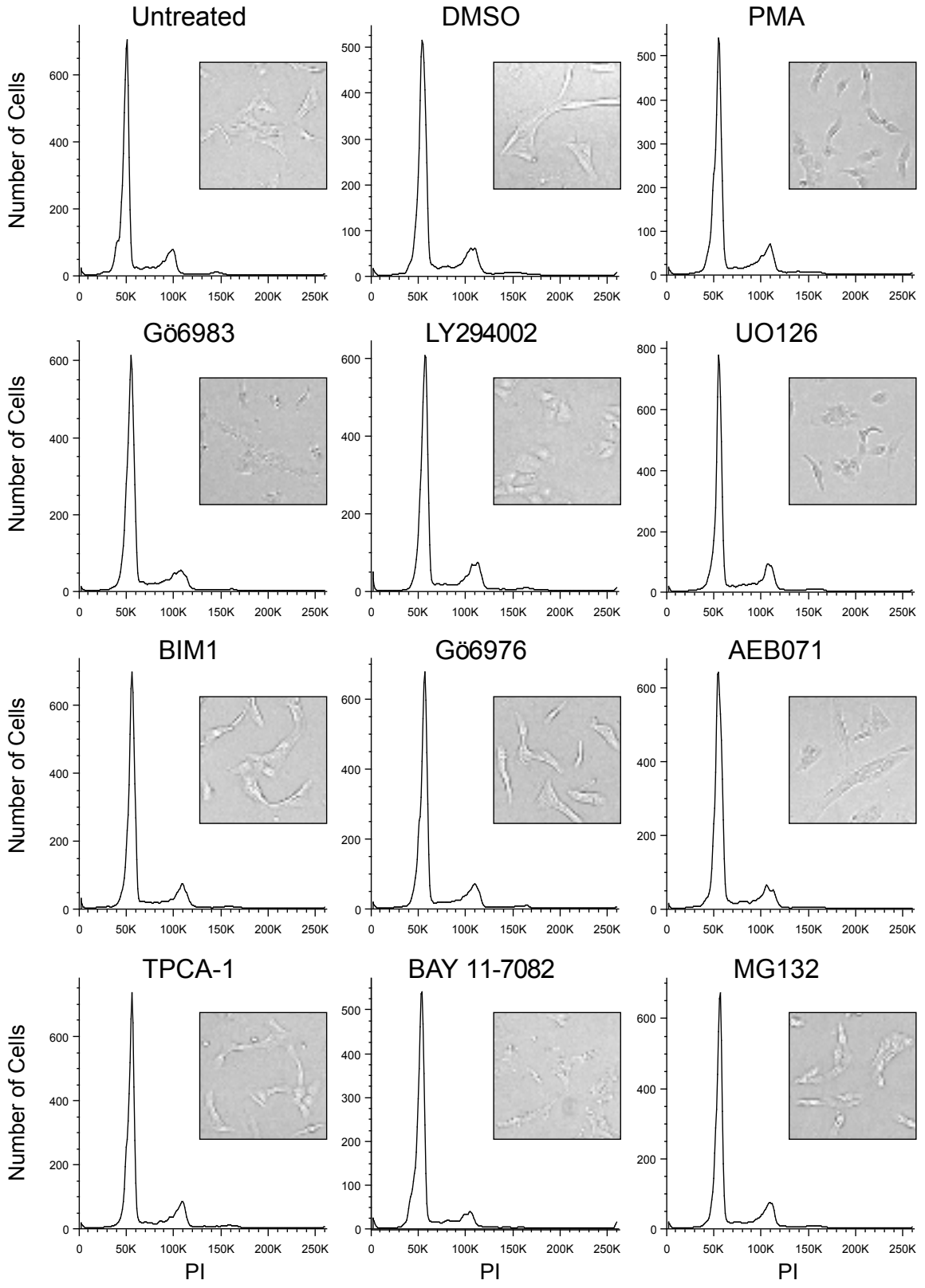


Figure 3.S4 Viability controls for MCF10A cells treated with small molecule inhibitors.

PI staining for cell cycle (histogram) and bright field microscopy for cellular morphology (images) for MCF10A cells treated with 10 μ M of the indicated small molecule inhibitor for 6 hrs. Microscopy images were taken at 40x magnification.

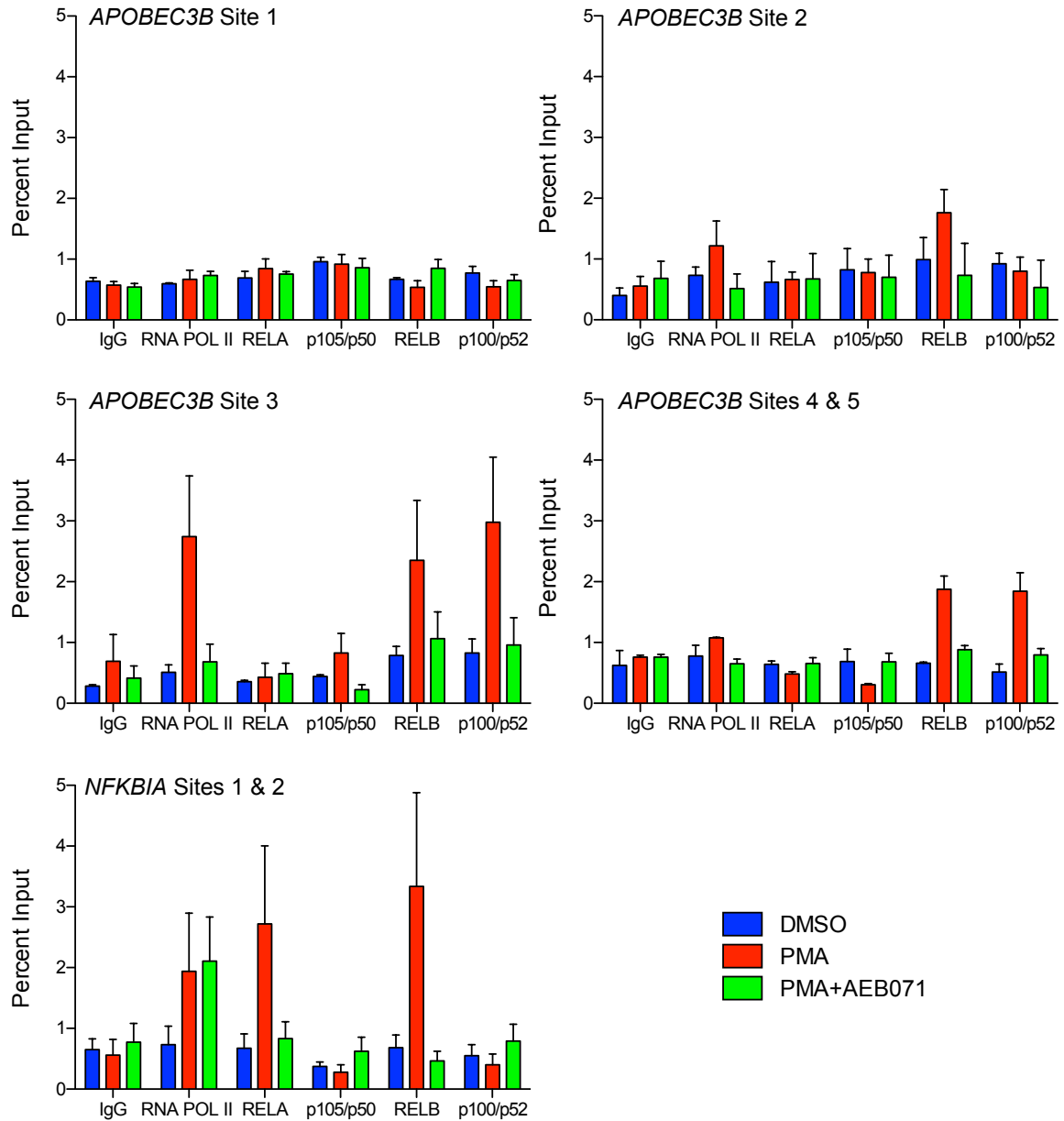


Figure 3.S5 Expanded ChIP data for MCF10A cells treated with PMA alone or in combination with AEB071.

ChIP was done for the indicated proteins after a treatment with vehicle control, PMA or PMA following a 2hr pretreatment with AEB071. *APOBEC3B* sites 4 & 5 and the two *NFKBIA* sites are reported together because they are too close to be distinguished by this procedure. qPCR results are reported as percent of the total chromatin input.

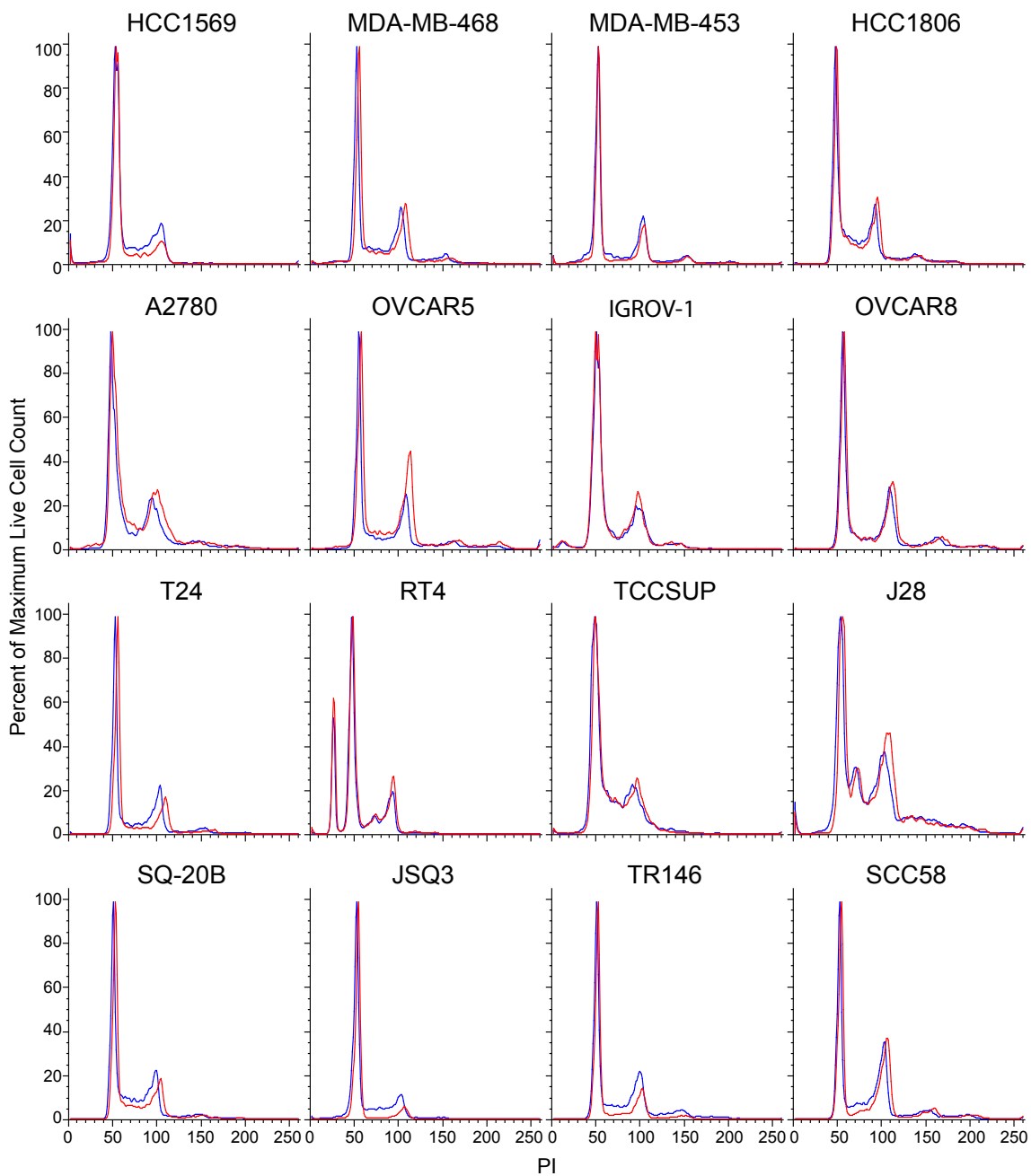


Figure 3.S6 Viability controls for cancer cell lines treated with AEB071.

PI staining for cell cycle for the indicated cancer cell lines treated for 48 hrs with either DMSO (blue) or 10 μM AEB071 (red).

CHAPTER 4:

***APOBEC3G* expression correlates with T cell infiltration and improved clinical outcomes in high-grade serous ovarian carcinoma**

Authors: Brandon Leonard,^{1,2,*} Gabriel J. Starrett,^{1,2,*} Matthew J. Maurer,³ Ann L. Oberg,³ Brett D. Anderson,^{1,2} William B. Brown,^{1,2} Kimberly R. Kalli,⁴ Scott H. Kaufmann,^{5,6} Reuben S. Harris^{1,2}

Affiliations: ¹Biochemistry, Molecular Biology and Biophysics Department, University of Minnesota, Minneapolis, MN 55455, USA. ²Masonic Cancer Center, University of Minnesota, Minneapolis, MN 55455, USA. ³Division of Biomedical Statistics and Informatics, Department of Health Sciences Research, Mayo Clinic, Rochester, MN 55905, USA. ⁴Women's Cancer Program, Mayo Clinic Cancer Center, Rochester, MN 55905 USA. ⁵Division of Oncology Research, Department of Oncology, Mayo Clinic, Rochester, MN 55905 USA. ⁶Department of Molecular Pharmacology & Experimental Therapeutics, Mayo Clinic, Rochester, MN 55905, USA.

* These authors contributed equally to this work

SUMMARY

The main physiological function of the APOBEC family of DNA cytosine deaminases is defending against viral infection and endogenous retroelement replication in human cells. Expression of one family member, APOBEC3B, has emerged as a major source of mutation in cancer with adverse pathological consequences. Other APOBEC family members may also contribute to carcinogenesis. However, given the known roles of this family in immunity, especially in T cells, detection of APOBECs in heterogeneous tumor specimens is likely to be confounded by immune cell infiltration. Because T cell infiltration has been shown to be a prognostic marker in high-grade serous ovarian cancer (HGSOC), we asked whether correlations exist between *APOBEC* gene expression and T cell markers in a cohort of 354 HGSOC patients. We identified a strong linear correlation between several T cell markers, including *CD3D*, *CD4*, *CD8A*, *GZMB*, and *PRF1*, and the expression of the HIV-1 restriction factor *APOBEC3G*, but not the cancer genome mutator *APOBEC3B*. Using clinical data, we show that high *APOBEC3G* expression correlates more significantly with improved overall and progression-free survival than the previously validated T cell markers listed above. Finally, we analyzed publically available RNA sequencing data and found that *APOBEC3G* expression correlates with the T cell marker, *CD3D*, across multiple cancer types. Additional correlations were seen between the other HIV restrictive *APOBEC3s* and *CD3D*, and between the antibody diversification gene, *AID*, and the B cell marker, *CD20*. Our results highlight the complexity of the tumor microenvironment and identify *APOBEC3G* as a new biomarker for HGSOC.

INTRODUCTION

In addition to genome instability, immune infiltration is an enabling hallmark of cancer (1). Both genome instability and immune infiltration have the unique capability of

driving several other hallmarks by increasing genetic and cellular heterogeneity, respectively. One challenge in the field of cancer genomics has been to resolve this dynamic and complex heterogeneity within the new wealth of deep sequencing data. Deconvolution of these data is not trivial because observed differences between cancer cells, immune infiltrates, and stromal cells complicate many experimental approaches including gene expression profiling and mutation calling.

Recently, the APOBECs have been implicated as drivers of cancer progression [(80,147,148) and references therein]. The APOBECs are an 11-member family of cytosine deaminases that convert cytosines to uracils (C-to-U) in ssDNA (48). Their enzymatic activity has been shown to be a critical component of both the adaptive and innate immune systems [(32) and references therein]. AID is arguably the most studied APOBEC due to its known roles in antibody diversification through somatic hypermutation and class switch recombination in B cells (33). APOBEC3D, F, G, and H are highly established restriction factors of human immunodeficiency virus-1 (HIV-1) replication in CD4+ T cells (34). All 4 of these APOBEC3s can be induced upon T cell activation or viral infection and are capable of introducing C-to-U lesions in viral cDNA intermediates that manifest as G-to-A mutations in proviral genomes (36,37,44).

While the APOBEC3s have been shown to have important physiologic roles in protecting cells from endogenous and exogenous pathogens, their dysregulation has also been linked to pathologic consequences. The most significant example is the recent finding that APOBEC3B is a major contributor of mutation in breast, ovarian, and several other cancers (13,21-23,74). APOBEC3B can deaminate cytosines to promutagenic uracil lesions in genomic DNA, which will result in mutations if they are not repaired properly. In addition, APOBEC3B is significantly upregulated in multiple cancers and its mutation signature is overrepresented in cancer genomes, which is defined by C-to-T/G mutations primarily in TCW trinucleotide contexts. Elevated expression of APOBEC3B

has also been linked to poor prognosis in estrogen receptor (ER)-positive breast cancers (26,27).

In addition to the identification of APOBEC3B as a major contributor to the mutations that drive cancer progression, other APOBECs have also been implicated as potential contributors to mutagenesis in cancer (50,65,149). Because many APOBEC family members are highly expressed in immune cells, a major confounding factor in the quantification of APOBEC expression levels from expression profiling of tumors is cellular heterogeneity driven by immune infiltration, as discussed above. To address this issue and determine the contribution of immune cell infiltrates to expression of the APOBECs within tumor samples, we first examined a cohort of high-grade serous ovarian carcinoma (HGSOC) samples, where increased expression of T cell markers is known to be associated with improved prognosis (76-79). We found a strong correlation between APOBEC3G expression and markers of T cell infiltration. Moreover, APOBEC3G was significantly associated with improved prognosis. We also applied these findings to multiple cancer types through an analysis of publically available RNA sequencing (RNAseq) data from The Cancer Genome Atlas (TCGA). Together our data elucidate the complexity of APOBEC expression profiling in heterogeneous tumor specimens and identify APOBEC3G as a new biomarker for HGSOC.

RESULTS

***APOBEC3G* expression correlates with T-cell activation in HGSOC**

APOBEC3D, F, G, and H are known to be highly expressed in T cells, where they form an overlapping innate immune defense against HIV-1 replication (36,37,44). Using a cohort of 354 primary HGSOC tumor samples, we asked whether one of these family members, *APOBEC3G*, also associates with T cell infiltrates in heterogeneous tumor samples (clinical characteristics in **Table 4.1**). In addition to *APOBEC3G*, we also

quantified *APOBEC3B* expression levels both as a negative control and because of its known role in ovarian cancer genome mutagenesis (74). To determine the relative amount of T cell infiltration we analyzed several markers, including *CD3D* (total T cells), *CD4* (helper T cells), *CD8A* (cytotoxic T cells), *GZMB* (activated cytotoxic T cells), *PRF1* (activated cytotoxic T cells), and *RNF128* (anergic T cells) (150,151). As expected, we did not observe any remarkable correlations between *APOBEC3B* and any of the T cell markers (**Fig. 4.1A-F**). We did find significant correlations between *APOBEC3G* and all T cell markers except *RNF128* which is a marker of T cell anergy (**Fig. 4.1G-L**). Interestingly, we found that *APOBEC3G* had a slightly stronger positive, linear correlation with *CD8A* than *CD4* (**Fig. 4.1H vs. 4.1I**), which is interesting because there have not been any studies focused on elucidating the function of *APOBEC3G* in cytotoxic T cells (CTLs). This discovery was further corroborated by additional correlations between *APOBEC3G* and two markers of CTL activation, *GZMB* and *PRF1* (**Fig. 4.1J and 4.1K**). The data shown here not only supported previous studies that describe *APOBEC3G* expression in T cells (44,45), but also show an unanticipated association between *APOBEC3G* and CTL activation.

***APOBEC3G* is a biomarker of improved patient outcomes in HGSOC**

Given the strong correlation between *APOBEC3G* expression and markers of T cell infiltration (**Fig. 4.1G-K**) and previous studies identifying T cell infiltration as a marker of improved patient outcomes in HGSOC (76-79), we next asked whether *APOBEC3G* could be a useful clinical biomarker for HGSOC patient outcomes. Long-term clinical follow-up data was available for all of the patients from which the above samples were taken. We used these clinical data and the expression profiling performed above to determine whether *APOBEC3G* expression could predict progression free survival (PFS) and/or overall survival (OS) in HGSOC. As a positive control we also

looked at the T cell markers above. Although we did not see a significant difference in PFS with respect to *CD3D* expression, we did observe significantly improved PFS in patients with tumor samples expressing higher levels of *CD4* and *PRF1* (**Fig. 4.2A**). A trend toward a similar result was also observed for *CD8A* and *GZMB* (**Fig. 4.2A**). As expected, *RNF128* did not correlate with PFS (**Fig. 4.2A**). Interestingly, *APOBEC3G* surpassed all of these genes as the most indicative marker of improved PFS in HGSOE (**Fig. 4.2A**). The results compiled from an analysis of OS largely mirrored those of PFS (**Fig. 4.2B**).

***APOBEC3B* expression is not significantly associated with patient outcomes in HGSOE**

APOBEC3B has recently been implicated as an endogenous mutagen in several human cancers [(80,147,148) and references therein], including ovarian cancer (74). Moreover, its expression has been linked to poor patient outcomes in ER-positive breast cancer (26,27). Using the expression data and clinical information from above, we asked if *APOBEC3B* affects patient outcomes in HGSOE. While there was a slight trend toward high *APOBEC3B* and improved, rather than worsened, outcome, we did not observe any striking correlation between *APOBEC3B* and patient outcome in HGSOE (**Fig. 4.2A and 4.2B**). These data suggest that *APOBEC3B* may not have as great of an effect on the ovarian cancer genome as it does in breast cancer.

***APOBEC* expression correlates with immune cell markers in multiple human cancers**

To apply our findings from HGSOE to several additional human cancers, we analyzed publically available RNAseq data from TCGA. At the time of these analyses, the TCGA had RNAseq data available for 7,861 samples spanning 22 different tumor

types (**Table 4.S1**). For each tumor type, we quantified the expression of the *APOBEC* family members and determined correlations with the T cell marker *CD3D* (**Fig. 4.3A**; heat map). We also performed hierarchical clustering to elucidate similar correlation patterns between cancer types (**Fig. 4.3A** and **4.3B**; dendrogram). These analyses revealed that, in addition to *APOBEC3G*, *APOBEC3D* and *H* also correlated significantly with *CD3D* across multiple cancer types (**Fig. 4.3A**). Interestingly, *APOBEC3F*, which is also known to restrict HIV replication, did not correlate as strongly. We also performed the same analysis with *CD20*, which is a well-known marker for B cells (**Fig 4.3B**). The expression of the antibody diversification gene, *AID*, was the only *APOBEC* family member that significantly correlated with *CD20* in a majority of cancer types (**Fig. 4.3B**). These analyses reveal that a majority of the expression of several *APOBEC* family members is likely due to T and B cell immune infiltrates into the tumor microenvironment of several cancer types.

DISCUSSION

The global and HGSOC specific analyses performed here have led to the identification of *APOBEC3G* as a novel biomarker for improved patient outcomes in HGSOC. Our analysis of a cohort of 354 HGSOC patients identified a strong correlation between *APOBEC3G* and several markers of T cell infiltration (**Fig 4.1G-K**). Furthermore, clinical data revealed that *APOBEC3G* also associates with improved outcome better than previously validated T cell markers (**Fig 4.2A** and **4.2B**). Finally, our global analysis across 22 cancer types identified a striking correlation between several additional HIV restrictive *APOBECs* and a marker of T cells, *CD3D*, in several heterogeneous tumor specimens from the TCGA (**Fig 4.3A**). Together, our data suggest that *APOBEC3G* predicts improved clinical outcomes by acting as a biomarker for anti-cancer T cell responses in heterogeneous tumor samples.

While APOBEC3B and AID remain the only substantially supported cytosine deaminases to catalyze cancer genome mutagenesis, several other APOBEC family members have been implicated as well (50,65,149). APOBEC3B is thought to contribute to cancer mutation in several human cancers, including breast, lung, bladder, cervical, head/neck, and ovarian cancer (13,21-23,74). Conversely, the carcinogenic effects of AID are more limited, as it has only been shown to cause certain types of B cell lymphomas (52,53). This idea is supported by our data showing that AID correlates with a marker of B cells in several solid tumor types (**Fig. 4.3B**). It has also been proposed that APOBEC3G drives hepatocellular carcinoma tumorigenesis (50). This is unlikely given that most of the APOBEC3G expression seen in primary tumor specimens is likely confined to T cell infiltrates (**Fig 4.1G-K and 4.3A**).

While we saw a strong correlation between *APOBEC3D*, *G*, and *H* and *CD3D* in our analysis of TCGA data, the correlation was substantially diminished for *APOBEC3F* (**Fig. 4.3A**). This is interesting because APOBEC3F is thought to play an equally important role in HIV-1 restriction in CD4+ T cells as APOBEC3D, G, and H, and prior studies have found that *APOBEC3F* is expressed at comparable levels to *APOBEC3D* and higher than *APOBEC3H* in human primary CD4+ T cells (36,37,44). Our data suggest that either *APOBEC3F* is not as consistently expressed in T cells associated with the tumor microenvironment or that *APOBEC3F* is highly expressed in other cell types within tumor samples. The latter is consistent with previous reports that *APOBEC3F* is readily detectable in several breast and ovarian cancer cell lines where immune infiltrates are not present (23,74).

It is also interesting that *APOBEC3G* correlates more significantly with cytotoxic T cell activation markers than *CD4* expression (**Fig. 4.1H vs. 4.1I-K**). The primary host cell for HIV replication is CD4+ T cells and it is here that APOBEC3G is known to restrict viral replication through the deamination of cDNA intermediates. Nevertheless, there has

been a previous study that detected *APOBEC3G* expression in CD8+ T cells isolated from primary peripheral blood mononuclear cells (45). Together, these data indicate that *APOBEC3G* may have additional roles in other cell types, such as cytotoxic T cells. Indeed, alternative functions have been suggested for this cytosine deaminase, including the restriction of endogenous retroelements (152) and the long-term evolutionary conflict between primates and retroviruses besides HIV-1 (153,154), both of which likely take place in multiple cell types.

Our parallel analysis to determine how *APOBEC3B* expression affects patient outcomes in HGSOE found that *APOBEC3B* does not have a major impact on clinical prognosis (**Fig 4.2A** and **4.2B**). This surprising finding differs significantly from breast cancer, where high *APOBEC3B* expression is associated with poor clinical outcome (26,27). One major difference between these two cancer types is the therapeutic options available for treatment. There are multiple targeted therapeutics available for the treatment of breast cancer that are administered based on molecular markers. In contrast, nearly all ovarian cancer patients are treated with frontline platinum-based therapies. Because platinum-based therapies induce DNA damage, it would also be interesting to determine if these drugs are synergistic with *APOBEC3B* catalyzed cytosine deamination and create a synthetic lethal state in cancer cells. This hypothesis is not unfounded as a study has shown that increased mutation loads correlates with improved clinical outcomes in HGSOE patients treated with cisplatin (155). Furthermore, a negative synergistic effect created by these two forms of DNA damage could explain the slight trend toward a correlation between increased *APOBEC3B* expression and improved outcomes. Another, and potentially more likely scenario, is that the levels of *APOBEC3B* mutagenesis in ovarian cancer are not high enough to manifest clinically. Indeed, the strength of the *APOBEC3B* mutation signature was not as strong in ovarian cancer as many other cancer types despite similar expression levels (13,21-23,74). The

underlying causes for this discrepancy are currently unknown, but several factors could be involved, including DNA repair efficiency and regulatory protein modifications. Regardless, more work is needed to determine the threshold of APOBEC3B mutagenesis needed to confer a clinical impact.

MATERIALS AND METHODS

Ovarian cancer cohort analysis

Primary tumor samples from 354 HGSOC patients were selected based on morphology, grade, stage, and availability of clinical outcome data (IRB #13-002487). TRIzol based RNA extractions were performed following crysectioning of each snap frozen tissue specimen. cDNA was synthesized in triplicate using Transcriptor Reverse Transcriptase (Roche) and RT-qPCR for *APOBEC3B*, *APOBEC3G*, *CD3D*, *CD4*, *CD8A*, *GZMB*, *PRF1*, *RNF128*, and *TBP* was performed using the primer and probe combinations listed in **Table 4.S2** and validation in **Fig 4.S1**. Correlations were determined using Spearman's correlation and Spearman's correlation coefficient (r_s) and p-values are reported. Kaplan-Meier plots were constructed in GraphPad Prism and p-values were calculated using the Mantel-Cox log-rank test.

TCGA analysis

The most recent version of all normalized RNAseqV2 data as of July 2015 was acquired from TCGA. mRNA expression for each *APOBEC* family member, *CD3D*, and *CD20* were quantified based on normalized read counts. r_s and p-values for linear models of *APOBEC* versus immune-marker genes were calculated using Spearman's correlation with the R statistical package.

Table 4.1 HGSOC clinical characteristics

| | Total (n=354) |
|------------------------------|---------------|
| Morphology | |
| Serous | 354 (100%) |
| Grade | |
| 2 | 11 (3.1%) |
| 3 | 343 (96.9%) |
| Stage | |
| 1 | 14 (3.9%) |
| 2 | 8 (2.3%) |
| 3 | 253 (71.5%) |
| 4 | 79 (22.3%) |
| Debulking Status | |
| No residual disease | 162 (45.8%) |
| <=1 cm remaining | 144 (40.7%) |
| <=1 cm remaining, possibly 0 | 48 (13.5%) |

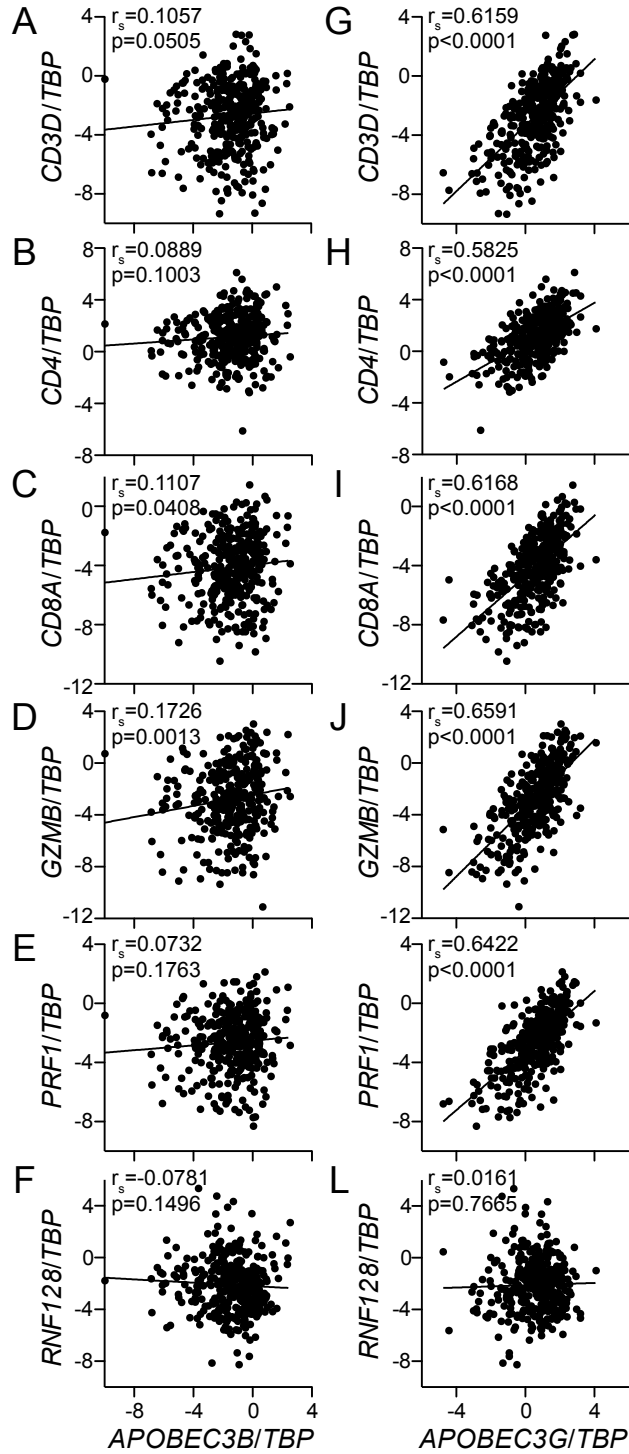


Figure 4.1 Correlations between *APOBEC3* expression and T cell markers in HGSOC.

Dot plots illustrating correlations between *APOBEC3B* (A-F) or *APOBEC3G* (G-L) expression and the indicated T cell marker. mRNA expression was determined using

RT-qPCR and all data was normalized to the housekeeping gene, *TBP*. Spearman's correlation coefficients (ρ) and p-values were calculated using Spearman's correlation. Best-fit lines are shown for qualitative comparison, and were calculated using linear regression models.

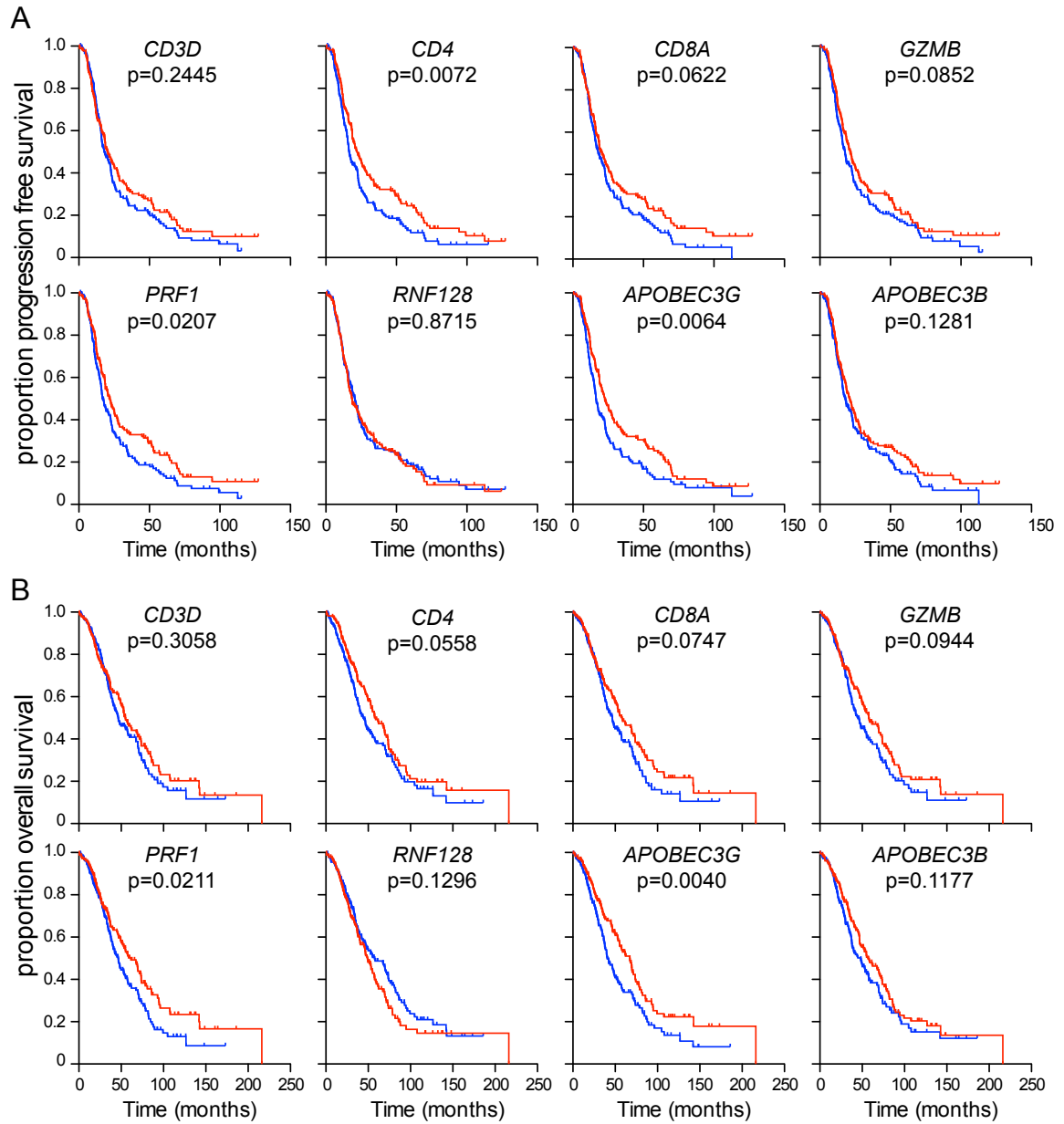


Figure 4.2 Clinical Correlates of *APOBEC3* and T cell marker expression in HGSOC.

Kaplan-Meier plots illustrating associations between progression free survival (**A**) or overall survival (**B**) and either one of the T cell markers or *APOBEC* expression. Samples were split at the median and p-values were calculated using the Mantel-Cox log-rank test.

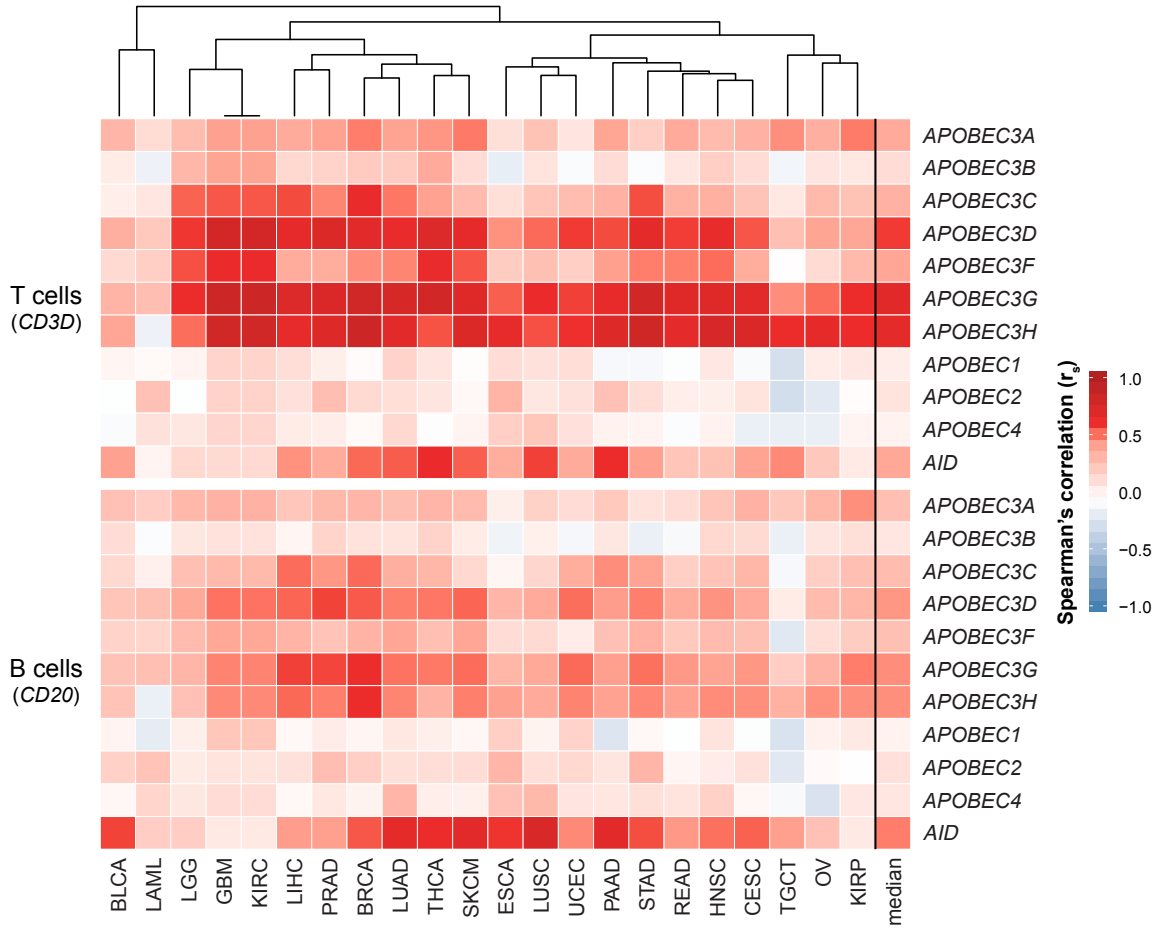


Figure 4.3 Correlations between *APOBEC* expression and immune cell markers across 22 cancer types.

Heat map of Spearman's correlation coefficients calculated from the comparison of *CD3D* (**A**) or *CD20* (**B**) with the indicated *APOBEC* family member. Expression levels were determined using TCGA RNAseq data. Annotation of the cancer abbreviations can be found in **Table 4.S1**. Dark red squares indicate strong positive correlations, dark blue squares indicate strong negative correlations and white squares indicate a lack of correlation.

Table 4.S1 Summary of samples used in TCGA analysis

| Cancer type | TCGA Abbreviation | Number of samples |
|---|------------------------------|--------------------------|
| Bladder urothelial carcinoma | BLCA | 408 |
| Breast invasive carcinoma | BRCA | 1,066 |
| Cervical squamous cell carcinoma and endocervical adenocarcinoma | CESC | 306 |
| Esophageal carcinoma | ESCA | 185 |
| Glioblastoma multiforme | GBM | 169 |
| Head and neck squamous cell carcinoma | HNSC | 521 |
| Kidney renal clear cell carcinoma | KIRC | 103 |
| Kidney renal papillary cell carcinoma | KIRP | 291 |
| Acute Myeloid Leukemia | LAML | 173 |
| Brain lower grade glioma | LGG | 534 |
| Liver hepatocellular carcinoma | LIHC | 327 |
| Lung adenocarcinoma | LUAD | 513 |
| Lung squamous cell carcinoma | LUSC | 502 |
| Ovarian serous cystadenocarcinoma | OV | 266 |
| Pancreatic adenocarcinoma | PAAD | 99 |
| Prostate adenocarcinoma | PRAD | 498 |
| Rectum adenocarcinoma | READ | 167 |
| Skin cutaneous melanoma | SKCM | 472 |
| Stomach adenocarcinoma | STAD | 415 |
| Testicular germ cell tumors | TGCT | 156 |
| Thyroid carcinoma | THCA | 513 |
| Uterine corpus endometrial carcinoma | UCEC | 177 |
| | Total | 7,861 |

Table 4.S2 RT-qPCR primer and probe sets

| Gene symbol | mRNA NCBI accession | 5' Primer sequence | 3' Primer sequence | Probe name |
|--------------------|----------------------------|----------------------------|---------------------------|-------------------|
| <i>APOBEC3B</i> | NM_004900 | gaccctttggtccttcgac | gcacagccccaggagaag | UPL1 |
| <i>APOBEC3G</i> | NM_021822 | ccgaggacccgaaggttac | tccaacagtgctgaaattcg | UPL79 |
| <i>CD3D</i> | NM_000732 | ctaccgtgcaagttcattatcg | aaggagcagagtggcaatga | UPL83 |
| <i>CD4</i> | NM_000616 | gatacttacatctgtgaagtggagga | agcaggtgggtgtcagagtt | UPL63 |
| <i>CD8A</i> | NM_001768 | tcatggccttaccagtgacc | aggttccagggtccgatcc | UPL51 |
| <i>GZMB</i> | NM_004131 | gagacgacttcgtgctgaca | ccccaagggtgacatttatgg | UPL60 |
| <i>PRF1</i> | NM_001083116 | ccgcttctctatacgggattc | gcagcagcaggagaaggat | UPL68 |
| <i>RNF128</i> | NM_024539 | gtgcacctcttgcccttacg | ccttttatttcacaacgacagaaa | UPL51 |
| <i>TBP</i> | NM_003194 | cccatgactcccatgacc | tttacaaccaagattcactgtgg | UPL51 |

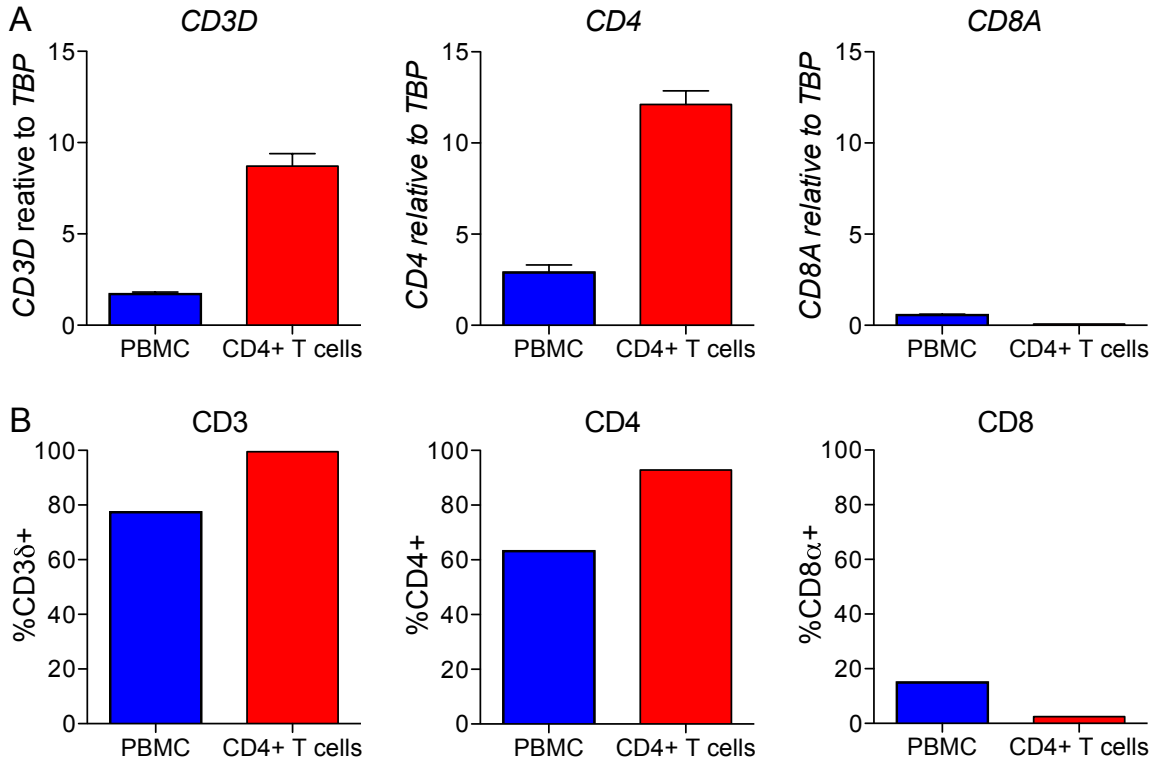


Figure 4.S1 Validation of RT-qPCR assays

(A) Histograms reporting mRNA levels of *CD3D*, *CD4*, and *CD8A* in peripheral blood mononuclear cells and CD4+ T cells isolated from the same donor. mRNA levels were quantified by RT-qPCR and represent the average of triplicate reactions. Error bars denote standard deviation (SD).

(B) Histograms reporting surface expression of CD3 δ , CD4, and CD8 α in peripheral blood mononuclear cells and CD4+ T cells isolated from the same donor. Each bar represents the percent of live cells that are positive for each marker as quantified by flow cytometry.

CHAPTER 5:
Conclusions and Discussion

Author: Brandon Leonard

Affiliations: Microbiology, Immunology and Cancer Biology Graduate Program,
University of Minnesota, Minneapolis, MN 55455, USA. Biochemistry, Molecular Biology
and Biophysics Department, University of Minnesota, Minneapolis, MN 55455, USA.
Masonic Cancer Center, University of Minnesota, Minneapolis, MN 55455, USA.

CONCLUSIONS

Chapter 2: APOBEC3B upregulation and genomic mutation patterns in serous ovarian carcinoma

Following our initial studies in breast cancer (23), we were interested in applying our findings of APOBEC3B mutagenesis to other cancer types. Given the similar mutation spectra observed in early sequencing studies of breast and ovarian cancer (73), we performed an in depth analysis of APOBEC3B expression and mutation in ovarian cancer [(74) and **Chapter 2**]. These studies identified *APOBEC3B* mRNA upregulation in a majority of ovarian cancer cell lines and primary tumors. Functional studies using a FRET-based DNA cytosine deaminase activity assay showed that *APOBEC3B* mRNA upregulation correlates with cytosine deaminase activity in several *APOBEC3B* high and low cell lines. Using the same assay, in combination with knockdown and fractionation procedures, we further revealed that APOBEC3B is responsible for all detectable cytosine deaminase activity and that this activity is primarily limited to the nuclear compartment. Furthermore, our collaborators at the Mayo Clinic had performed whole genome deep sequencing on 16 of the low stage ovarian tumors used in this study. We were able to use these data together with our *APOBEC3B* RT-qPCR results to positively correlate *APOBEC3B* mRNA expression with total numbers of mutations in these tumors. Interestingly, we found that there were more transversion mutations at C/G base pairs than transition mutations, suggesting that this is the major outcome of DNA damage at these sites in ovarian cancer. Consistent with this finding, we also saw a significant positive correlation between *APOBEC3B* mRNA expression and the total number of transversion mutations at C/G base pairs rather than transitions, which we had previously reported in breast cancer. The transversion mutations also appeared to be processed at the expense of transition mutations, as a trend toward a negative

correlation with transition mutations at C/G base pairs was observed. The APOBEC3B trinucleotide signature was also more enriched at the sites of transversions than transistions, further suggesting that APOBEC3B is in fact responsible for the initiation of transversion mutations in ovarian cancer.

Chapter 3: APOBEC3B upregulation by the PKC-NFκB pathway in multiple human cancers

The most common question that is asked when discussing the role of APOBEC3B in cancer mutation is: How does this protein become upregulated in cancer? We have, therefore, put much effort into answering this question, and have made advances in determining multiple pathways that contribute to APOBEC3B upregulation [(69,156) and **Chapter 3**]. Global analyses of APOBEC3B expression and signatures of mutation in cancer identified that cervical and head/neck cancer both had high APOBEC3B expression and an enrichment for the predicted APOBEC3B mutation signature (13,21,22). Because human papilloma virus (HPV) is known to be a major driver of these cancer types and the APOBEC3 family has well known roles in innate immunity to viral infections including HPV (35), we hypothesized that APOBEC3B upregulation in cancer may be a result of HPV infection. Indeed, several studies have shown this to be the case through functional experiments and bioinformatic analyses (16,69-72,117). Nevertheless, this mechanism can only explain APOBEC3B upregulation in the relatively small subset of cancers that are caused by HPV (i.e. >90% of cervical cancers (157) and ~13% of head/neck cancers (117)).

In the studies described in Chapter 3, we successfully determined a mechanism of APOBEC3B upregulation in non-viral cancers (156). Early studies examining genes altered by phorbol stimulation of oral keratinocytes were the first to clone a cDNA with sequence similarities to APOBEC3A and APOBEC3B (75). With this knowledge, we

were able to determine that PMA is capable of specifically upregulating APOBEC3B in several human cell lines, including the breast epithelial cell line, MCF10A. Using this cell line as a model system, we further determined that PMA signals through PKC α to activate non-canonical NF κ B driven transcription of the *APOBEC3B* locus. This was determined using a combination of pharmacologic, biochemical, genetic, and bioinformatic approaches. To extend these findings to cancer cells, we treated a panel of cancer cell lines with the pre-clinical PKC inhibitor, AEB071, and observed at least a 50% decrease in APOBEC3B expression in nearly half of the cell lines. In conclusion, we have identified a novel mechanism of APOBEC3B regulation in which alterations along the PKC-NF κ B signaling axis lead to increased expression of APOBEC3B in several tumor types.

Chapter 4: APOBEC3G expression correlates with T cell infiltration and improved clinical outcomes in high-grade serous ovarian carcinoma

Genetic and cellular heterogeneity often complicate the analysis of primary tumor specimens. While identifying cytosine deamination as a novel source of genetic heterogeneity in cancer has been a major focus of my thesis research, our lab is also interested in understanding how cellular heterogeneity within tumor samples can affect the detection of APOBEC expression. A focused study of high-grade serous ovarian cancer (HGSOC) showed that *APOBEC3G* closely associates with markers of T cell infiltration. The availability of clinical data allowed us to examine clinical outcome in our cohort, as well. Interestingly, high *APOBEC3G* expression correlates with improved outcomes. Based on our data and prior literature showing that additional T cell markers also correlate with improved outcomes in HGSOC (76-79), we hypothesize that APOBEC3G is a biomarker for anti-tumor immune responses. In addition to these findings, we also determined that *APOBECB* does not significantly associate with clinical

outcome in HGSOC. This is in contrast to multiple publications identifying APOBEC3B as a positive prognostic marker in estrogen receptor (ER)-positive breast cancer (26,27), and suggests that an effective anti-tumor immune response may outweigh the mutagenic contribution from APOBEC3B in ovarian cancer cells. Finally, we apply our findings in HGSOC to several other cancer types by performing a bioinformatic analysis of publicly available RNA sequencing (RNAseq) data from the The Cancer Genome Atlas (TCGA), and show correlations between several HIV-1 restrictive *APOBEC3* family members and the T cell marker, *CD3D*.

DISCUSSION

In depth vs global analyses of mutation signatures

Our studies of ovarian cancer in conjunction with global analyses of mutation signatures in cancer highlight the importance of in depth analyses in individual cancer types. Several studies mining publically available data sets of thousands of tumor genomes (primarily exomic regions) were unable to identify a significant APOBEC3B mutation signature in ovarian cancer (13,21,22). Conversely, the work shown here elucidates a distinguishable APOBEC3B mutation signature in whole genome sequences of just 16 ovarian tumors [(74) and **Chapter 2**]. Multiple factors may contribute to these differential results. First, whole genome sequencing is likely to allow for a more accurate quantification of mutation signature than exome sequencing, since, on average, over 10-fold more mutations were detected in each tumor used in our study. This is significant because some of the TCGA tumors had as few as 2 somatic mutations in their exomes (83). Second, it is important to carefully choose the samples used in any mutational analysis. Many of the treatments for ovarian and other cancers are mutation-inducing genotoxic agents, and, therefore, these drugs are likely to skew the mutation spectra and hide signatures of additional sources of mutation. Samples taken from

patients that have not been treated with DNA damaging agents are therefore important for mutation analyses. Furthermore, the stage and grade of the specimens should be considered as the age and aggressiveness of the tumor can also have an effect on mutation loads. Overall, in depth study of individual cancer types are likely to identify additional mutation sources that may be overlooked by large-scale analyses.

Fundamental differences between APOBEC3B catalyzed mutation in breast and ovarian cancer

A recent publication from the TCGA identified several similarities between a specific subtype of breast cancer called triple negative breast cancer (TNBC) and HGSOE (91). Of note, these analyses revealed comparable frequently mutated genes (including *TP53*, *RB1*, and *BRCA1/2*), mRNA expression profiles, and responses to platinum-based drugs and taxanes as therapeutic approaches for these cancer types. Interestingly, our studies highlight some of the differences observed between breast and ovarian cancer with respect to APOBEC3B catalyzed mutation. These distinctions are discussed below.

First, the mutagenic outcome of cytosine deamination is different in breast and ovarian cancer [(23,74) and **Chapter 2**]. While both observations are substantiated by work on AID in antibody diversification (33), it is interesting to speculate on the underlying mechanisms responsible for differential uracil repair in cancer. In breast cancer, the most likely source of the observed correlation between APOBEC3B and transition mutations is a lack of effective uracil excision, which forces uracils to go through DNA replication. Uracil is known to template as a T and the resulting C-to-T mutation will be fixed in the genome following an additional round of DNA synthesis. It is possible that, in ovarian cancer, increased uracil excision rates create abasic sites that act as substrates for translesion DNA synthesis. It is currently unknown whether there

are differential rates of uracil excision in these two cancer types, but functional studies have shown that eliminating uracil excision or translesion synthesis in yeast results in a loss of transversion mutations resulting from active DNA cytosine deamination (28,59). If the underlying pathways are identified in human cancer cells, they may provide a new therapeutic intervention strategy aimed at increasing APOBEC3B mutagenesis through inhibition of the dominant uracil processing pathways. This strategy has been termed synthetic lethality and is currently being leveraged clinically through the use of PARP inhibitors in BRCA1/2 mutant tumors [(158,159) and reviewed recently by (160)].

Second, the enrichment of the APOBEC3B signature was significantly less than that of breast cancer (21-23,74). This was a surprising observation given that *APOBEC3B* mRNA overexpression in these tumor types is nearly identical (21,23,74). At the time of these studies, antibodies capable of detecting endogenous APOBEC3B protein levels were not available, so the correlation between APOBEC3B mRNA and protein expression was unclear. Some studies since, including the data presented in Chapter 3, have shown a close association between APOBEC3B mRNA and protein expression, suggesting that this discrepancy is likely not due to differential protein expression. Future studies will be needed to determine whether APOBEC3B is regulated at the posttranslational level, including protein modification, negative regulation through interactions with other proteins and/or nucleic acids, or the requirement for a binding partner for catalytic activity as has been shown for APOBEC1 and RNA binding proteins ACF and RBM47 (161,162). An additional confounding factor may be that the repair of uracil lesions is more efficient in ovarian cancer samples or that the repair pathway utilized in ovarian cancer introduces a mutation signature of its own.

Third, is that APOBEC3B does not have a clear clinical impact in ovarian cancer as it does in ER-positive breast cancer (26,27). This discrepancy may be explained by several of the above discussion points, including the weaker mutation signature

observed in ovarian cancer genomes and complications due to differential therapeutic options. The most probable source of the difference in clinical impact is that the enrichment of the APOBEC3B mutation signature in ovarian cancer genomes is weaker than breast cancer [(23,74) (21) and **Chapter 2**]. As discussed above, additional studies will be needed to determine why the mutation signature is not as evident in ovarian cancer. An alternative hypothesis is that the many targeted therapies available to treat breast cancer are more susceptible to resistance driven by APOBEC3B catalyzed mutation. In fact, some studies have found that resistance can be acquired with only one mutation (163-165). This is in stark contrast to the therapeutic options approved for the treatment of ovarian cancer. Nearly all ovarian cancers are initially treated with cisplatin and the underlying reasons why over half of patients relapse are not well defined. If this is the case, it may be important to avoid treating tumors expressing high levels of APOBEC3B with certain targeted therapies.

Elucidating the complete APOBEC3B regulatory network in cancer

While HPV infection and activation of the PKC-NFκB pathway have the potential to explain a majority of APOBEC3B upregulation in cancer, several observations indicate that there may also be additional mechanisms. The clearest evidence is that several of the known HPV negative cell lines analyzed above did not show significant downregulation of APOBEC3B expression upon PKC inhibition. This is particularly evident in bladder cancer. Several alternative hypotheses must be tested to determine why this is the case. First, activation of the PKC-NFκB pathway may take place downstream of PKC. Activation of these proteins would eliminate the dependency on PKC and could explain the lack of an effect upon PKC inhibition. To conclusively test this hypothesis, better inhibitors for these downstream proteins need to be developed. Second, there may be alternative ways of activating non-canonical NFκB signaling. For

example, it is known that lymphotoxin- β receptor mediated activation of NIK is a potent agonist of this pathway (135,136). This hypothesis could be test by either stimulating this pathway with lymphotoxin- β ligand or inhibiting the pathway with either lymphotoxin- β receptor blocking antibodies or NIK inhibitors. Third, there may be one or more completely independent mechanisms present in the nonresponsive cell lines, especially those that are derived from bladder tumors. This may be the case since no correlations have been identified between APOBEC3B and the expression of other genes within large publically available sequencing datasets, suggesting that the complete transcriptional regulatory network of APOBEC3B expression in cancer may be complex.

It is also interesting to speculate whether the mechanism responsible for upregulation of APOBEC3B expression by HPV infection feeds into the PKC-NF κ B axis or if this is a completely independent pathway. As stated above, parallel studies suggests that the E6 oncoprotein encoded by HPV is sufficient to induce APOBEC3B expression in cervical and head/neck cancer (69). E6 is known to degrade the tumor suppressor TP53 (166,167), suggesting that HPV could alleviate APOBEC3B transcriptional repression through the degradation of TP53 by E6. While this mechanistic linkage needs to be tested experimentally, it is consistent with our finding that APOBEC3B upregulation correlates with TP53 mutation in breast cancer cell lines (23). It is also possible that the mechanism employed by HPV converges with the regulatory pathway elucidated here. Indeed, there is evidence that HPV E6 can stimulate NF κ B signaling (168-171).

Our studies also suggest a new strategy for the inhibition of APOBEC3B catalyzed mutagenesis in cancer through transcriptional downregulation of APOBEC3B expression using inhibitors of the PKC-NF κ B pathway. In fact, the AEB071 PKC inhibitor used throughout our work has shown promising results in preclinical and clinical studies as an anti-cancer agent (131-134). While the goal of this approach would not necessarily

be to kill cancer cells, inhibitors of the PKC-NFκB pathway may be used to decrease A3B mutagenesis in order to reduce the likelihood of drug resistance and recurrence.

Developing *APOBEC3G* as a biomarker in ovarian cancer

In addition to our discovery of the impact and regulation of *APOBEC3B* in ovarian cancer, our comprehensive clinical analysis of *APOBEC3* expression in HGSOV also identified *APOBEC3G* as positive prognostic marker (**Chapter 4**). The correlations between *APOBEC3G* expression and markers of T cell infiltration together with previous work demonstrating that several T cell markers correlate with improved prognosis (76-79), indicate that *APOBEC3G* functions in a similar capacity. In fact, *APOBEC3G* correlated more significantly with improved outcomes than several canonical T cell markers, including *CD3D*, *CD4*, *CD8A*, *GZMB1*, and *PRF1*. These studies must be coupled with additional functional studies to determine why *APOBEC3G* correlates strongly with CTL activation, since nearly all of the research performed on *APOBEC3G* has focused on CD4+ T cell biology. It would also be interesting to determine if this anti-tumor CTL response helps to explain the lack of a clinical effect that *APOBEC3B* has on ovarian cancer. Perhaps this response shadows the effect of *APOBEC3B* catalyzed mutation in ovarian cancer cells.

CLOSING REMARKS

Cancer is a major health concern in the United States and worldwide. Over 1,500 people die from this disease every day in the United states alone (172). Because many of the aggressive characteristics that lead to poor outcomes for cancer patients are driven by tumor heterogeneity, a more comprehensive understanding of the sources of this diversity will likely lead to new and improved therapies. This is especially true for ovarian cancer where genetic diversity driven genomic instability is a major underlying

cause of tumorigenesis (83) and few therapeutic options are available. The main goal of my thesis research has been to determine how the DNA cytosine deaminase, APOBEC3B, contributes to genetic diversity in ovarian cancer with the ultimate goal of making a translational impact on patient outcomes. Here, I show that APOBEC3B upregulation leads to increased mutation in ovarian cancer genomes (**Chapter 2**) and that the PKC-NF κ B pathway drives this upregulation in multiple human cancers (**Chapter 3**). These findings suggest new therapeutic strategies aimed at leveraging existing PKC inhibitors to transcriptionally downregulated APOBEC3B, slow tumor evolution, lengthen the durability of existing anti-cancer drugs and improve patient outcomes.

BIBLIOGRAPHY

1. Hanahan D, Weinberg RA. Hallmarks of cancer: the next generation. *Cell*. 2011;144:646–74.
2. Pfeifer GP, You Y-H, Besaratinia A. Mutations induced by ultraviolet light. *Mutat Res*. 2005;571:19–31.
3. Lo JA, Fisher DE. The melanoma revolution: from UV carcinogenesis to a new era in therapeutics. *Science*. 2014;346:945–9.
4. Proctor RN. Tobacco and the global lung cancer epidemic. *Nat Rev Cancer*. 2001;1:82–6.
5. Wiencke JK. DNA adduct burden and tobacco carcinogenesis. *Oncogene*. 2002;21:7376–91.
6. King M-C, Marks JH, Mandell JB, New York Breast Cancer Study Group. Breast and ovarian cancer risks due to inherited mutations in BRCA1 and BRCA2. *Science*. 2003;302:643–6.
7. Tutt A, Ashworth A. The relationship between the roles of BRCA genes in DNA repair and cancer predisposition. *Trends Mol Med*. 2002;8:571–6.
8. D'Andrea AD, Grompe M. The Fanconi anaemia/BRCA pathway. *Nat Rev Cancer*. 2003;3:23–34.
9. Fishel R, Lescoe MK, Rao MRS, Copeland NG, Jenkins NA, Garber J, et al. The human mutator gene homolog MSH2 and its association with hereditary nonpolyposis colon cancer. *Cell*. 1993;75:1027–38.
10. Bronner CE, Baker SM, Morrison PT, Warren G, Smith LG, Lescoe MK, et al. Mutation in the DNA mismatch repair gene homologue hMLH1 is associated with hereditary non-polyposis colon cancer. *Nature*. 1994;368:258–61.
11. Papadopoulos N, Nicolaidis NC, Wei YF, Ruben SM, Carter KC, Rosen CA, et al. Mutation of a mutL homolog in hereditary colon cancer. *Science*.

1994;263:1625–9.

12. Barnes DE, Lindahl T. Repair and genetic consequences of endogenous DNA base damage in mammalian cells. *Annu Rev Genet.* 2004;38:445–76.
13. Alexandrov LB, Nik-Zainal S, Wedge DC, Aparicio SAJR, Behjati S, Biankin AV, et al. Signatures of mutational processes in human cancer. *Nature.* 2013;500:415–21.
14. Nik-Zainal S, Alexandrov LB, Wedge DC, Van Loo P, Greenman CD, Raine K, et al. Mutational processes molding the genomes of 21 breast cancers. *Cell.* 2012;149:979–93.
15. Lawrence MS, Stojanov P, Polak P, Kryukov GV, Cibulskis K, Sivachenko A, et al. Mutational heterogeneity in cancer and the search for new cancer-associated genes. *Nature.* 2013;499:214–8.
16. Henderson S, Chakravarthy A, Su X, Boshoff C, Fenton TR. APOBEC-mediated cytosine deamination links PIK3CA helical domain mutations to human papillomavirus-driven tumor development. *Cell Rep.* 2014;7:1833–41.
17. de Bruin EC, McGranahan N, Mitter R, Salm M, Wedge DC, Yates L, et al. Spatial and temporal diversity in genomic instability processes defines lung cancer evolution. *Science.* 2014;346:251–6.
18. Zhang L, Zhou Y, Cheng C, Cui H, Cheng L, Kong P, et al. Genomic analyses reveal mutational signatures and frequently altered genes in esophageal squamous cell carcinoma. *Am J Hum Genet.* 2015;96:597–611.
19. Patch A-M, Christie EL, Etemadmoghadam D, Garsed DW, George J, Fereday S, et al. Whole-genome characterization of chemoresistant ovarian cancer. *Nature.* 2015;521:489–94.
20. Poon SL, Pang S-T, McPherson JR, Yu W, Huang KK, Guan P, et al. Genome-wide mutational signatures of aristolochic acid and its application as a screening

- tool. *Sci Transl Med*. 2013;5:197ra101.
21. Burns MB, Temiz NA, Harris RS. Evidence for APOBEC3B mutagenesis in multiple human cancers. *Nat Genet*. 2013;45:977–83.
 22. Roberts SA, Lawrence MS, Klimczak LJ, Grimm SA, Fargo D, Stojanov P, et al. An APOBEC cytidine deaminase mutagenesis pattern is widespread in human cancers. *Nat Genet*. 2013;45:970–6.
 23. Burns MB, Lackey L, Carpenter MA, Rathore A, Land AM, Leonard B, et al. APOBEC3B is an enzymatic source of mutation in breast cancer. *Nature*. 2013;494:366–70.
 24. Cancer Genome Atlas Research Network. Comprehensive molecular characterization of urothelial bladder carcinoma. *Nature*. 2014;507:315–22.
 25. Rebhandl S, Huemer M, Gassner FJ, Zaborsky N, Hebenstreit D, Catakovic K, et al. APOBEC3 signature mutations in chronic lymphocytic leukemia. *Leukemia*. 2014;28:1929–32.
 26. Sieuwerts AM, Willis S, Burns MB, Look MP, Meijer-Van Gelder ME, Schlicker A, et al. Elevated APOBEC3B correlates with poor outcomes for estrogen-receptor-positive breast cancers. *Horm Cancer*. 2014;5:405–13.
 27. Cescon DW, Haibe-Kains B, Mak TW. APOBEC3B expression in breast cancer reflects cellular proliferation, while a deletion polymorphism is associated with immune activation. *Proceedings of the National Academy of Sciences*. 2015;112:2841–6.
 28. Taylor BJ, Nik-Zainal S, Wu YL, Stebbings LA, Raine K, Campbell PJ, et al. DNA deaminases induce break-associated mutation showers with implication of APOBEC3B and 3A in breast cancer kataegis. *Elife*. 2013;2:e00534.
 29. Shinohara M, Ito K, Shindo K, Matsui M, Sakamoto T, Tada K, et al. APOBEC3B can impair genomic stability by inducing base substitutions in genomic DNA in

- human cells. *Sci Rep.* 2012;2:806.
30. Teng B, Burant CF, Davidson NO. Molecular cloning of an apolipoprotein B messenger RNA editing protein. *Science.* 1993;260:1816–9.
 31. Conticello SG. The AID/APOBEC family of nucleic acid mutators. *Genome Biol.* 2008;9:229.
 32. Refsland EW, Harris RS. The APOBEC3 family of retroelement restriction factors. *Curr Top Microbiol Immunol.* 2013;371:1–27.
 33. Di Noia JM, Neuberger MS. Molecular mechanisms of antibody somatic hypermutation. *Annu Rev Biochem.* 2007;76:1–22.
 34. Harris RS, Hultquist JF, Evans DT. The restriction factors of human immunodeficiency virus. *Journal of Biological Chemistry.* 2012;287:40875–83.
 35. Vieira VC, Soares MA. The role of cytidine deaminases on innate immune responses against human viral infections. *Biomed Res Int.* 2013;2013:683095.
 36. Hultquist JF, Lengyel JA, Refsland EW, LaRue RS, Lackey L, Brown WL, et al. Human and rhesus APOBEC3D, APOBEC3F, APOBEC3G, and APOBEC3H demonstrate a conserved capacity to restrict Vif-deficient HIV-1. *Journal of Virology.* 2011;85:11220–34.
 37. Refsland EW, Hultquist JF, Harris RS. Endogenous origins of HIV-1 G-to-A hypermutation and restriction in the nonpermissive T cell line CEM2n. *PLoS Pathog.* 2012;8:e1002800.
 38. Stenglein MD, Harris RS. APOBEC3B and APOBEC3F inhibit L1 retrotransposition by a DNA deamination-independent mechanism. *Journal of Biological Chemistry.* 2006;281:16837–41.
 39. Bogerd HP, Wiegand HL, Doehle BP, Lueders KK, Cullen BR. APOBEC3A and APOBEC3B are potent inhibitors of LTR-retrotransposon function in human cells. *Nucleic Acids Res.* 2006;34:89–95.

40. Stenglein MD, Burns MB, Li M, Lengyel J, Harris RS. APOBEC3 proteins mediate the clearance of foreign DNA from human cells. *Nat Struct Mol Biol.* 2010;17:222–9.
41. Bulliard Y, Narvaiza I, Bertero A, Peddi S, Röhrig UF, Ortiz M, et al. Structure-function analyses point to a polynucleotide-accommodating groove essential for APOBEC3A restriction activities. *Journal of Virology.* 2011;85:1765–76.
42. Carpenter MA, Li M, Rathore A, Lackey L, Law EK, Land AM, et al. Methylcytosine and normal cytosine deamination by the foreign DNA restriction enzyme APOBEC3A. *Journal of Biological Chemistry.* 2012;287:34801–8.
43. LaRue RS, Jónsson SR, Silverstein KAT, Lajoie M, Bertrand D, El-Mabrouk N, et al. The artiodactyl APOBEC3 innate immune repertoire shows evidence for a multi-functional domain organization that existed in the ancestor of placental mammals. *BMC Mol Biol.* 2008;9:104.
44. Refsland EW, Stenglein MD, Shindo K, Albin JS, Brown WL, Harris RS. Quantitative profiling of the full APOBEC3 mRNA repertoire in lymphocytes and tissues: implications for HIV-1 restriction. *Nucleic Acids Res.* 2010;38:4274–84.
45. Koning FA, Newman ENC, Kim E-Y, Kunstman KJ, Wolinsky SM, Malim MH. Defining APOBEC3 expression patterns in human tissues and hematopoietic cell subsets. *Journal of Virology.* 2009;83:9474–85.
46. Yamanaka S, Balestra ME, Ferrell LD, Fan J, Arnold KS, Taylor S, et al. Apolipoprotein B mRNA-editing protein induces hepatocellular carcinoma and dysplasia in transgenic animals. *Proceedings of the National Academy of Sciences.* 1995;92:8483–7.
47. Saraconi G, Severi F, Sala C, Mattiuz G, Conticello SG. The RNA editing enzyme APOBEC1 induces somatic mutations and a compatible mutational signature is present in esophageal adenocarcinomas. *Genome Biol.* 2014;15:417.

48. Harris RS, Petersen-Mahrt SK, Neuberger MS. RNA editing enzyme APOBEC1 and some of its homologs can act as DNA mutators. *Mol Cell*. 2002;10:1247–53.
49. Petersen-Mahrt SK, Harris RS, Neuberger MS. AID mutates *E. coli* suggesting a DNA deamination mechanism for antibody diversification. *Nature*. 2002;418:99–103.
50. Ding Q, Chang C-J, Xie X, Xia W, Yang J-Y, Wang S-C, et al. APOBEC3G promotes liver metastasis in an orthotopic mouse model of colorectal cancer and predicts human hepatic metastasis. *J Clin Invest*. 2011;121:4526–36.
51. Okazaki I-M, Hiai H, Kakazu N, Yamada S, Muramatsu M, Kinoshita K, et al. Constitutive expression of AID leads to tumorigenesis. *Journal of Experimental Medicine*. 2003;197:1173–81.
52. Robbiani DF, Nussenzweig MC. Chromosome translocation, B cell lymphoma, and activation-induced cytidine deaminase. *Annu Rev Pathol*. 2013;8:79–103.
53. Ramiro AR, Jankovic M, Eisenreich T, Difilippantonio S, Chen-Kiang S, Muramatsu M, et al. AID Is Required for c-myc/IgH Chromosome Translocations In Vivo. *Cell*. 2004;118:431–8.
54. Lackey L, Demorest ZL, Land AM, Hultquist JF, Brown WL, Harris RS. APOBEC3B and AID have similar nuclear import mechanisms. *J Mol Biol*. 2012;419:301–14.
55. Lackey L, Law EK, Brown WL, Harris RS. Subcellular localization of the APOBEC3 proteins during mitosis and implications for genomic DNA deamination. *Cell Cycle*. 2013;12:762–72.
56. Stenglein MD, Matsuo H, Harris RS. Two regions within the amino-terminal half of APOBEC3G cooperate to determine cytoplasmic localization. *Journal of Virology*. 2008;82:9591–9.
57. Pak V, Heidecker G, Pathak VK, Derse D. The role of amino-terminal sequences in cellular localization and antiviral activity of APOBEC3B. *Journal of Virology*.

2011;85:8538–47.

58. Krokan HE, Sætrom P, Aas PA, Pettersen HS, Kavli B, Slupphaug G. Error-free versus mutagenic processing of genomic uracil--relevance to cancer. *DNA Repair (Amst)*. 2014;19:38–47.
59. Chan K, Resnick MA, Gordenin DA. The choice of nucleotide inserted opposite abasic sites formed within chromosomal DNA reveals the polymerase activities participating in translesion DNA synthesis. *DNA Repair (Amst)*. 2013;12:878–89.
60. Kidd JM, Newman TL, Tuzun E, Kaul R, Eichler EE. Population stratification of a common APOBEC gene deletion polymorphism. *PLoS Genet*. 2007;3:e63.
61. Komatsu A, Nagasaki K, Fujimori M, Amano J, Miki Y. Identification of novel deletion polymorphisms in breast cancer. *Int J Oncol*. 2008;33:261–70.
62. Xuan D, Li G, Cai Q, Deming-Halverson S, Shrubsole MJ, Shu X-O, et al. APOBEC3 deletion polymorphism is associated with breast cancer risk among women of European ancestry. *Carcinogenesis*. 2013;34:2240–3.
63. Long J, Delahanty RJ, Li G, Gao Y-T, Lu W, Cai Q, et al. A common deletion in the APOBEC3 genes and breast cancer risk. *J Natl Cancer Inst*. 2013;105:573–9.
64. Qi G, Xiong H, Zhou C. APOBEC3 deletion polymorphism is associated with epithelial ovarian cancer risk among Chinese women. *Tumour Biol*. 2014;35:5723–6.
65. Nik-Zainal S, Wedge DC, Alexandrov LB, Petljak M, Butler AP, Bolli N, et al. Association of a germline copy number polymorphism of APOBEC3A and APOBEC3B with burden of putative APOBEC-dependent mutations in breast cancer. *Nat Genet*. 2014;46:487–91.
66. Land AM, Law EK, Carpenter MA, Lackey L, Brown WL, Harris RS. Endogenous APOBEC3A DNA cytosine deaminase is cytoplasmic and nongenotoxic. *Journal of Biological Chemistry*. 2013;288:17253–60.

67. Thielen BK, McNevin JP, McElrath MJ, Hunt BVS, Klein KC, Lingappa JR. Innate immune signaling induces high levels of TC-specific deaminase activity in primary monocyte-derived cells through expression of APOBEC3A isoforms. *Journal of Biological Chemistry*. 2010;285:27753–66.
68. Hausen zur H. Papillomaviruses in the causation of human cancers - a brief historical account. *Virology*. 2009;384:260–5.
69. Vieira VC, Leonard B, White EA, Starrett GJ, Temiz NA, Lorenz LD, et al. Human papillomavirus E6 triggers upregulation of the antiviral and cancer genomic DNA deaminase APOBEC3B. *MBio*. 2014;5:e02234–14.
70. Warren CJ, Xu T, Guo K, Griffin LM, Westrich JA, Lee D, et al. APOBEC3A functions as a restriction factor of human papillomavirus. *Journal of Virology*. 2015;89:688–702.
71. Mori S, Takeuchi T, Ishii Y, Kukimoto I. Identification of APOBEC3B promoter elements responsible for activation by human papillomavirus type 16 E6. *Biochem Biophys Res Commun*. 2015;460:555–60.
72. Ohba K, Ichiyama K, Yajima M, Gemma N, Nikaido M, Wu Q, et al. *in vivo* and *in vitro* studies suggest a possible involvement of HPV infection in the early stage of breast carcinogenesis via APOBEC3B induction. *PLoS ONE*. 2014;9:e97787.
73. Greenman C, Stephens P, Smith R, Dalgliesh GL, Hunter C, Bignell G, et al. Patterns of somatic mutation in human cancer genomes. *Nature*. 2007;446:153–8.
74. Leonard B, Hart SN, Burns MB, Carpenter MA, Temiz NA, Rathore A, et al. APOBEC3B upregulation and genomic mutation patterns in serous ovarian carcinoma. *Cancer Research*. 2013;73:7222–31.
75. Madsen P, Anant S, Rasmussen HH, Gromov P, Vorum H, Dumanski JP, et al. Psoriasis upregulated phorbolin-1 shares structural but not functional similarity

- to the mRNA-editing protein apobec-1. *Journal of Investigative Dermatology*.
Nature Publishing Group; 1999;113:162–9.
76. Callahan MJ, Nagymanyoki Z, Bonome T, Johnson ME, Litkouhi B, Sullivan EH, et al. Increased HLA-DMB expression in the tumor epithelium is associated with increased CTL infiltration and improved prognosis in advanced-stage serous ovarian cancer. *Clin Cancer Res*. 2008;14:7667–73.
 77. Nielsen JS, Sahota RA, Milne K, Kost SE, Nesslinger NJ, Watson PH, et al. CD20+ tumor-infiltrating lymphocytes have an atypical CD27- memory phenotype and together with CD8+ T cells promote favorable prognosis in ovarian cancer. *Clin Cancer Res*. 2012;18:3281–92.
 78. Milne K, Köbel M, Kalloger SE, Barnes RO, Gao D, Gilks CB, et al. Systematic analysis of immune infiltrates in high-grade serous ovarian cancer reveals CD20, FoxP3 and TIA-1 as positive prognostic factors. *PLoS ONE*. 2009;4:e6412.
 79. Han LY, Fletcher MS, Urbauer DL, Mueller P, Landen CN, Kamat AA, et al. HLA class I antigen processing machinery component expression and intratumoral T-Cell infiltrate as independent prognostic markers in ovarian carcinoma. *Clin Cancer Res*. 2008;14:3372–9.
 80. Burns MB, Leonard B, Harris RS. APOBEC3B: pathological consequences of an innate immune DNA mutator. *Biomedical Journal*. 2015;38:102–10.
 81. Hultquist JF, Harris RS. Leveraging APOBEC3 proteins to alter the HIV mutation rate and combat AIDS. *Future Virol*. 2009;4:605.
 82. Siegel R, Naishadham D, Jemal A. Cancer statistics, 2013. *CA Cancer J Clin*. 2013;63:11–30.
 83. Cancer Genome Atlas Research Network. Integrated genomic analyses of ovarian carcinoma. *Nature*. 2011;474:609–15.
 84. Walsh T, Casadei S, Lee MK, Pennil CC, Nord AS, Thornton AM, et al. Mutations

- in 12 genes for inherited ovarian, fallopian tube, and peritoneal carcinoma identified by massively parallel sequencing. *Proceedings of the National Academy of Sciences*. 2011;108:18032–7.
85. Kelland L. The resurgence of platinum-based cancer chemotherapy. *Nat Rev Cancer*. 2007;7:573–84.
 86. Markman M. Antineoplastic agents in the management of ovarian cancer: current status and emerging therapeutic strategies. *Trends Pharmacol Sci*. 2008;29:515–9.
 87. Norquist B, Wurz KA, Pennil CC, Garcia R, Gross J, Sakai W, et al. Secondary somatic mutations restoring BRCA1/2 predict chemotherapy resistance in hereditary ovarian carcinomas. *J Clin Oncol*. 2011;29:3008–15.
 88. Pasqualucci L, Bhagat G, Jankovic M, Compagno M, Smith P, Muramatsu M, et al. AID is required for germinal center-derived lymphomagenesis. *Nat Genet*. 2008;40:108–12.
 89. Klemm L, Duy C, Iacobucci I, Kuchen S, Levetzow von G, Feldhahn N, et al. The B cell mutator AID promotes B lymphoid blast crisis and drug resistance in chronic myeloid leukemia. *Cancer Cell*. 2009;16:232–45.
 90. Lohr JG, Stojanov P, Lawrence MS, Auclair D, Chapuy B, Sougnez C, et al. Discovery and prioritization of somatic mutations in diffuse large B-cell lymphoma (DLBCL) by whole-exome sequencing. *Proceedings of the National Academy of Sciences*. 2012;109:3879–84.
 91. Cancer Genome Atlas Network. Comprehensive molecular portraits of human breast tumours. *Nature*. 2012;490:61–70.
 92. Smith NL, Welch P, Press JZ, Agnew KJ, Garcia R, Swisher EM. E2F3b over-expression in ovarian carcinomas and in BRCA1 haploinsufficient fallopian tube epithelium. *Genes Chromosomes Cancer*. 2012;51:1054–62.

93. Rausch JW, Chelico L, Goodman MF, Le Grice SFJ. Dissecting APOBEC3G substrate specificity by nucleoside analog interference. *Journal of Biological Chemistry*. 2009;284:7047–58.
94. Kohli RM, Maul RW, Guminski AF, McClure RL, Gajula KS, Saribasak H, et al. Local sequence targeting in the AID/APOBEC family differentially impacts retroviral restriction and antibody diversification. *Journal of Biological Chemistry*. 2010;285:40956–64.
95. Wang M, Rada C, Neuberger MS. Altering the spectrum of immunoglobulin V gene somatic hypermutation by modifying the active site of AID. *Journal of Experimental Medicine*. 2010;207:141–53.
96. Wijesinghe P, Bhagwat AS. Efficient deamination of 5-methylcytosines in DNA by human APOBEC3A, but not by AID or APOBEC3G. *Nucleic Acids Res*. 2012.
97. Kim N, Mudrak SV, Jinks-Robertson S. The dCMP transferase activity of yeast Rev1 is biologically relevant during the bypass of endogenously generated AP sites. *DNA Repair (Amst)*. 2011;10:1262–71.
98. Conover CA, Hartmann LC, Bradley S, Stalboerger P, Klee GG, Kalli KR, et al. Biological characterization of human epithelial ovarian carcinoma cells in primary culture: the insulin-like growth factor system. *Exp Cell Res*. 1998;238:439–49.
99. Li H, Durbin R. Fast and accurate short read alignment with Burrows-Wheeler transform. *Bioinformatics*. 2009;25:1754–60.
100. DePristo MA, Banks E, Poplin R, Garimella KV, Maguire JR, Hartl C, et al. A framework for variation discovery and genotyping using next-generation DNA sequencing data. *Nat Genet*. 2011;43:491–8.
101. Larson DE, Harris CC, Chen K, Koboldt DC, Abbott TE, Dooling DJ, et al. SomaticSniper: identification of somatic point mutations in whole genome

- sequencing data. *Bioinformatics*. 2012;28:311–7.
102. Sherry ST, Ward MH, Kholodov M, Baker J, Phan L, Smigielski EM, et al. dbSNP: the NCBI database of genetic variation. *Nucleic Acids Res*. 2001;29:308–11.
103. 1000 Genomes Project Consortium, Abecasis GR, Altshuler D, Auton A, Brooks LD, Durbin RM, et al. A map of human genome variation from population-scale sequencing. *Nature*. 2010;467:1061–73.
104. Trapnell C, Pachter L, Salzberg SL. TopHat: discovering splice junctions with RNA-Seq. *Bioinformatics*. 2009;25:1105–11.
105. Hong GF. Sequencing of large double-stranded DNA using the dideoxy sequencing technique. *Biosci Rep*. 1982;2:907–12.
106. Chien J, Narita K, Rattan R, Giri S, Shridhar R, Staub J, et al. A role for candidate tumor-suppressor gene TCEAL7 in the regulation of c-Myc activity, cyclin D1 levels and cellular transformation. *Oncogene*. 2008;27:7223–34.
107. Kruk PA, Godwin AK, Hamilton TC, Auersperg N. Telomeric instability and reduced proliferative potential in ovarian surface epithelial cells from women with a family history of ovarian cancer. *Gynecol Oncol*. 1999;73:229–36.
108. Langdon SP, Lawrie SS, Hay FG, Hawkes MM, McDonald A, Hayward IP, et al. Characterization and properties of nine human ovarian adenocarcinoma cell lines. *Cancer Research*. 1988;48:6166–72.
109. Hamilton TC, Young RC, McKoy WM, Grotzinger KR, Green JA, Chu EW, et al. Characterization of a human ovarian carcinoma cell line (NIH:OVCAR-3) with androgen and estrogen receptors. *Cancer Research*. 1983;43:5379–89.
110. Subramanian IV, Bui Nguyen TM, Truskinovsky AM, Tolar J, Blazar BR, Ramakrishnan S. Adeno-associated virus-mediated delivery of a mutant endostatin in combination with carboplatin treatment inhibits orthotopic growth of ovarian cancer and improves long-term survival. *Cancer Research*.

2006;66:4319–28.

111. Berchuck A, Rodriguez G, Olt G, Whitaker R, Boente MP, Arrick BA, et al. Regulation of growth of normal ovarian epithelial cells and ovarian cancer cell lines by transforming growth factor-beta. *Am J Obstet Gynecol.* 1992;166:676–84.
112. Buick RN, Pullano R, Trent JM. Comparative properties of five human ovarian adenocarcinoma cell lines. *Cancer Research.* 1985;45:3668–76.
113. Provencher DM, Lounis H, Champoux L, Tetrault M, Manderson EN, WANG JC, et al. Characterization of four novel epithelial ovarian cancer cell lines. *In Vitro Cell Dev Biol Anim.* 2000;36:357–61.
114. Bénard J, Da Silva J, De Blois M-C, Boyer P, Duvillard P, Chiric E, et al. Characterization of a human ovarian adenocarcinoma line, IGROV1, in tissue culture and in nude mice. *Cancer Research.* 1985;45:4970–9.
115. Rose WC, Basler GA. In vivo model development of cisplatin-resistant and -sensitive A2780 human ovarian carcinomas. *In Vivo.* 1990;4:391–6.
116. Kuong KJ, Loeb LA. APOBEC3B mutagenesis in cancer. *Nat Genet.* 2013;45:964–5.
117. Cancer Genome Atlas Network. Comprehensive genomic characterization of head and neck squamous cell carcinomas. *Nature.* 2015;517:576–82.
118. Roberts SA, Sterling J, Thompson C, Harris S, Mav D, Shah R, et al. Clustered mutations in yeast and in human cancers can arise from damaged long single-strand DNA regions. *Mol Cell.* 2012;46:424–35.
119. Rathore A, Carpenter MA, Demir Ö, Ikeda T, Li M, Shaban NM, et al. The local dinucleotide preference of APOBEC3G can be altered from 5'-CC to 5'-TC by a single amino acid substitution. *J Mol Biol.* 2013;425:4442–54.
120. Nabel CS, Lee JW, Wang LC, Kohli RM. Nucleic acid determinants for selective

- deamination of DNA over RNA by activation-induced deaminase. *Proceedings of the National Academy of Sciences*. 2013;110:14225–30.
121. Rosse C, Linch M, Kermorgant S, Cameron AJM, Boeckeler K, Parker PJ. PKC and the control of localized signal dynamics. *Nat Rev Mol Cell Biol*. 2010;11:103–12.
122. Griner EM, Kazanietz MG. Protein kinase C and other diacylglycerol effectors in cancer. *Nat Rev Cancer*. 2007;7:281–94.
123. Spitaler M, Cantrell DA. Protein kinase C and beyond. *Nat Immunol*. 2004;5:785–90.
124. Mackay HJ, Twelves CJ. Targeting the protein kinase C family: are we there yet? *Nat Rev Cancer*. 2007;7:554–62.
125. Gschwendt M, Dieterich S, Rennecke J, Kittstein W, Mueller HJ, Johannes FJ. Inhibition of protein kinase C mu by various inhibitors. Differentiation from protein kinase c isoenzymes. *FEBS Lett*. 1996;392:77–80.
126. Toullec D, Pianetti P, Coste H, Bellevergue P, Grand-Perret T, Ajakane M, et al. The bisindolylmaleimide GF 109203X is a potent and selective inhibitor of protein kinase C. *Journal of Biological Chemistry*. 1991;266:15771–81.
127. Martiny-Baron G, Kazanietz MG, Mischak H, Blumberg PM, Kochs G, Hug H, et al. Selective inhibition of protein kinase C isozymes by the indolocarbazole Gö 6976. *Journal of Biological Chemistry*. 1993;268:9194–7.
128. Evenou J-P, Wagner J, Zenke G, Brinkmann V, Wagner K, Kovarik J, et al. The potent protein kinase C-selective inhibitor AEB071 (sotrastaurin) represents a new class of immunosuppressive agents affecting early T-cell activation. *J Pharmacol Exp Ther*. 2009;330:792–801.
129. Wagner J, Matt von P, Sedrani R, Albert R, Cooke N, Ehrhardt C, et al. Discovery of 3-(1H-indol-3-yl)-4-[2-(4-methylpiperazin-1-yl)quinazolin-4-yl]pyrrole-2,5-dione

- (AEB071), a potent and selective inhibitor of protein kinase C isotypes. *J Med Chem.* 2009;52:6193–6.
130. Wagner J, Matt von P, Faller B, Cooke NG, Albert R, Sedrani R, et al. Structure-activity relationship and pharmacokinetic studies of sotrastaurin (AEB071), a promising novel medicine for prevention of graft rejection and treatment of psoriasis. *J Med Chem.* 2011;54:6028–39.
131. Wu X, Li J, Zhu M, Fletcher JA, Hodi FS. Protein kinase C inhibitor AEB071 targets ocular melanoma harboring GNAQ mutations via effects on the PKC/Erk1/2 and PKC/NF- κ B pathways. *Mol Cancer Ther.* 2012;11:1905–14.
132. Chen X, Wu Q, Tan L, Porter D, Jager MJ, Emery C, et al. Combined PKC and MEK inhibition in uveal melanoma with GNAQ and GNA11 mutations. *Oncogene.* 2013.
133. Musi E, Ambrosini G, de Stanchina E, Schwartz GK. The phosphoinositide 3-kinase α selective inhibitor BYL719 enhances the effect of the protein kinase C inhibitor AEB071 in GNAQ/GNA11-mutant uveal melanoma cells. *Mol Cancer Ther.* 2014;13:1044–53.
134. Piperno-Neumann S, Kapiteijn E, Larkin JMG, Carvajal RD, Luke JJ, Seifert H, et al. Phase I dose-escalation study of the protein kinase C (PKC) inhibitor AEB071 in patients with metastatic uveal melanoma. *J Clin Oncol.* 2014;32:5s(suppl–abstr9030).
135. Vallabhapurapu S, Karin M. Regulation and function of NF-kappaB transcription factors in the immune system. *Annu Rev Immunol.* 2009;27:693–733.
136. Karin M, Cao Y, Greten FR, Li Z-W. NF-kappaB in cancer: from innocent bystander to major culprit. *Nat Rev Cancer.* 2002;2:301–10.
137. Strickson S, Campbell DG, Emmerich CH, Knebel A, Plater L, Ritorto MS, et al. The anti-inflammatory drug BAY 11-7082 suppresses the MyD88-dependent

- signalling network by targeting the ubiquitin system. *Biochem J.* 2013;451:427–37.
138. Podolin PL, Callahan JF, Bolognese BJ, Li YH, Carlson K, Davis TG, et al. Attenuation of murine collagen-induced arthritis by a novel, potent, selective small molecule inhibitor of I κ B Kinase 2, TPCA-1 (2-[(aminocarbonyl)amino]-5-(4-fluorophenyl)-3-thiophenecarboxamide), occurs via reduction of proinflammatory cytokines and antigen-induced T cell Proliferation. *J Pharmacol Exp Ther.* 2005;312:373–81.
139. Foxwell B, Browne K, Bondeson J, Clarke C, de Martin R, Brennan F, et al. Efficient adenoviral infection with I κ B alpha reveals that macrophage tumor necrosis factor alpha production in rheumatoid arthritis is NF-kappaB dependent. *Proceedings of the National Academy of Sciences.* 1998;95:8211–5.
140. Liu H, Sidiropoulos P, Song G, Pagliari LJ, Birrer MJ, Stein B, et al. TNF-alpha gene expression in macrophages: regulation by NF-kappa B is independent of c-Jun or C/EBP beta. *J Immunol.* 2000;164:4277–85.
141. Lucifora J, Xia Y, Reisinger F, Zhang K, Stadler D, Cheng X, et al. Specific and nonhepatotoxic degradation of nuclear hepatitis B virus cccDNA. *Science.* 2014;343:1221–8.
142. Snyder A, Makarov V, Merghoub T, Yuan J, Zaretsky JM, Desrichard A, et al. Genetic basis for clinical response to CTLA-4 blockade in melanoma. *N Engl J Med.* 2014;371:2189–99.
143. Van Raamsdonk CD, Bezrookove V, Green G, Bauer J, Gaugler L, O'Brien JM, et al. Frequent somatic mutations of GNAQ in uveal melanoma and blue naevi. *Nature.* 2009;457:599–602.
144. Van Raamsdonk CD, Griewank KG, Crosby MB, Garrido MC, Vemula S, Wiesner T, et al. Mutations in GNA11 in uveal melanoma. *N Engl J Med.* 2010;363:2191–

9.

145. Love MI, Huber W, Anders S. Moderated estimation of fold change and dispersion for RNA-seq data with DESeq2. *Genome Biol.* 2014;15:550.
146. Trapnell C, Roberts A, Goff L, Pertea G, Kim D, Kelley DR, et al. Differential gene and transcript expression analysis of RNA-seq experiments with TopHat and Cufflinks. *Nat Protoc.* 2012;7:562–78.
147. Swanton C, McGranahan N, Starrett GJ, Harris RS. APOBEC enzymes: mutagenic fuel for cancer evolution and heterogeneity. *Cancer Discovery.* 2015;5:704–12.
148. Roberts SA, Gordenin DA. Hypermutation in human cancer genomes: footprints and mechanisms. *Nat Rev Cancer.* 2014;14:786–800.
149. Caval V, Suspène R, Shapira M, Vartanian J-P, Wain-Hobson S. A prevalent cancer susceptibility APOBEC3A hybrid allele bearing APOBEC3B 3'UTR enhances chromosomal DNA damage. *Nat Commun.* 2014;5:5129.
150. Sabek O, Dorak MT, Kotb M, Gaber AO, Gaber L. Quantitative detection of T-cell activation markers by real-time PCR in renal transplant rejection and correlation with histopathologic evaluation. *Transplantation.* 2002;74:701–7.
151. Zheng Y, Zha Y, Gajewski TF. Molecular regulation of T-cell anergy. *EMBO Rep.* 2008;9:50–5.
152. Schumacher AJ, Nissley DV, Harris RS. APOBEC3G hypermutates genomic DNA and inhibits Ty1 retrotransposition in yeast. *Proceedings of the National Academy of Sciences.* 2005;102:9854–9.
153. Duggal NK, Emerman M. Evolutionary conflicts between viruses and restriction factors shape immunity. *Nat Rev Immunol.* 2012;12:687–95.
154. Stoye JP. Studies of endogenous retroviruses reveal a continuing evolutionary saga. *Nat Rev Microbiol.* 2012;10:395–406.
155. Sohn I, Jung WY, Sung CO. Somatic hypermutation and outcomes of platinum

- based chemotherapy in patients with high grade serous ovarian cancer. *Gynecol Oncol.* 2012;126:103–8.
156. Leonard B, McCann JL, Starrett GJ, Kosyakovski L, Luengas EM, Molan AM, et al. APOBEC3B upregulation by the PKC-NFκB pathway in multiple human cancers. *Cancer Research.* in review.
157. Muñoz N, Bosch FX, de Sanjosé S, Herrero R, Castellsagué X, Shah KV, et al. Epidemiologic classification of human papillomavirus types associated with cervical cancer. *N Engl J Med.* 2003;348:518–27.
158. Farmer H, McCabe N, Lord CJ, Tutt ANJ, Johnson DA, Richardson TB, et al. Targeting the DNA repair defect in BRCA mutant cells as a therapeutic strategy. *Nature.* 2005;434:917–21.
159. Bryant HE, Schultz N, Thomas HD, Parker KM, Flower D, Lopez E, et al. Specific killing of BRCA2-deficient tumours with inhibitors of poly(ADP-ribose) polymerase. *Nature.* 2005;434:913–7.
160. Lord CJ, Tutt ANJ, Ashworth A. Synthetic lethality and cancer therapy: lessons learned from the development of PARP inhibitors. *Annu Rev Med.* 2015;66:455–70.
161. Dance GSC, Sowden MP, Cartegni L, Cooper E, Krainer AR, Smith HC. Two proteins essential for apolipoprotein B mRNA editing are expressed from a single gene through alternative splicing. *Journal of Biological Chemistry.* 2002;277:12703–9.
162. Fossat N, Tourle K, Radziewicz T, Barratt K, Liebhold D, Studdert JB, et al. C to U RNA editing mediated by APOBEC1 requires RNA-binding protein RBM47. *EMBO Rep.* 2014;15:903–10.
163. Barber LJ, Sandhu S, Chen L, Campbell J, Kozarewa I, Fenwick K, et al. Secondary mutations in BRCA2 associated with clinical resistance to a PARP

- inhibitor. *J Pathol*. 2013;229:422–9.
164. Bouwman P, Jonkers J. Molecular pathways: how can BRCA-mutated tumors become resistant to PARP inhibitors? *Clin Cancer Res*. 2014;20:540–7.
165. Robinson DR, Wu Y-M, Vats P, Su F, Lonigro RJ, Cao X, et al. Activating ESR1 mutations in hormone-resistant metastatic breast cancer. *Nat Genet*. 2013;45:1446–51.
166. Scheffner M, Werness BA, Huibregtse JM, Levine AJ, Howley PM. The E6 oncoprotein encoded by human papillomavirus types 16 and 18 promotes the degradation of p53. *Cell*. 1990;63:1129–36.
167. Scheffner M, Huibregtse JM, Vierstra RD, Howley PM. The HPV-16 E6 and E6-AP complex functions as a ubiquitin-protein ligase in the ubiquitination of p53. *Cell*. 1993;75:495–505.
168. James MA, Lee JH, Klingelutz AJ. Human papillomavirus type 16 E6 activates NF-kappaB, induces cIAP-2 expression, and protects against apoptosis in a PDZ binding motif-dependent manner. *Journal of Virology*. 2006;80:5301–7.
169. Yan M, Peng J, Jabbar IA, Liu X, Filgueira L, Frazer IH, et al. Activation of dendritic cells by human papillomavirus-like particles through TLR4 and NF-kappaB-mediated signalling, moderated by TGF-beta. *Immunol Cell Biol*. 2005;83:83–91.
170. An J, Mo D, Liu H, Veena MS, Srivatsan ES, Massoumi R, et al. Inactivation of the CYLD deubiquitinase by HPV E6 mediates hypoxia-induced NF-kappaB activation. *Cancer Cell*. 2008;14:394–407.
171. Vuillier F, Gaud G, Guillemot D, Commere P-H, Pons C, Favre M. Loss of the HPV-Infection Resistance EVER2 Protein Impairs NF-kB Signaling Pathways in Keratinocytes. *PLoS ONE*. 2014;9:e89479.
172. American Cancer Society. *Cancer Facts & Figures: 2015*. Atlanta: American Cancer Society; 2015.